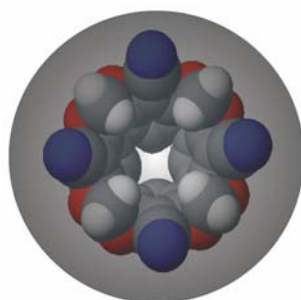


Cavitands, Helicates and Macrocycles – Unleashing the Power of Weak Non-Covalent Interactions



Dissertation

zur

Erlangung des Doktorgrades (Dr. rer. nat.)

der

Mathematisch-Naturwissenschaftlichen Fakultät

der

Rheinischen Friedrich-Wilhelms-Universität Bonn

vorgelegt von

Sascha Shuxia Zhu

aus

Jiangsu

Bonn 2009

**Cavitands, Helicates and Macrocycles –
Unleashing the Power of Weak Non-Covalent Interactions**

Dissertation

zur

Erlangung des Doktorgrades (Dr. rer. nat.)

der

Mathematisch-Naturwissenschaftlichen Fakultät

der

Rheinischen Friedrich-Wilhelms-Universität Bonn

vorgelegt von

Sascha Shuxia Zhu

aus

Jiangsu

Bonn 2009

Angefertigt mit Genehmigung der Mathematisch-Naturwissenschaftlichen Fakultät
der Rheinischen Friedrich-Wilhelms-Universität Bonn

1. Referent: Prof. Dr. Christoph A. Schalley (FU Berlin)
2. Referent: Prof. Dr. Arne Lützen
3. Referent: Prof. Dr. Klaus Wandelt
4. Referent: Prof. Dr. Karl Maier

Tag der Promotion: 03.11.2009

Die vorliegende Arbeit wurde in der Zeit von März 2006 bis Februar 2009 unter der Leitung von Herrn Prof. Dr. Christoph A. Schalley am Kekulé-Institut für Organische Chemie und Biochemie der Rheinischen Friedrich-Wilhelms-Universität Bonn angefertigt.

Teile dieser Arbeit sind bereits veröffentlicht:

- 1.** *Anionen bindende Resorcinaren-Cavitanden: die Bedeutung von C–H...Anion-Wechselwirkungen* /
Anion Binding to Resorcinarene-Based Cavitands: The Importance of C–H...Anion Interactions
S. S. Zhu, H. Staats, K. Brandhorst, J. Grunenberg, F. Gruppi, E. Dalcanale, A. Lützen, K. Rissanen, C. A. Schalley, *Angew. Chem.* **2008**, *120*, 800-804; *Angew. Chem. Int. Ed.* **2008**, *47*, 788-792.
- 2.** *A Modular "Toolbox" Approach to Flexible Branched Multimacrocyclic Hosts as Precursors for Multiply Interlocked Architectures*
B. Baytekin, S. S. Zhu, B. Brusilowskij, J. Illigen, J. Ranta, J. Huuskonen, L. Russo, K. Rissanen, L. Kaufmann, C. A. Schalley, *Chem. Eur. J.* **2008**, *14*, 10012-10028.
- 3.** *Self-assembly of Heterodinuclear Triple-stranded Helicates: Control by Coordination Number and Charge*
M. Albrecht, Y. Liu, S. S. Zhu, C. A. Schalley, R. Fröhlich, *Chem. Commun.* **2009**, 1195-1197.
- 4.** *Conformational Flexibility of Tetralactam Macrocycles and Their Intermolecular Hydrogen-Bonding Patterns in the Solid State*
S. S. Zhu, M. Nieger, J. Daniels, T. Felder, I. Kossev, T. Schmidt, M. Sokolowski, F. Vögtle, C. A. Schalley, *Chem. Eur. J.* **2009**, *15*, 5040-5046.

Dedicated to my parents and my wife

*“Now I do not know
whether I was then a man dreaming I was a butterfly,
or whether I am now a butterfly, dreaming I am a man.”*

– Zhuangzi (about 370-290 B.C.), a Chinese philosopher

Table of Contents (Overview)

Preface	V
A. Anion Binding in Resorcinarene-Based Cavitands: An MS Study	1
B. Self-Assembled Metallosupramolecular Helicates: An MS Study	27
C. Multimacrocyclic Hosts as Precursors for Multiply Interlocked Systems: A Study on Modular Synthesis	45
D. Conformationally Flexible Tetralactam Macrocycles: An X-ray Study	70
E. Experimental Section	79
F. References and Notes	110
Appendix I: Acknowledgement	119
Appendix II: Curriculum Vitae / Lebenslauf	121
Appendix III: Publication List / Publikationsliste	125
Appendix IV: Summary / Zusammenfassung	128

Table of Contents (Detailed)

Preface.....	V
A. Anion Binding in Resorcinarene-Based Cavitands: An MS Study	1
A1 Purpose of the Study and Introduction	1
A1.1 Anion Binding in General	1
A1.2 Resorcinarene-based Cavitands and Their Anion-binding Properties	4
A1.3 Advantages of Using Mass Spectrometry for Our Studies	6
A2 Anion Binding in Monotopic Methylene-bridged Cavitands – Results and Discussion.....	8
A2.1 Brief Overview	8
A2.2 Small Monoanions and Dianions as Guests	9
A2.3 Tandem MS Experiments with Cavitand-Sulfate Complexes.....	10
A2.4 Large Monoanions as Guests	13
A2.5 Large Di- and Tetraanions as Guests – Gas Phase Ranking for the Cavitand-Anion Interaction.....	14
A2.6 Preliminary Conclusions from the MS Experiments.....	16
A2.7 Quantum Chemical Calculations.....	17
A3 Anion Binding in Cavitands Other Than Monotopic Methylene-bridged Analogues – Results and Discussion	19
A3.1 Brief Overview	19
A3.2 Ethylene-bridged Cavitand.....	20
A3.3 Non-bridged Cavitands	22
A3.4 Ditopic Methylene-bridged Cavitand.....	23
A4 Final Conclusions and Outlook.....	26
B. Self-Assembled Metallosupramolecular Helicates: An MS Study	27
B1 Purpose of the Study and Introduction	27
B1.1 Helicates in General	27
B1.2 Helicates Obtained through Hierarchical Self-Assembly	30
B1.3 Advantages of Using Mass Spectrometry for Our Studies	32
B2 Hierarchically Assembled Helicates – Results and Discussion	33
B2.1 Brief Overview	33
B2.2 Homodinuclear Homoleptic Helicates – Kinetic Effects in Their Formation..	34

B2.3	Mixtures (not) Leading to Heterodinuclear Homoleptic Helicates.....	35
B2.4	Mixtures Leading to Homodinuclear Heteroleptic Helicates (Pathway <i>B</i>).....	38
B2.5	Mixtures Leading to Heterodinuclear Heteroleptic Helicates (Pathway <i>A</i>).....	39
B3	Heterodinuclear Helicates Assembled from Heteroditopic Ligands – Results and Discussion.....	41
B3.1	Brief Overview	41
B3.2	MS Characterization of the Reaction Product of a Ga-La-Helicate.....	42
B3.3	MS Characterization of a Ti-Ca-Helicate.....	43
B4	Final Conclusions and Outlook.....	44
C.	Multimacrocyclic Hosts as Precursors for Multiply Interlocked Systems:	
	A Study on Modular Synthesis.....	45
C1	Purpose of the Study and Introduction.....	45
C2	Results and Discussion.....	48
C2.1	Brief Overview	48
C2.2	Synthesis of a Tetralactam Macrocycle via the Pre-Macrocyclization Pathway	49
C2.3	Crystal Structure of Macrocycle 3	50
C2.4	Synthesis of Key Intermediates and Synthesis of Macrocyclic Ligands via the Post-Macrocyclization Pathway	52
C2.5	Rotaxane Synthesis	54
C2.6	Synthesis of Covalently Linked, Cross-Coupled Macrocycle Dimers and Trimers	56
C2.7	Synthesis of Chromophore-Substituted Macrocycles	58
C2.8	Self-Assembly of Macrocyclic Ligands to Metal-Centered FBMHs – Pyridine Coordination.....	60
C2.9	Crystal Structure of Metal-Centered FBMH 34.....	63
C2.10	Synthesis and Molecular Modeling of MIA 40.....	64
C2.11	Self-Assembly of Macrocyclic Ligands to Metal-Centered FBMHs – Terpyridine Coordination.....	66
C3	Final Conclusions and Outlook.....	68
D.	Conformationally Flexible Tetralactam Macrocycles: An X-ray Study.....	70
D1	Purpose of the Study and Introduction.....	70
D2	Results and Discussion.....	71
D3	Final Conclusions and Outlook.....	78

E.	Experimental Section	79
E1	Instruments for NMR spectroscopy	79
E2	Instruments and General Settings for Mass Spectrometry	79
E3	Chemicals and Miscellaneous.....	81
E4	Abbreviations.....	81
E5	Synthetic Procedures.....	84
E6	Data of crystal structures	94
F.	References and Notes	110
	Appendix I: Acknowledgement	119
	Appendix II: Curriculum Vitae / Lebenslauf.....	121
	Appendix III: Publication List / Publikationsliste	125
	Appendix IV: Summary / Zusammenfassung.....	128

Preface

Scientific progress is closely intertwined with the change of basic principles and concepts – also referred to as “paradigm shifts”^[i] if a certain significance level is reached. The best examples for these shifts are Einstein’s theory of relativity or the theory of quantum mechanics, involving fundamental rethinking in classical physics. Despite lacking such spectacular examples, the discipline of chemistry has witnessed some more or less eye-catching paradigm shifts over the past few decades, for instance:

- i. Within the old paradigm, the evaluation of chemical processes was focused on the chemical yield. With the emergence of green chemistry in the 1990s, a new paradigm evolved, shifting the focus to sustainability-related aspects such as atom efficiency, waste prevention and the use of alternative reaction media (green solvents, solventless reactions).^[ii]
- ii. According to the old paradigm, there were either properties of the macroscopic matter or properties of the molecules themselves, furthermore, the only feasible way to obtain small, sub-micron structures was believed to be the top-down approach. A paradigm shift came along with the advent of nanoscience in the 1980s, showing the properties of nano-scale materials to be unique and unlike that of bulk matter or discrete molecules, and establishing the bottom-up approach as the route of choice to fabricate these materials.^[iii]
- iii. In the context of the old paradigm, the experimentally observed properties of a chemical system were mostly attributed to the properties of the molecules involved. The environment was usually thought of as negligible, because the interactions between a molecule and its environment are so much weaker than the covalent bonds within the molecule. Nowadays supramolecular chemistry came into existence, when chemists became more and more aware of the fact that the intrinsic properties of a molecule are much more significantly altered by the environment than believed before. Non-covalent bonds came into the focus of chemical research and defined a whole new research field.^[iv]

Paradigm shift (iii.) and the change to the bottom-up approach (ii.) could not be viable if *weak non-covalent interactions* would still remain unknown. Although there is no precise definition of these interactions, the boundary to strong non-covalent bonds can be set at approximately 50 kJ/mol (see Figure I). Owing to the development of modern analytical techniques and the fabrication of novel materials over the last decades, more and more types of weak non-covalent interactions have been discovered, for example cation- π interactions^[v] or very weak hydrogen bonds such as C–H \cdots O^[vi] and C–H \cdots π interactions^[vii]. Basically, weak non-

covalent interactions are ubiquitous in all fields of chemistry: from liquid crystals within displays and screens, in some of which π - π interactions play a major role^[viii], to biochemical systems such as proteins, in which weak hydrogen bonds and van-der-Waals forces contribute to the secondary or tertiary structures^[ix] – just to name two examples from everyday life.

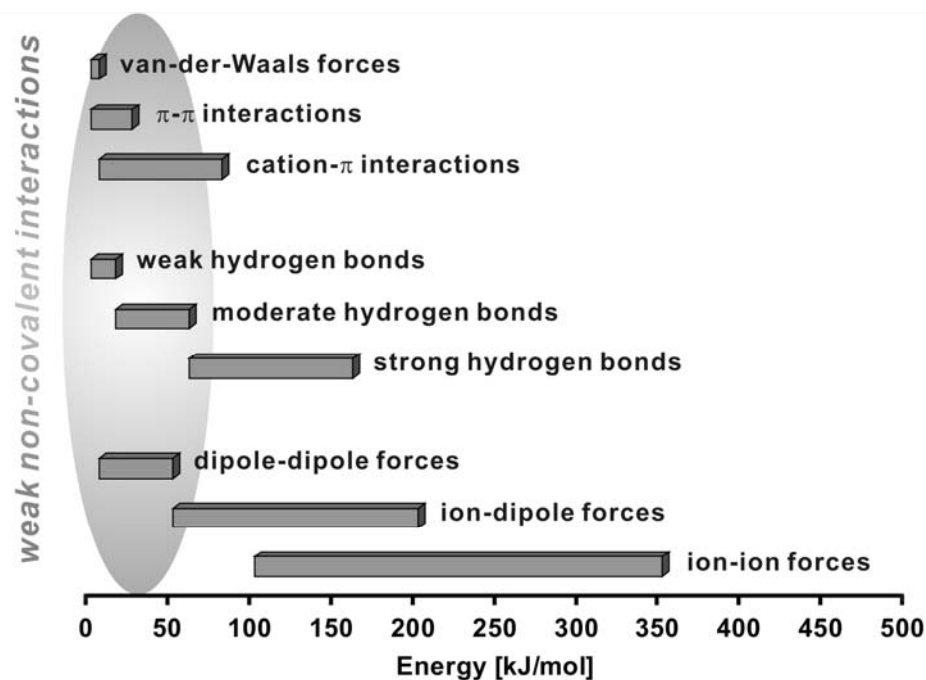


Figure I: Energy ranges of different kinds of non-covalent interactions^[iv,x]

This thesis will reveal very different and somehow unexpected facets of weak non-covalent interactions – for instance in **cavitands** in which C–H \cdots anion interactions are operative, in **helicates** in which the self-assembly process is assisted by Li⁺ \cdots O=C interactions, and in **macrocycles** in which moderate to weak hydrogen bonds have a great impact on threading processes and crystal structures. The work tries to contribute to a more comprehensive understanding of these interactions and of supramolecular phenomena, and might be a further step on the long road towards the next paradigm shift.

References (Preface section)

- [i] T. S. Kuhn, *The Structure of Scientific Revolutions* (3rd edition); University of Chicago Press: Chicago, **1996**.
- [ii] a) P. T. Anastas, J. C. Warner, *Green Chemistry: Theory and Practice*; Oxford Science Publications: New York, **1998**; b) G. W. V. Cave, C. L. Raston, J. L. Scott, *Chem. Commun.* **2001**, 2159-2169; c) R. A. Sheldon, *Green Chem.* **2005**, 7, 267-278.
- [iii] a) J. R. Heath, *Acc. Chem. Res.* **1999**, 32, 388; b) G. M. Whitesides, *Small* **2005**, 1, 172-179.
- [iv] C. A. Schalley, *Introduction*, in: C. A. Schalley (Ed.), *Analytical Methods in Supramolecular Chemistry*, Wiley-VCH: Weinheim, **2007**.
- [v] J. C. Ma, D. A. Dougherty, *Chem. Rev.* **1997**, 97, 1303-1324.
- [vi] Y. L. Gu, T. Kar, S. Scheiner, *J. Am. Chem. Soc.* **1999**, 121, 9411-9422.
- [vii] M. Nishio, *CrystEngComm* **2004**, 6, 130-158.
- [viii] a) F. Würthner, C. Thalacker, S. Diele, C. Tschierske, *Chem.-Eur. J.* **2001**, 7, 2245-2253; b) Y. F. Wang, Y. L. Chen, R. J. Li, S. Q. Wang, W. Su, P. Ma, M. R. Wasielewski, X. Y. Li, J. Z. Jiang, *Langmuir* **2007**, 23, 5836-5842.
- [ix] W. Amann, W. Eisner, P. Gietz, J. Maier, W. Schierle, R. Stein, *Elemente Chemie II*, Ernst Klett: Stuttgart, **1998**.
- [x] a) P. Andrews, M. Dooley, *Role of molecular recognition in drug design*, in: P. Krogsgaard-Larsen, T. Liljefors, U. Madsen (Eds.), *Textbook of drug design and discover* (3rd Edition); Taylor and Francis: London, New York, **2002**; b) H. J. Schneider, *Angew. Chem.* **2009**, 121, 3982-4036; *Angew. Chem. Int. Ed.* **2009**, 48, 3924-3977.

A. Anion Binding in Resorcinarene-Based Cavitands: An MS Study

A1 Purpose of the Study and Introduction

A1.1 Anion Binding in General

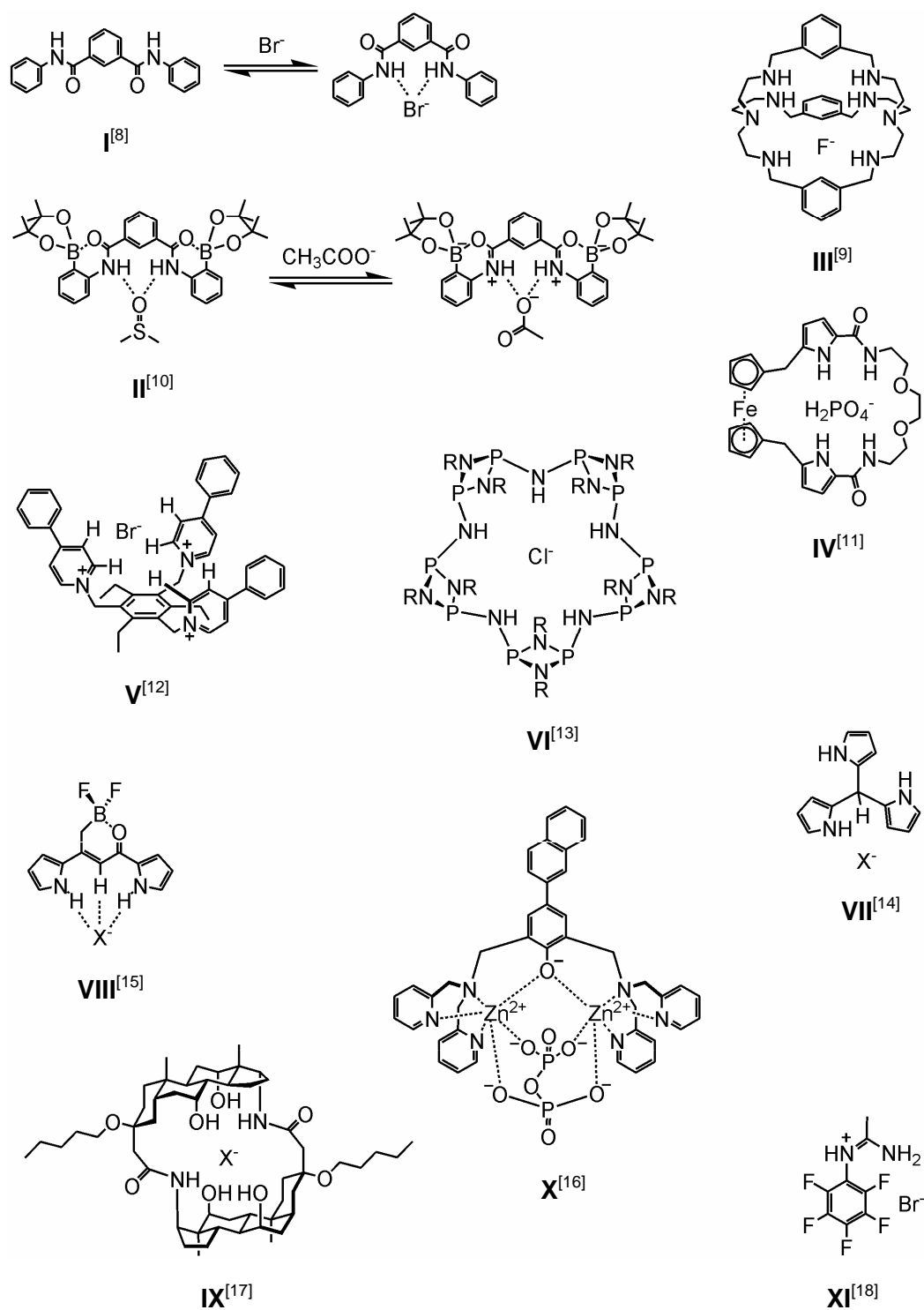
In recent years, anion binding chemistry has become a field of growing interest in the interdisciplinary framework of biological^[1], analytical^[2], and supramolecular chemistry^[3]. In the development of anion binding hosts, much endeavour has been directed towards applications such as sensors or membrane transport agents for biologically significant anionic species,^[4] anion separation agents,^[5] and catalytically active receptors.^[6]

Generally, as regards the binding situation in solution, anion binding is more challenging than cation binding due to the following reasons:

- Anions adopt very different geometries, for example linear (azide), spherical (halides), planar (nitrate), tetrahedral (tetrafluoroborate), octahedral (hexafluorophosphate) or more complex geometries (citrate).^[7]
- If anions and cations of comparable size – for example F^- (ionic radius 1.33 Å) and K^+ (1.38 Å) – are considered, the free energy of solvation is considerably higher for anions than for cations. Therefore, anion binding hosts have to compete more effectively with the solvent molecules.^[7]
- Many anions only exist in a limited pH range.^[7]

Anion binding hosts can be classified into the following categories:

(see Table A1 on page 3)



Scheme A1: Examples for anion binding hosts (Abbreviations: X^- = halide, R = tert-butyl)

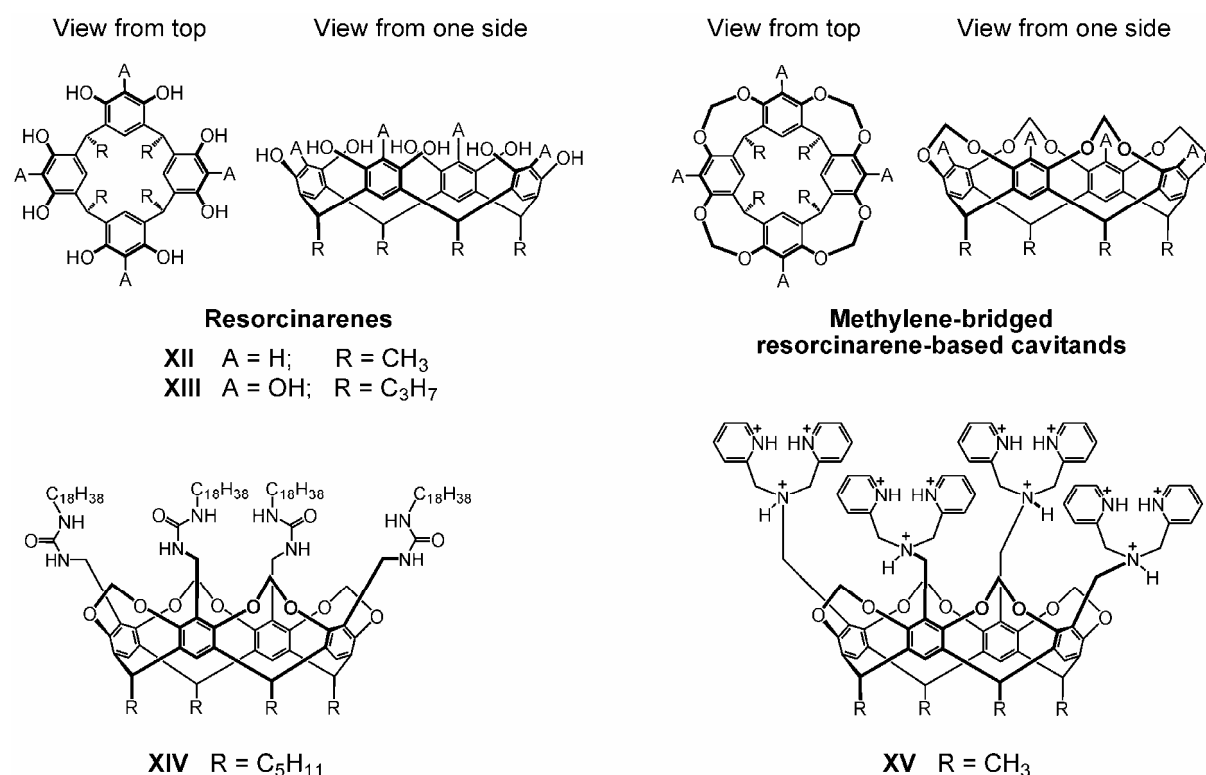
Criteria for classification	Categories	Subcategories	Examples (numbers refer to Scheme A1)
Charge	neutral	non-zwitterionic	all except II/V/X/XI
		zwitterionic	II
	cationic		V/X/XI
Framework	organic	non-metallated	all except IV/VI/X
		metallated	IV/X
	inorganic		VI
“Cyclicity”	acyclic ^[19]		all except II/IV/VI/IX
	macro-cyclic	macromonocyclic	IV/VI/IX
		macrobicyclic	III
Preorganisation	preorganized		II-IV/VI/IX/X
	non-preorganized		I/V/VII/VIII/XI
State of matter in which anion binding is observed (analytical technique)	solid state (<i>X-ray diffraction</i>)		I-III/V-VII/XI
	solution state (<i>NMR, calorimetry</i>)		I/II/IV/VII-X
	gas phase (<i>MS</i>)		VII
Interactions between anion and host	hydrogen bonds	NH•••anion	I-IV/VI-VIII/XI
		OH•••anion	IX
		aromatic CH•••anion	V
		non-aromatic CH•••anion	VIII
	electrostatic interactions		X
	anion- π interactions		XI

Table A1: Classification of anion binding hosts; Sub-categories on which the study is focused are marked gray.

As neutral, non-metallated organic receptors are considered, anion binding is mainly based on rather strong hydrogen bonds provided by a donor group. Well-known examples for these hydrogen bond donors are N–H or O–H groups. In quite a number of anion receptors, anion binding is supported by additional weaker interactions of the anion with *aromatic* C–H bonds (see **V** in Scheme A1).^[12,20] In this context, interactions **between anions and non-aromatic C–H** as a weak hydrogen bond donor are, however, extremely rare and only appear in company with N–H•••anion hydrogen bonds (see **VIII** in Scheme A1).^[15,21] Up to date, versatile anion receptors completely based on non-aromatic C–H•••anion hydrogen bonds are yet unknown. Answering the question whether any of them exist is one of the main objectives of this study.

A1.2 Resorcinarene-based Cavitands and Their Anion-binding Properties

As one class of the traditional workhorses in supramolecular chemistry, resorcinarenes^[22] represent a highly interesting multi-purpose scaffold. Their numerous applications range from the assembly of, for example, capsules^[23] such as the resorcinarene hexamers (see Figure A1a/b),^[24] of coordination cages (see Figure A1c/d),^[25] or of molecular loops^[26] to supramolecular sensors,^[27] and phase-transfer catalysts.^[28]



Scheme A2: Chemical structures of some resorcinarenes and cavitands

The simplest resorcinarenes such as **XII** (Scheme A2) are held in a cone conformation through O–H•••O hydrogen bonding along the upper rim. They are well known for accommodating guest cations, e.g. quaternary ammonium ions,^[29] or neutral solvent molecules^[30] inside their cavities.

For anion binding instead, more elaborate cavitand receptors were developed so far,^[31] in which the resorcinarene merely represents the scaffold, while **explicit anion-binding sites** – such as (thio)urea, N-heterocyclic or quaternary ammonium groups (see **XIV**^[31a] and **XV**^[31d] in Scheme A2) – are located in the apical positions on the edge of the cavity. Furthermore,

two recent NMR spectroscopic and crystallographic studies^[32] reported C–H•••X hydrogen bonding involving the inwards oriented acetal hydrogen atoms of methylene-bridged resorcinarene cavitanDs comparable to the one shown in Scheme A2, where X is the halide part of an alkyl halide. The question emerging from this observation is: Can this type of hydrogen bonds be utilized for anion binding? Is a resorcinarene cavitanD **without** the above-mentioned “explicit anion-binding sites” capable of binding anions? Answering these questions is a further, crucial goal of this study.

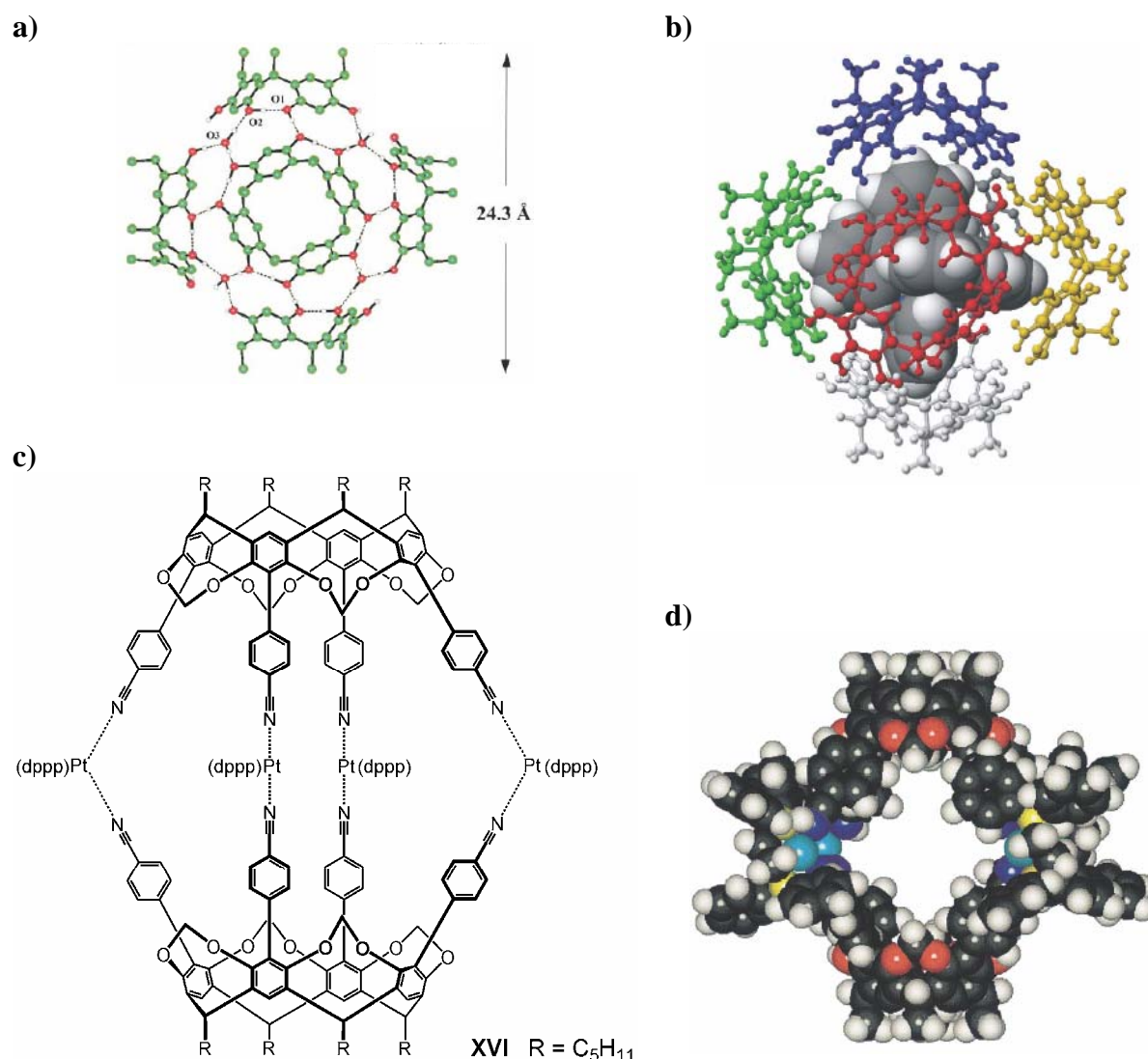


Figure A1: a) Hexameric capsule formed by **XII** (see Scheme A2) and eight water molecules,^[24a]
 b) Hexameric capsule formed by **XIII** (see Scheme A2) and the included metal template $[\text{Ru}(2,2'\text{-bipy})_3]^{2+}$,^[24c]
 c/d) Schematic and space-filling representation (pentyl replaced by methyl) of coordination cage **XVI**^[25a]

A1.3 Advantages of Using Mass Spectrometry for Our Studies

In general, gas-phase experiments are a powerful tool to examine the anion binding capabilities of resorcinarene cavitands, because the absence of the environment waives unexpected effects of solvent or counterions and enables us to study the intrinsic properties of the anion-cavitand complexes.

For our studies, we use the specific technique of Electrospray ionization Fourier-transform ion-cyclotron resonance mass spectrometry (**ESI-FTICR-MS**).

ESI works as follows.^[33]

Using nebulizing gas, the solution is sprayed into a chamber which is held under atmospheric pressure. At the same time, the drying gas flows in opposite direction to the nebulizing stream in this chamber. The voltage between the capillary and the chamber wall (3 to 5 kV) leads to the formation of charged droplets. Due to solvent evaporation within the counter-flow of drying gas, these droplets are gradually shrinking until completely desolvated ions are generated. The electric field directs the ions via a glass capillary into the analyzer's prechamber. Finally, the ion beam is focused through an electrostatic lens system and transferred into the mass analyzer.

FTICR works as follows.^[34]

- a) *Trapping*: The ions from the ionization chamber are trapped by a magnetic field perpendicular to the direction of ion movement and by an electric field between two trapping plates.
- b) *Excitation*: The excitation of the ion-cyclotron movement, which is required for the variation of the cyclotron radius, occurs through a uniform electric field. If the frequency of the oscillating electric field perpendicular to the magnetic field equals the cyclotron frequency of the ions with specific mass-to-charge-ratio, resonance occurs, causing the ions to be accelerated to a larger cyclotron radius and to move in phase as an "ion packet".
- c) *Detection*: When the "ion packet" cyclotrons between a pair of detector plates, an image charge is generated, inducing an image current. This current is proportional to the ICR signal which appears as an FID ("free induction decay") in the time domain. The FID is a superposition of sine waves and can be converted into the frequency domain by a Fourier-Transform technique to output the final mass spectrum.

Using ESI-FTICR-MS has many advantages: ESI is one of the softest ionization techniques and the method of choice for analyzing supramolecular assemblies. FTICR is a mass analyzer technique featuring high resolution, high accuracy, fast measurement and large mass range.

Furthermore, FTICR is an optimal technique for tandem-MS. During **tandem-MS** experiments, precursor ions are isolated and activated, before they dissociate to product ions through collision-induced dissociation (CID) or infrared multiphoton dissociation (IRMPD). The product ions are finally detected in the mass analyzer.

Tandem-MS can also be used in the following way: If heterodimeric ions $[X_1 \cdots Y \cdots X_2]^{+/-}$ (see Table A2) can be formed in the gas phase and subjected to tandem-MS experiments, the relative binding affinities of X_1/X_2 for Y can be determined by the so-called **Cooks' kinetic method**^[35] through comparing the intensities of the fragments $[X_1 \cdots Y]^{+/-}$ and $[Y \cdots X_2]^{+/-}$. This opens up a possibility to determine binding strengths of anion-cavitand complexes in the gas phase.

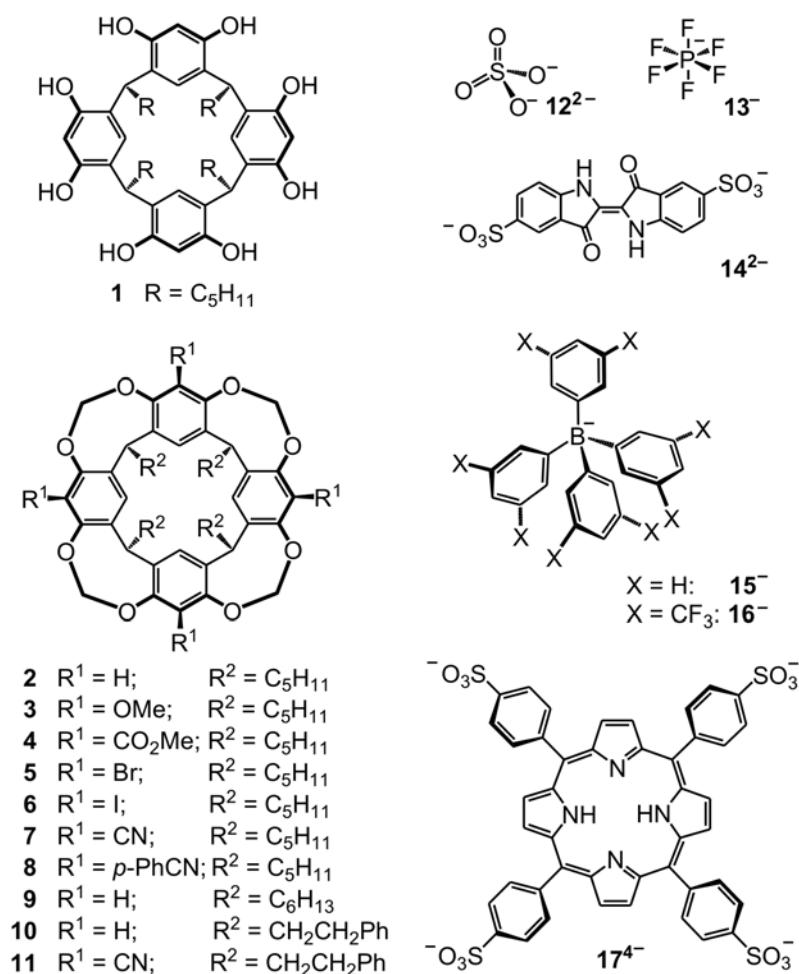
Dissociation of a generalized heterodimer bound to core Y:	$[X_1 \cdots Y \cdots X_2]^{+/-}$	fragments into	$[X_1 \cdots Y]^{+/-} + [X_2]$ or $[X_1] + [Y \cdots X_2]^{+/-}$
Example: Dissociation of proton-bound heterodimers (B_1 and B_2 are neutral bases)	$[B_1 \cdots H \cdots B_2]^+$	fragments into	$[B_1 \cdots H]^+ + [B_2]$ or $[B_1] + [H \cdots B_2]^+$

Table A2: Dissociation of heteodimeric species in Tandem-MS experiments, based on Cooks' kinetic method

A2 Anion Binding in Monotopic Methylene-bridged Cavitands – Results and Discussion ^[a] [36]

A2.1 Brief Overview

The anion-binding behavior of resorcinarene **1** and monotopic methylene-bridged cavitands **2–11**^[37] and **18**^[38] (Scheme A3; for **18**, see Scheme A4) were investigated using ESI-FTICR-MS experiments.



Scheme A3: Resorcinarene **1**, monotopic methylene-bridged cavitands **2–11** and anions **12**²⁻–**17**⁴⁻.

[a] The results of section A2 were obtained in collaboration with Holger Staats, Prof. Dr. Arne Lützen (both at Kekulé-Institut für Organische Chemie und Biochemie, Universität Bonn / University of Bonn, Germany), Kai Brandhorst, Priv.-Doz. Dr. Jörg Grunenberg (both at Institut für Organische Chemie, TU Braunschweig, Germany), Francesca Gruppi, Prof. Dr. Enrico Dalcanale (both at Dipartimento di Chimica Organica ed Industriale, Università degli Studi di Parma / University of Parma, Italy) and Prof. Dr. Kari Rissanen (Nanoscience Center, Department of Chemistry, University of Jyväskylä, Finland). H. Staats, Prof. Dr. A. Lützen, F. Gruppi, and Prof. Dr. E. Dalcanale contributed to synthesis of the resorcinarenes and cavitands studied in section A2. K. Brandhorst and Priv.-Doz. Dr. J. Grunenberg contributed to the quantum chemical calculations. Main parts of the results of section A2 were published in ref. [36].

A2.2 Small Monoanions and Dianions as Guests

When an acetone solution of $\text{Me}_4\text{N}(\mathbf{13})$ with **1** was sprayed in the positive ion mode, intense signals for cation-host complexes were observed, while **2** gave no signals for complexes with the same guest cation at all. In marked contrast, **1** did not give intense anion-host complexes $[\mathbf{13}@\mathbf{1}]^-$ in the negative mode (Figure A2a) while a surprisingly clean mass spectrum (Figure A2b) was obtained with **2**. Host-guest complex $[\mathbf{13}@\mathbf{2}]^-$ is the by far predominating complex formed in the ion source. Thus, non-bridged resorcinarene **1** forms complexes with cations, even though it could bind anions through $\text{O-H}\cdots\text{anion}$ hydrogen bonds. Methylene-bridged cavitands instead have a significant preference for suitable anions, even if cations are present which could compete for binding. Experiments with other anions such as chloride, bromide, iodide, or nitrate resulted also in the formation of anion-cavitand complexes with considerable abundance.

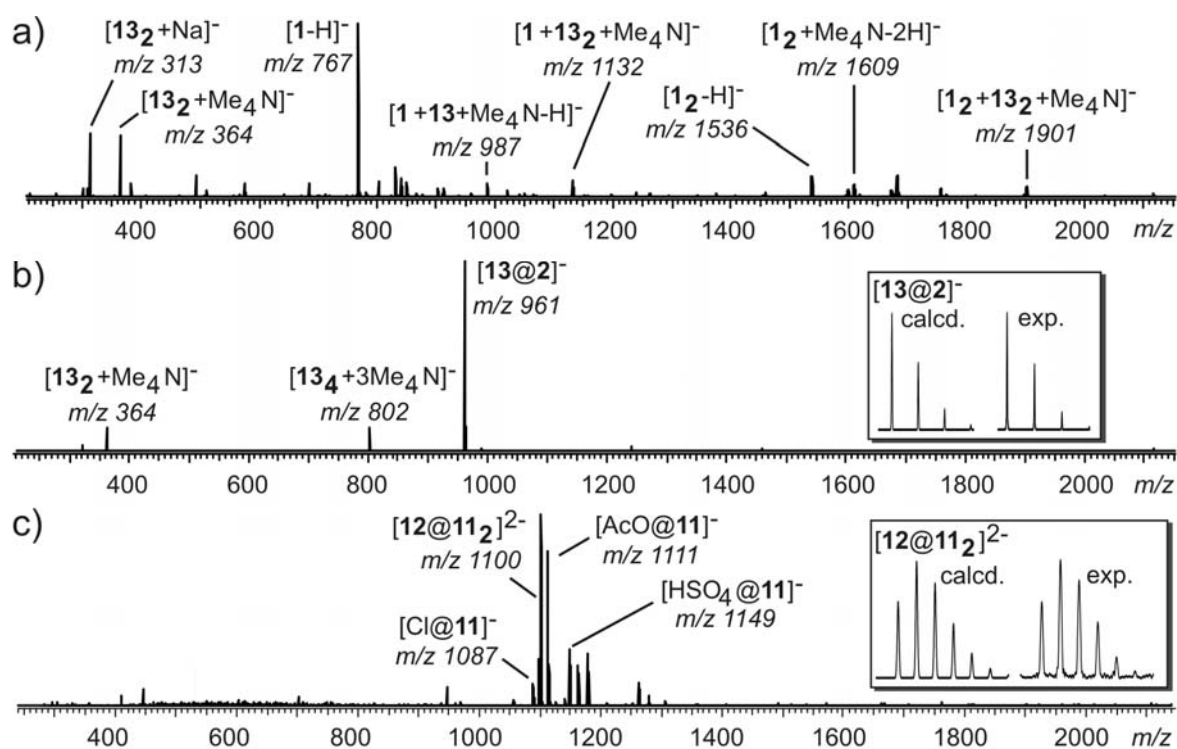
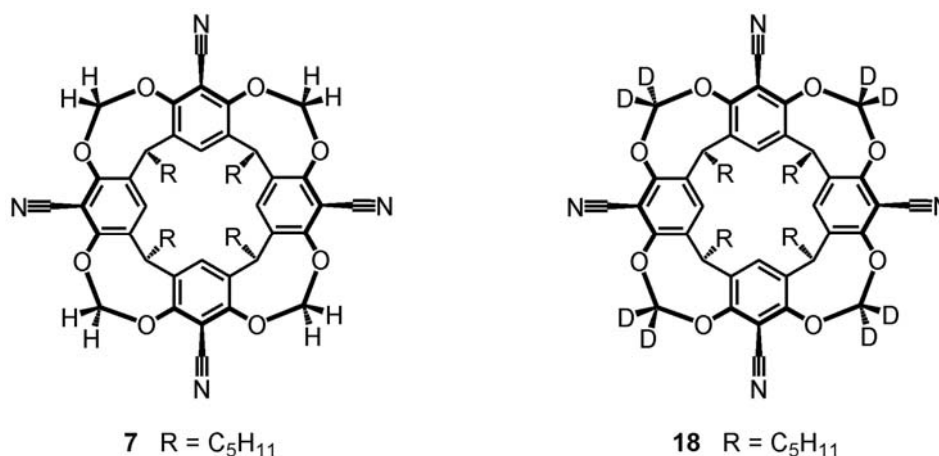


Figure A2: ESI-FTICR mass spectra (ESI) of solutions of

- a)** **1** + 1 eq. ($\text{Me}_4\text{N}(\mathbf{13})$) (200 μM in acetone); **b)** **2** + 1 eq. ($\text{Me}_4\text{N}(\mathbf{13})$) (200 μM in acetone);
c) **11** + 10 eq. ($\text{Me}_4\text{N})_2(\mathbf{12})$ (680 μM in acetone/MeOH = 40/7)

Encouraged by these results, the study was extended to sulfate as an example for a small dianion. Isolated sulfate dianions are calculated to be unstable by approximately 1.3–1.6 eV (~130–160 kJ/mol) and thus would spontaneously undergo electron autodetachment when generated under environment-free conditions.^[39] Therefore, sulfate can be observed in the gas phase only if solvated, e.g. by at least three water molecules.^[40] Despite the inherent instability of sulfate, the ESI-FTICR mass spectrum (Figure A2c) obtained from spraying an acetone/methanol solution of **11** and (Me₄N)₂(**12**) reveals the abundant formation of 2:1 complexes [**12**@**11**]₂²⁻. With cavitands **2** and **7**, formation of [**12**@**2**]₂²⁻ and [**12**@**7**]₂²⁻ was likewise observed.

A2.3 Tandem MS Experiments with Cavitand-Sulfate Complexes



Scheme A4: Cavitand **7** and its eightfold deuterated analogue **18**

To gain further insight, tandem MS experiments were conducted with mass-selected [**12**@**2**]₂²⁻, [**12**@**7**]₂²⁻, and [**12**@**18**]₂²⁻ ions (Schemes A3 and A4) (for experimental details, see section E2). In a CID experiment using argon as the collision gas, [**12**@**2**]₂²⁻ cleanly fragments through the loss of one cavitand (Figure A3, process A). The formation of 1:1 complex [**12**@**2**]₂²⁻ provides evidence for a sufficient stabilization of sulfate against electron autodetachment even through binding to only one cavitand. Even if theory^[39] overestimates the energy gain from electron autodetachment (130-160 kJ/mol) to some extent, the cavitand-anion binding energy must be higher than that and is thus substantial.

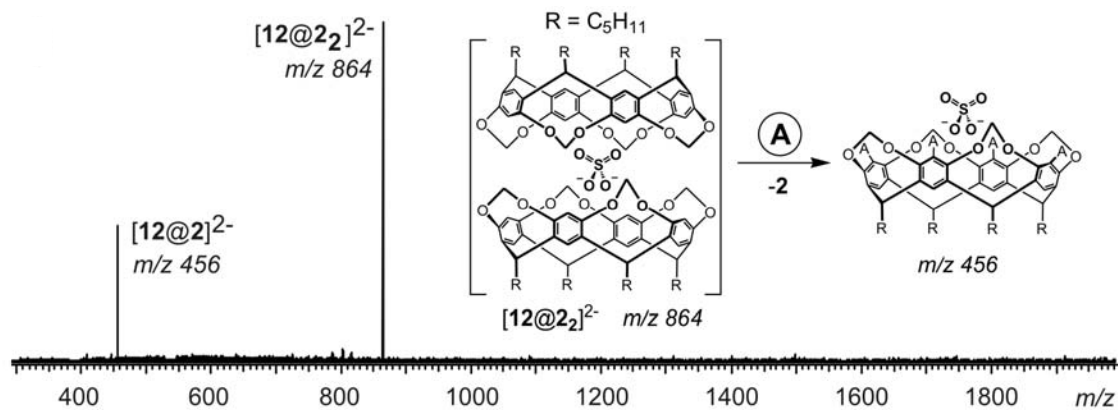


Figure A3: CID mass spectra with mass-selected [12@22]²⁻ (Spray solvent: acetone/MeOH = 40/7)

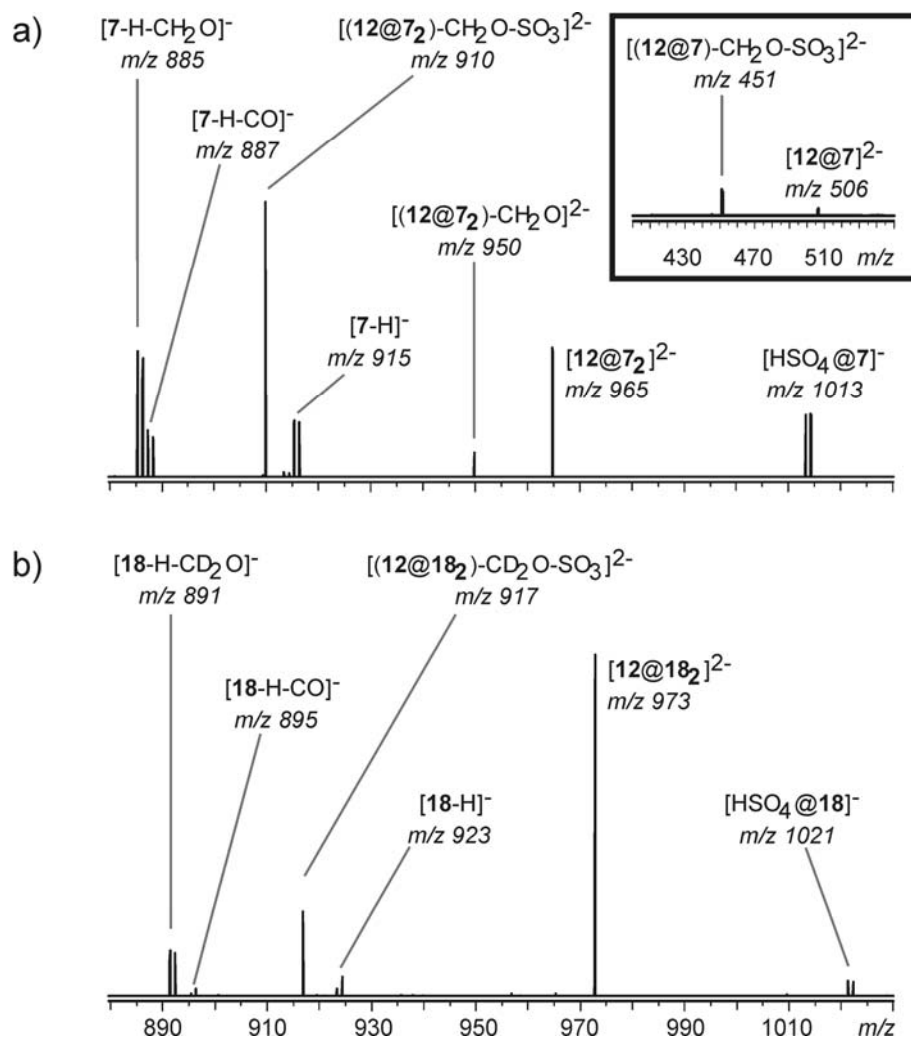
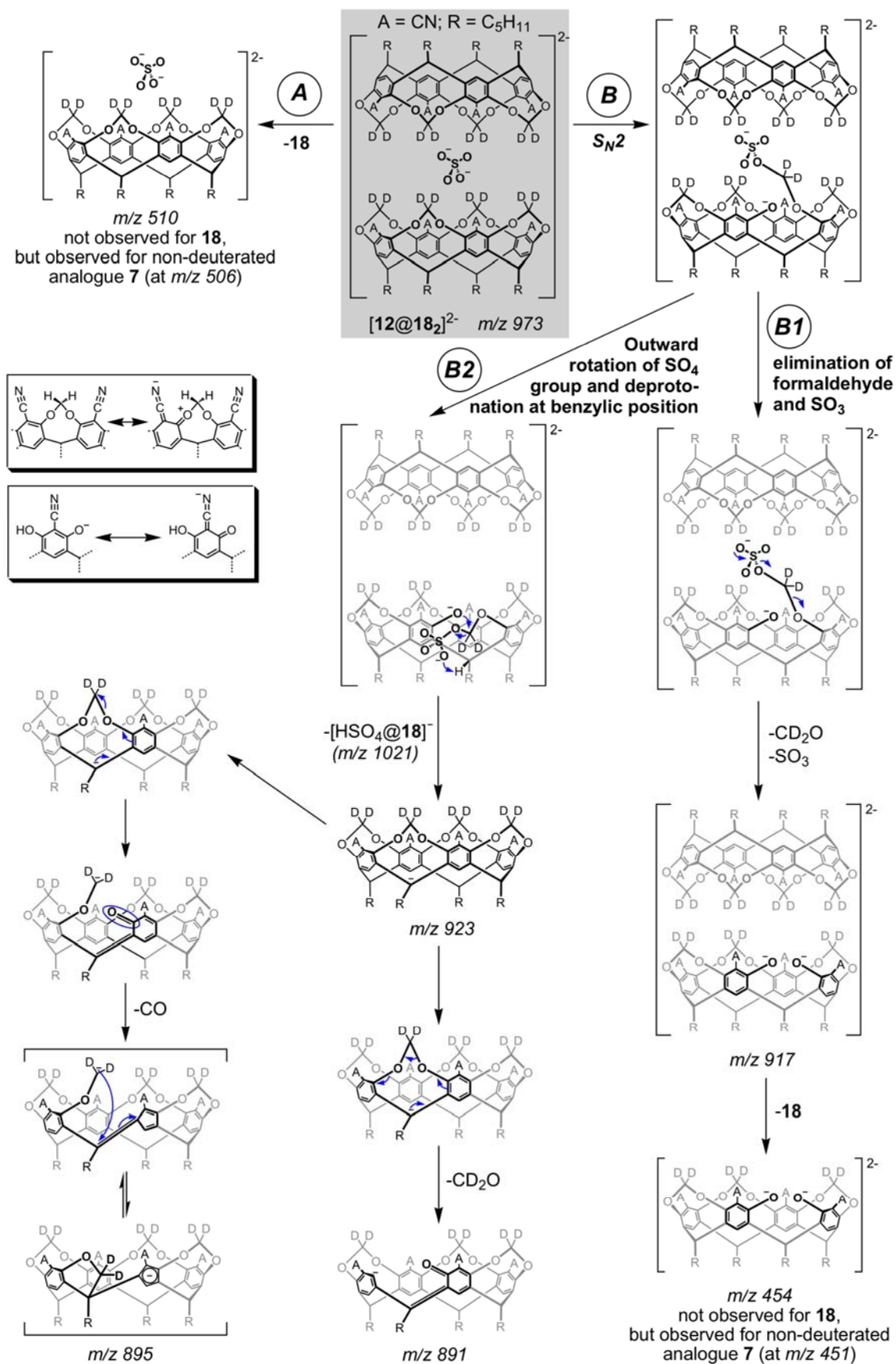


Figure A4^[41]: CID mass spectra with mass-selected (a) [12@7₂]²⁻ and (b) [12@18₂]²⁻ (Spray solvent: acetone/MeOH = 40/7); The inset on top right shows two additional fragments of [12@7₂]²⁻ which are not observed for [12@18₂]²⁻ due to insufficient signal-noise-ratio.



Scheme A5: Fragmentation pathways (**A**, **B**, **B1**, **B2**) of $[\text{12@18}_2]^{2-}$ as observed in the CID mass spectra. Due to insufficient signal-noise-ratio, some fragments are only observed for non-deuterated **7**. The insets (left) show the effect of EWGs such as nitrile on the acetal C–H polarization and the phenolate leaving group properties.

If the same experiment is performed with $[\mathbf{12@7_2}]^{2-}$ and $[\mathbf{12@18_2}]^{2-}$, which are sulfate complexes of cyano-substituted cavitand **7** and its eightfold deuterated analogue **18** (Figure A4), two main fragmentation pathways are populated (Scheme A5):

- (A) Loss of one neutral cavitand,
- (B) Nucleophilic attack of sulfate on the acetal carbon, with formation of a phenolate moiety.

In pathway **B**, two different subsequent reactions occur:

- (B1) Elimination of formaldehyde and sulfur trioxide
- (B2) Outward rotation of the covalently bound sulfate group and deprotonation at the benzylic position, with loss of $[\text{HSO}_4@\mathbf{7}]^-$ or $[\text{HSO}_4@\mathbf{18}]^-$

Pathway **B1** can result in a consecutive loss of a neutral cavitand, while the elimination of formaldehyde or of carbon monoxide follows the primary reaction in pathway **B2**. Through comparing the MS/MS spectra of $[\mathbf{12@7_2}]^{2-}$ and that of $[\mathbf{12@18_2}]^{2-}$, these fragmentation pathways can be determined with reasonable certainty.

The results are remarkable in that the loss of one neutral cavitand competes with breaking covalent interactions for $[\mathbf{12@7_2}]^{2-}$ or $[\mathbf{12@18_2}]^{2-}$, while this is not true for $[\mathbf{12@2_2}]^{2-}$. Consequently, the binding energy of **7** to sulfate must even be significantly higher than that of **2**. A rationalization for this feature is the direct conjugation of the acetal oxygen with the nitrile group (see insets in Scheme A5). An electron withdrawing substituent such as the nitrile group thus increases the positive partial charge on the acetal hydrogens and increases their interaction strengths with anions (also see section A2.5).

A2.4 Large Monoanions as Guests

Large monoanions such as tetraphenylborates $\mathbf{15}^-$ and $\mathbf{16}^-$ may provide insight into the binding mode through size selectivity experiments. Upon addition of 0.25 eq. Na(**15**) to a solution of **11**, dimeric, trimeric, and tetrameric complexes ($[\mathbf{15@11_2}]^-$, $[\mathbf{15@11_3}]^-$, $[\mathbf{15@11_4}]^-$) were observed in the mass spectrum as shown in Figure A5. Similar results were also obtained with cavitands **2**, **9**, and **10**. In marked contrast, cavitand **8** with its extended cavity, exclusively gave rise to 1:1 complex $[\mathbf{15@8}]^-$. Apparently, this is due to steric congestion caused by the longer and quite rigid side chains on the upper rim of **8** and points to anion binding in the cavitands cavity. In control experiments with the sterically more

demanding guest Na(**16**), no complex formation occurred with cavitands **9** and **11**, but free **16**⁻ was the only ion observed. Consequently, each phenyl group of tetraphenyl borate can dive into one cavitand cavity forming up to 4:1 complexes, while this binding mode is unavailable, when the size of the phenyl groups is increased by attaching two CF₃ groups in the 3- and 5-positions. Anion **16**⁻ is thus incongruent with the cavity in size and shape.

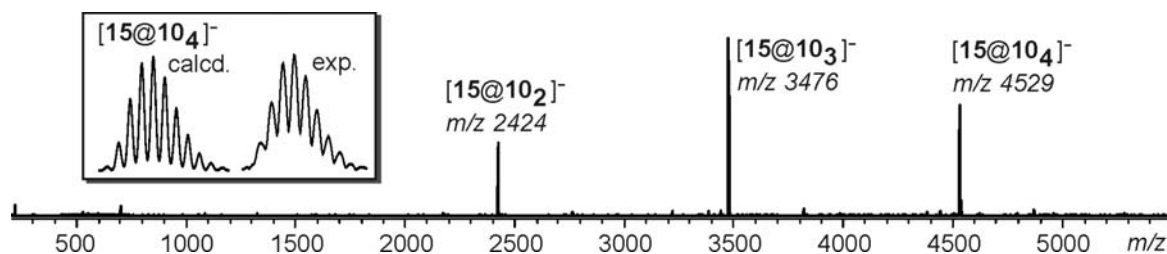


Figure A5: ESI-FTICR mass spectra (ESI) of a solution of **11** + 0.25 eq. Na(**15**) (250 μM in acetone)

A2.5 Large Di- and Tetraanions as Guests – Gas Phase Ranking for the Cavitand-Anion Interaction

In this section, larger dianions such as **14**²⁻ and tetraanionic species such as **17**⁴⁻ were studied. The mass spectrum (Figure A6a) obtained from a solution of **2** and Na₂(**14**) clearly shows the predominant presence of dimer-guest complex [**14@2**]²⁻ accompanied by the corresponding monomer-guest complex [**14@2**]²⁻. With the tetrasulfonated porphyrin **17**⁴⁻, 4:1 complexes [**17@2**]⁴⁻ of cavitand and tetraanion were observed as the base peak in the ESI mass spectrum (Figure A6b).

With guest **14**²⁻ and a 1:1 mixture of two different cavitands, it is possible to generate heterodimeric host-guest complexes. Upon addition of **14**²⁻ to a mixture of two cavitands such as **2** and **3** which have the same overall structure, but carry different substituents, heterodimeric cavitand-dianion complexes such as [**14@2₁3₁**]²⁻ were observed in the gas phase. After mass-selection of the heterodimeric complexes, CID experiments have been performed. Similar to Cooks' kinetic method, a qualitative ranking of the relative intrinsic strengths of the cavitand-sulfonate interactions can be easily determined by comparing the intensities of fragment ions such as [**14@2**]²⁻ and [**14@3**]²⁻ due to three reasons:^[42]

- (i) Fragmentation occurs exclusively through the loss of one neutral cavitand, which is not significantly influenced by the other due to the distance between the two anionic sites on the guest.

- (ii) The ratio of the above-mentioned fragment ions in the CID spectra is independent from ionization processes and spectrometer settings, because a true gas-phase experiment is performed.
- (iii) The number of vibrational degrees of freedom into which the internal energy can be distributed in either fragment is not significantly different.

Consequently, the question can be addressed how the electronic nature of electron-withdrawing or electron-donating substituents on the cavitands' upper rims influence complex stabilities. Following this protocol, CID experiments were conducted with mass-selected $[14@5_17_1]^{2-}$, $[14@5_16_1]^{2-}$, $[14@4_16_1]^{2-}$, $[14@2_14_1]^{2-}$, and $[14@2_13_1]^{2-}$ ions (Figure A7a-e). These CID spectra clearly show that the strengths of cavitand-sulfonate interactions increase as follows: $3 \leq 2 \ll 4 \ll 5 \approx 6 \ll 7$. In terms of the substituents' electronic nature, the order is: $\text{OMe} \leq \text{H} \ll \text{CO}_2\text{Me} \ll \text{Br} \approx \text{I} \ll \text{CN}$. The experimentally obtained tendency is in good agreement with the electron-withdrawing or donating ability of the aromatic substituents. The only exception is the CO_2Me group which apparently affects the complexation through its conformationally flexible methoxy arms, extending to the vicinity of the binding sites. Nevertheless, this effect is not too prominent since **4** still binds sulfonate far better than **2** and **3**.

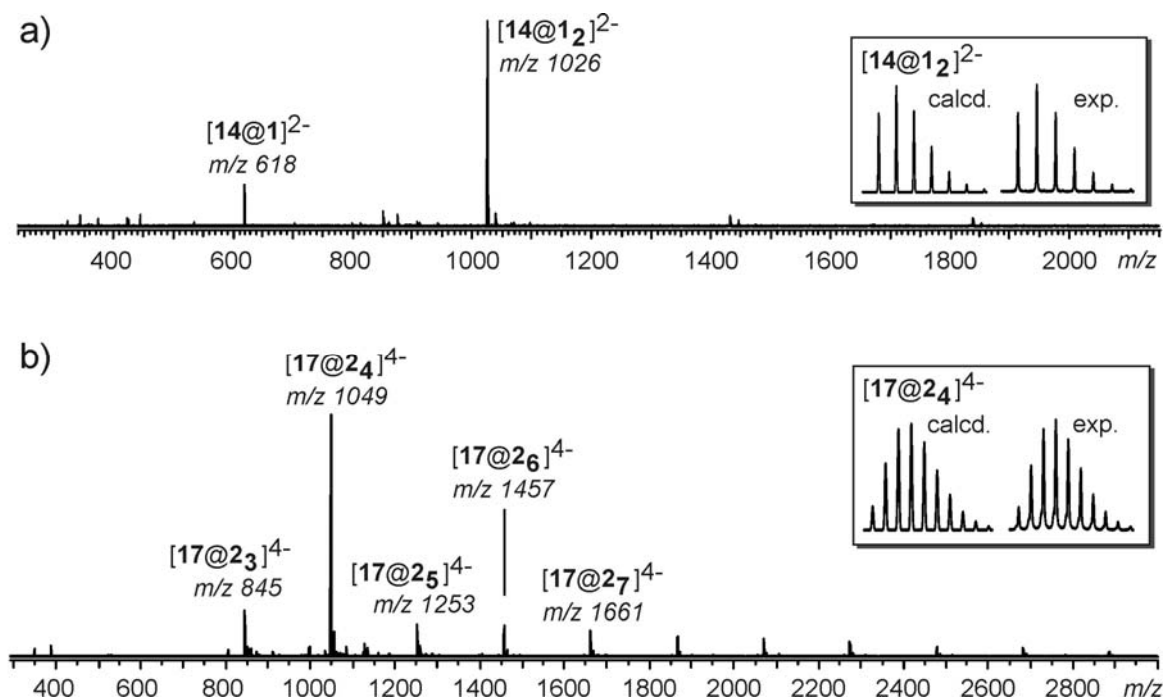


Figure A6: ESI-FTICR mass spectra (ESI⁻) of solutions of
a) **2** + 0.5 eq. $\text{Na}_2(\mathbf{14})$ (780 μM in acetone/MeOH = 40/1);
b) **2** + 1 eq. $\text{Na}_4(\mathbf{17})$ (200 μM in acetone/MeOH = 40/1)

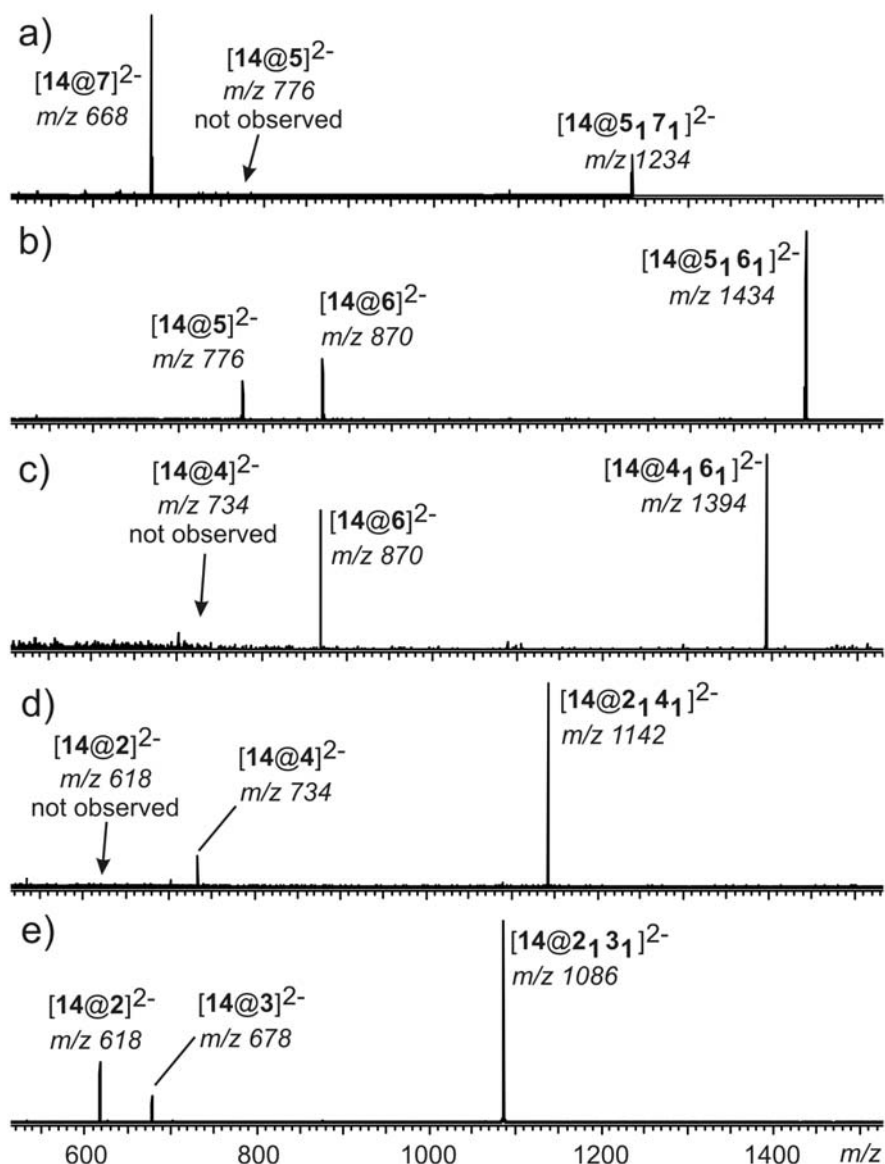


Figure A7: CID mass spectra with mass-selected, doubly charged heterodimeric cavitanD-indigo carmine complexes: **a)** $[14@5_17_1]^{2-}$, **b)** $[14@5_16_1]^{2-}$, **c)** $[14@4_16_1]^{2-}$, **d)** $[14@2_14_1]^{2-}$, **e)** $[14@2_13_1]^{2-}$. (Spray solvent: acetone/MeOH = 40/1)

A2.6 Preliminary Conclusions from the MS Experiments

The experiments conducted in the sections A2.2 to A2.5 provide evidence for a cavitanD-anion interaction mediated by C–H•••anion hydrogen bonds that involve the acetal protons pointing into the cavitanD bowl. The following reasons support this conclusion:

- (i) Anion- π interactions^[43] do not play a significant role, since otherwise, **1** would be expected to be a similarly good host for anions.

- (ii) The substantial stability of the anion-cavitand complexes, particularly that of $[\mathbf{12@11_2}]^{2-}$, indicates that complexation is mediated by multiple interactions and thus likely occurs inside the cavitand bowl.
- (iii) Cavitand **8** has the same alkyl feet as **2–7**, but reveals a significantly different complexation behavior with $\mathbf{14}^{2-}$ and $\mathbf{15}^-$. This excludes binding of the anions at the bottom rim, since then no such effects would be expected to occur. Steric effects due to the longer cyanophenyl substituents can however easily be understood, when anion binding inside the cavity is assumed.
- (iv) The fragmentation of $[\mathbf{12@7_2}]^{2-}$ includes the elimination of formaldehyde from the acetal position suggesting sulfate binding to occur close to the methylene inner protons.
- (v) Substituent effects revealed by the CID spectra of heterodimeric host-guest complexes with $\mathbf{14}^{2-}$ provide evidence for the binding sites to be located in the “influence region” of substituents at the upper rim, which in particular applies to the acetal protons which carry a higher positive partial charge, if electron-withdrawing substituents are present.

A2.7 Quantum Chemical Calculations

In order to get a more detailed insight into the thermodynamic forces driving anion binding to the cavitands through C–H•••anion interactions, a series of quantum chemical calculations were performed on a C_{4v} symmetric model system for $[\mathbf{13@2}]^-$ where the C_5H_{11} moieties were substituted simply by H, in the following named $[\mathbf{13@2}']^-$ (Figure A8). Geometry optimizations and energy second derivative calculations were done with the hybrid density functional B3LYP^[44] with a split valence double zeta basis set augmented with one set of polarization functions and diffuse functions on all atoms (6-31++G(d,p)) as implemented in Gaussian03.^[45] Adopting the rigid-rotor harmonic-oscillator approximation, the free energy of association at room temperature (ΔG°_{298}) for $[\mathbf{13@2}']^-$ is calculated to be -24.2 kJ/mol, which is quite substantial in view of 1) the assumed weak individual enthalpic contributions and 2) the entropic prize one has to pay in any associative mechanism. In a second step, generalized compliance constants^[46] were calculated in order to quantify the individual contributions and, if possible, to discriminate between C–H•••anion and possible anion- π interactions. To the best of our knowledge this is the first direct quantification of this type of weak, non-covalent

C–H⋯ion interaction. The anion- π contacts measured as displacements of the internal coordinates between the fluorine atoms of the PF_6^- anion and aromatic carbons in the resorcinarenes are very soft with compliance constants between 30 and 40 $\text{\AA}/\text{mdyne}$. Note, that a higher compliance constant is connected with a softer interaction. They can thus indeed be excluded as the enthalpic driving force during the association. On the other hand, the compliance constant for the $2'\text{C-H}\cdots\text{F-PF}_5^-$ interactions point to a hydrogen bond in the range between a strong N–H⋯O (~ 5 $\text{\AA}/\text{mdyne}$) and a C–H⋯O hydrogen bond (~ 20 $\text{\AA}/\text{mdyne}$). Its strength measured by generalized compliance constants is computed to be 15.2 $\text{\AA}/\text{mdyne}$. The four individual C–H⋯F contacts in $[\mathbf{13@2}']^-$, which are intensified through the negative charge on the guest molecule are therefore mainly responsible for the adduct stability.

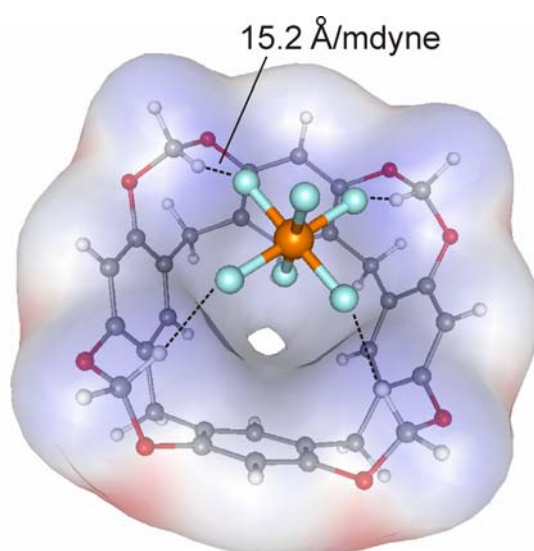
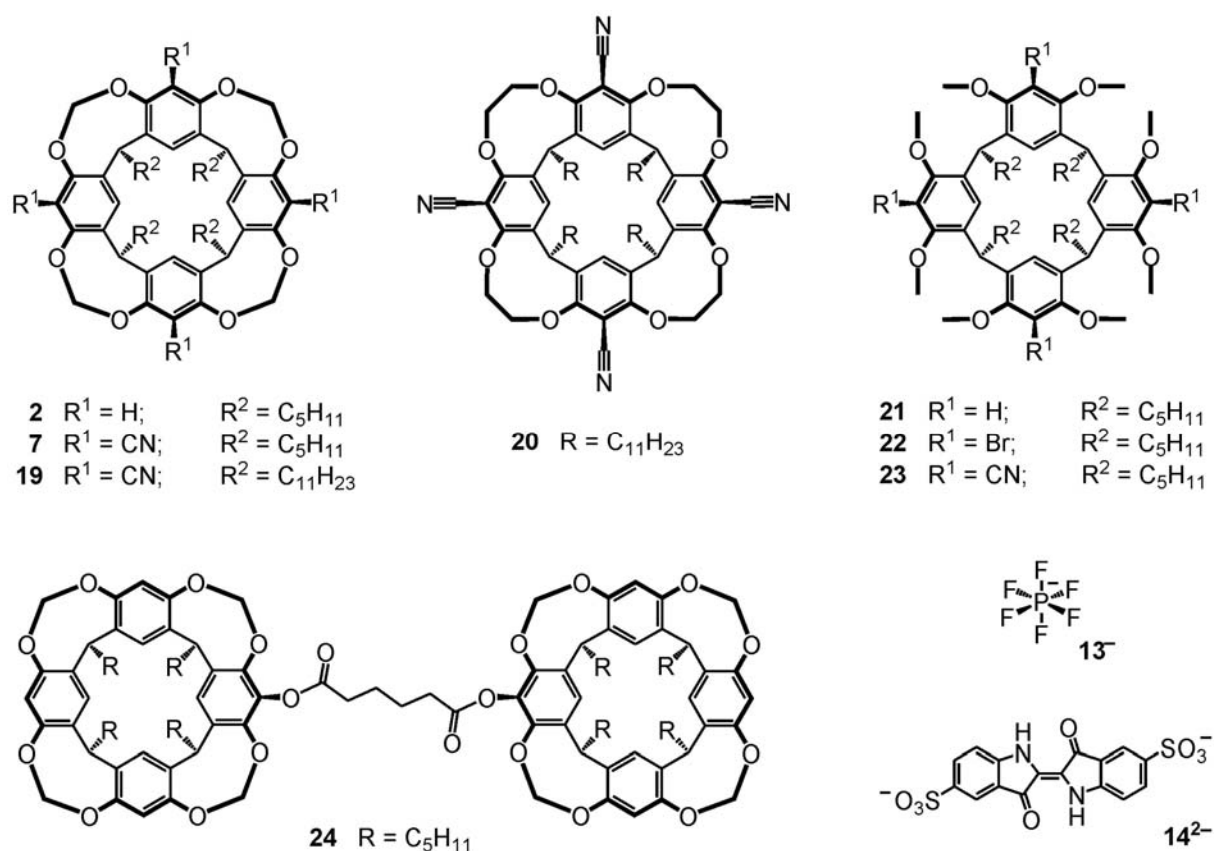


Figure A8. The B3LYP/6-31++G(d,p) optimized structure of the model complex $[\mathbf{13@2}']^-$ mapped with the electrostatic potential on the host surface. C–H⋯F hydrogen bonds are depicted

A3 Anion Binding in CavitanDs Other Than Monotopic Methylene-bridged Analogues – Results and Discussion ^[b]

A3.1 Brief Overview

After the anion-binding properties of monotopic methylene-bridged cavitanDs were investigated (see section A2), we have widened the scope of this ESI-FTICR-MS study to include ethylene-bridged cavitant **20**, non-bridged cavitant **21–23**, and ditopic methylene-bridged cavitant **24** (see Scheme A6).



Scheme A6: CavitanDs **7**, **19–24** and anions **13⁻** and **14²⁻** used in this study.

[b] The results of section A3 were obtained in collaboration with Holger Staats, Prof. Dr. Arne Lützen (both at Kekulé-Institut für Organische Chemie und Biochemie, Universität Bonn / University of Bonn, Germany), Prof. Dr. Enrico Dalcanale and co-workers of his group (at Dipartimento di Chimica Organica ed Industriale, Università degli Studi di Parma / University of Parma, Italy). H. Staats, Prof. Dr. A. Lützen, Prof. Dr. E. Dalcanale and co-workers of his group contributed to synthesis of the resorcinarenes and cavitanDs studied in section A3.

A3.2 Ethylene-bridged Cavitand

Compared with its methylene-bridged analogue **19**, ethylene-bridged cyano-substituted cavitand **20** have four additional methylene groups on the rim of the cavitand bowl. When an acetone solution of **20** and Bu₄NCl or Me₄N(**13**) was sprayed, clean mass spectra with [Cl@**20**]⁻ or [13@**20**]⁻ as base peaks were obtained (Figure A9), demonstrating **20** to be also suitable for anion binding.

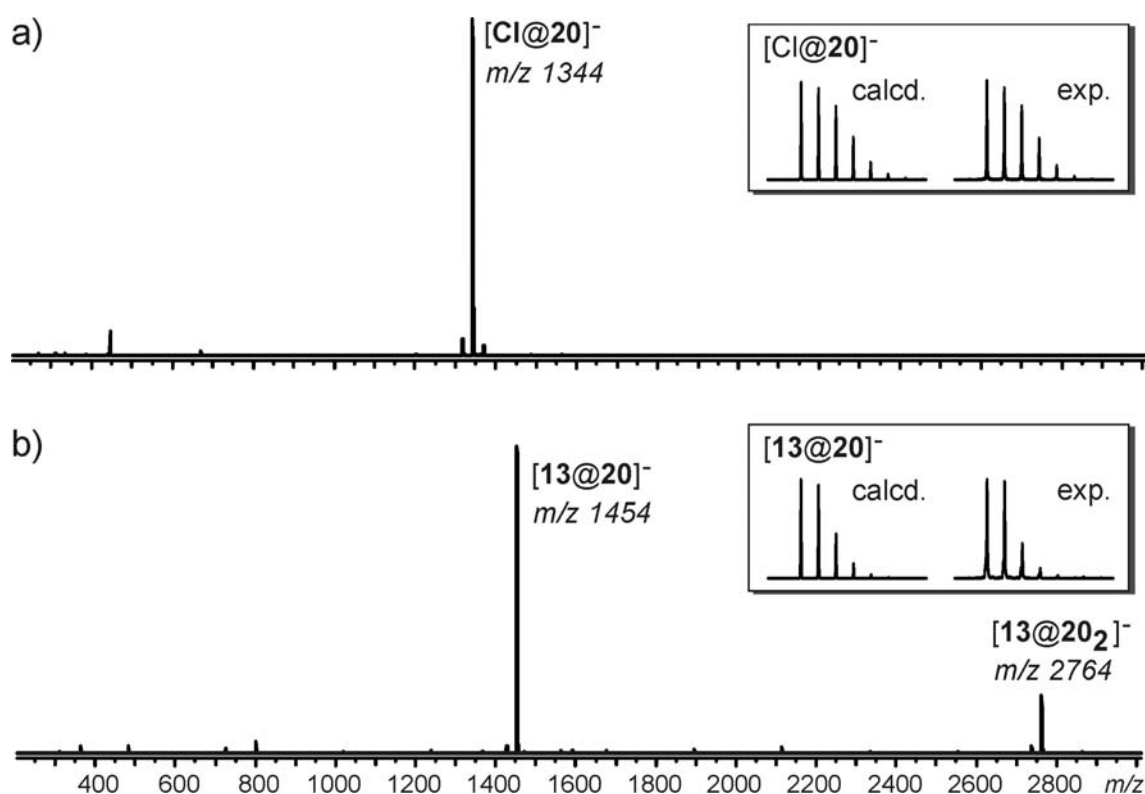


Figure A9: ESI-FTICR mass spectra (ESI⁻) of solutions of **a)** **20** + 1 eq. Bu₄NCl (200 μM in acetone);
b) **20** + 1 eq. (Me₄N)(**13**) (200 μM in acetone).

The question awaiting an answer is the one about the binding mode in the anion complexes of **20**. According to MM2 level calculations done with the CAChe program^[47] (see Figure A10), there is at least one example out of numerous possible low-energy conformations where four ethylenedioxy protons of **20'** point into the cavitand bowl. In this conformation, the geometry of the above-mentioned four protons resembles that of the four acetal protons in **19'** (compared with **19/20**, the alkyl feet C₁₁H₂₃ were replaced by H in **19'/20'**). Therefore we can assume that anion binding occurs through some of these four ethylenedioxy protons. Due to their higher conformational flexibility and lower electron-

deficiency, ethylenedioxy protons of **20** are expected to be less capable of binding anions than acetal protons of **19**, which means that **19** should be a better anion binding host than **20**.

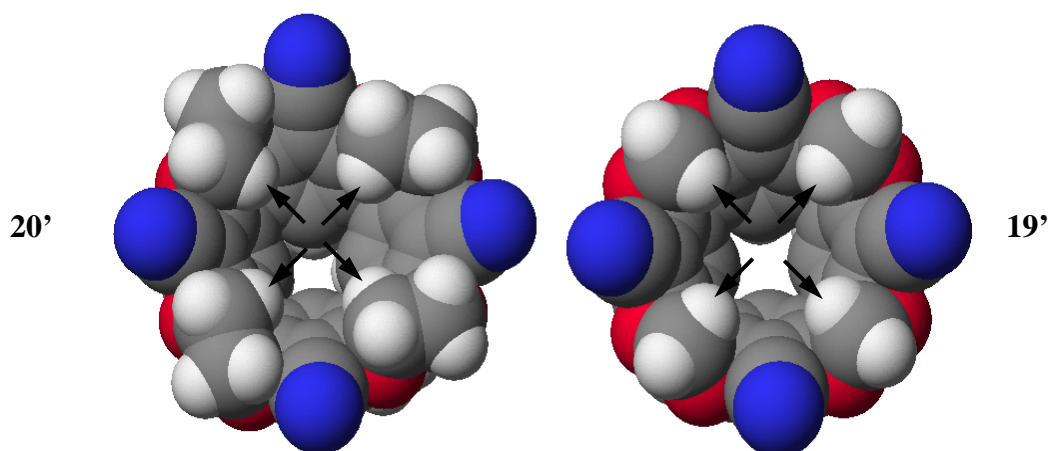


Figure A10: Space-filling representation of one example out of many possible low-energy conformations of **20'**/**19'** calculated at the MM2 level (view from top of the cavitanDs); The black arrows show the protons pointing into the cavitanD bowl; Color code: C gray, H white, N blue, O red;

To verify the assumption of **20** being a weaker anion binding host, a variant of Cooks' kinetic method was utilized^[42] (see also section A2.5). After an acetone solution containing a 1:1:1 mixture of **14**²⁻, **19** and **20** had been sprayed, heterodimeric cavitanD-dianion complexes $[\mathbf{14@19_120_1}]^{2-}$ were observed in the mass spectrum and mass-selected for the subsequent CID experiment. In the CID spectrum (Figure A11), the only fragment formed from the parent ion $[\mathbf{14@19_120_1}]^{2-}$ is $[\mathbf{14@19}]^{2-}$, showing that this cavitanD-anion interaction is indeed stronger for methylene-bridged **19** than for ethylene-bridged **20**.

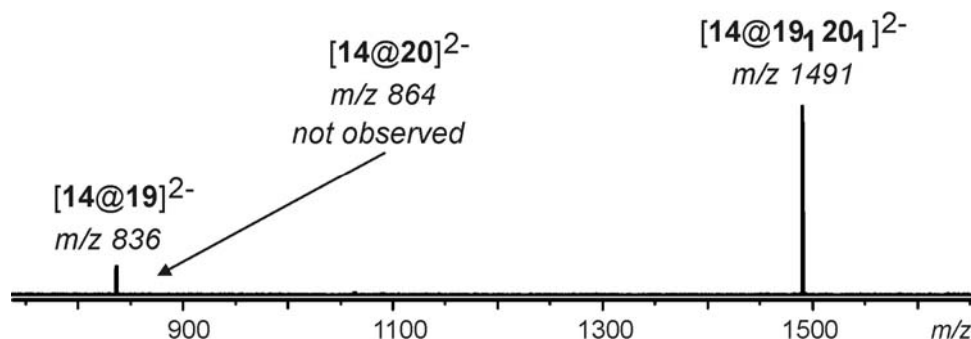


Figure A11: CID mass spectrum with mass-selected, doubly charged heterodimeric cavitanD-indigo carmine complex $[\mathbf{14@19_120_1}]^{2-}$ (Spray solvent: acetone/MeOH = 40/1)

A3.3 Non-bridged Cavitands

Compounds **21–23** are completely *O*-methyl protected resorcinarenes and can be regarded as non-bridged cavitands. When an acetone solution of cyano-substituted **23** is sprayed together with Bu_4NCl , an intense signal of the complex $[\text{Cl}@23]^-$ was observed in the mass spectrum, while the demethylated species $[23-\text{CH}_3]^-$ is also formed with sufficient abundance. In contrast to that, a clean mass spectrum showing only the signal for $[13@23]^-$ is obtained when spraying the acetone solution of **23** and $\text{Me}_4\text{N}(13)$ (Figure A12). This can be rationalized by the fact that chloride is a nucleophilic anion and can attack the methoxy carbon, liberating $[23-\text{CH}_3]^-$ and methyl chloride, whereas the non-nucleophilic hexafluorophosphate 13^- is not capable of undergoing such a reaction. Therefore, **23** is only an appropriate anion binding host for non-nucleophilic anions.

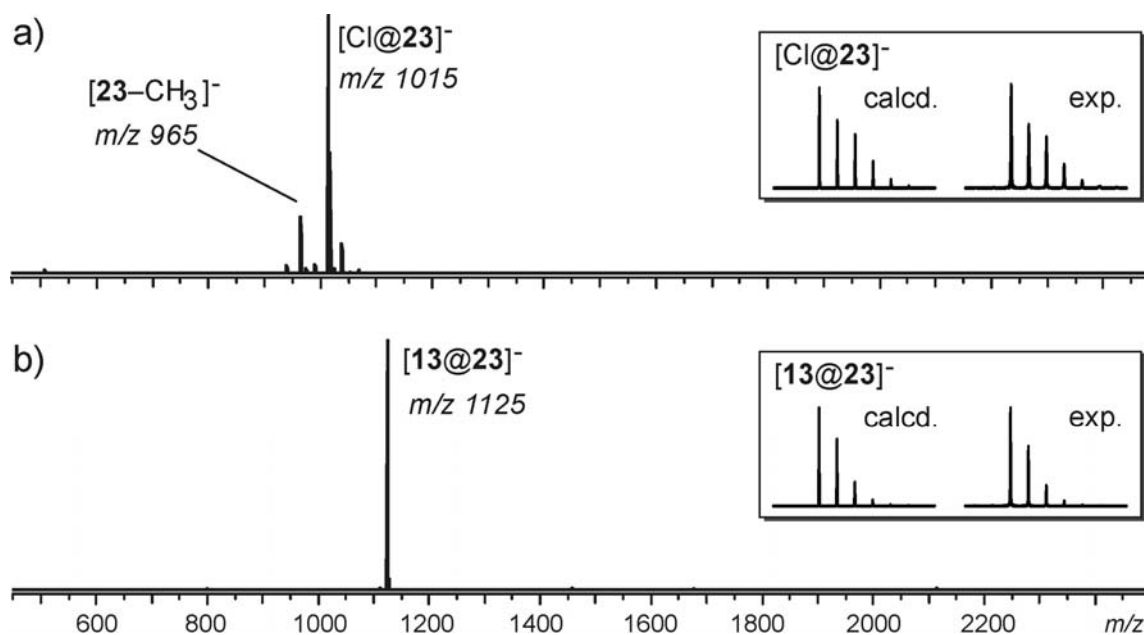


Figure A12: ESI-FTICR mass spectra (ESI⁻) of solutions of **a)** **23** + 1 eq. Bu_4NCl (200 μM in acetone); **b)** **23** + 1 eq. $(\text{Me}_4\text{N})(13)$ (200 μM in acetone).

Since we have observed from mass spectra that anion binding in unsubstituted and bromo-substituted resorcinarenes **21/22** is far weaker than in cyano-substituted **23**, we can assume from the substituent effect that anion binding occurs through some of the methoxy protons pointing into the cavitand bowl (see also (v) in section A2.6). This is very similar to the interaction between anions and acetal or ethylenedioxy protons in methylene- or ethylene-bridged cavitands. To assess the strength of this interaction in non-bridged cavitands, 14^{2-} was

added to a mixture of non-bridged **23** and methylene-bridged analogue **7**, generating heterodimeric cavitand-dianion complex $[\mathbf{14@7_123_1}]^{2-}$. These ions are mass-selected and subjected to a CID experiment which can be considered as a variant of Cooks' kinetic method^[42] (see also section A2.5). In the CID mass spectrum (Figure A13), the only fragment formed from the parent ion $[\mathbf{14@7_123_1}]^{2-}$ is $[\mathbf{14@7}]^{2-}$, indicating that methylene-bridged **7** is much more strongly bound to the indigo carmine anion than its non-bridged analogue **23**. This result was also expected because acetal protons are characterized by greater electron deficiency and less conformational flexibility than methoxy protons.

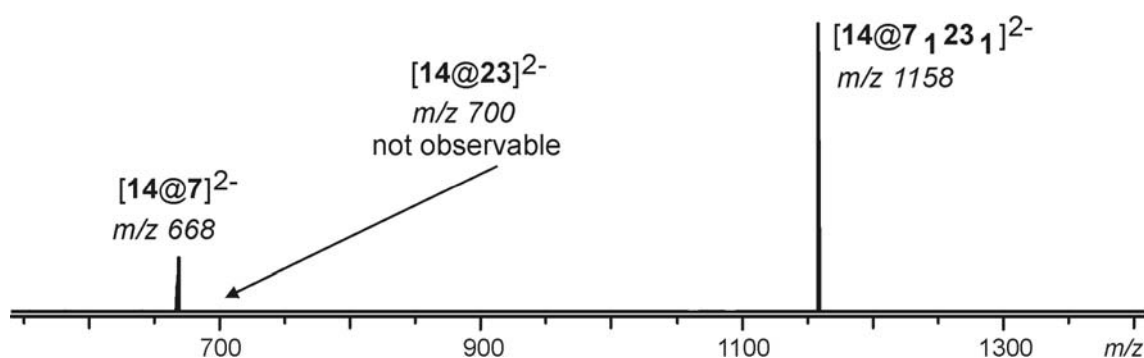


Figure A13: CID mass spectrum with mass-selected, doubly charged heterodimeric cavitand-indigo carmine complex $[\mathbf{14@7_123_1}]^{2-}$ (Spray solvent: acetone/MeOH = 40/1)

A3.4 Ditopic Methylene-bridged Cavitand

The ditopic methylene-bridged cavitand **24** was obtained after reacting two monohydroxy-cavitands with adipoyl dichloride. **24** was expected to be capable of binding two anions, each in one of its two cavitand bowls. However, when an acetone solution of the 1:1:1 mixture of **24**, Bu_4NCl and Bu_4NBr was sprayed, doubly charged species such as $[\text{Cl}_2@\mathbf{24}]^{2-}$, $[\text{Br}_1\text{Cl}_1@\mathbf{24}]^{2-}$ and $[\text{Br}_2@\mathbf{24}]^{2-}$ were observed with very low intensities in the mass spectrum, while singly charged 1:1 complexes such as $[\text{Cl}@\mathbf{24}]^-$ and $[\text{Br}@\mathbf{24}]^-$ were the by far dominating species (Figure A14). Furthermore, the doubly charged ions were only observable at rather soft ESI conditions, such as a capexit value of -60 V. Using $[\text{Br}_1\text{Cl}_1@\mathbf{24}]^{2-}$, Cooks' kinetic method^[42] can also be applied, but – in contrast to the heterodimeric cavitand-indigo carmine complexes (see sections A2.5, A3.2 and A3.3) – the ditopic cavitand host is here the central part on which two different anions are bound. After heterodimeric ions $[\text{Br}_1\text{Cl}_1@\mathbf{24}]^{2-}$ had been mass-selected, a CID experiment was performed, yielding $[\text{Cl}@\mathbf{24}]^-$ as the only

fragment (Figure A15). This result shows that chloride is much more strongly bound to **24** than bromide.

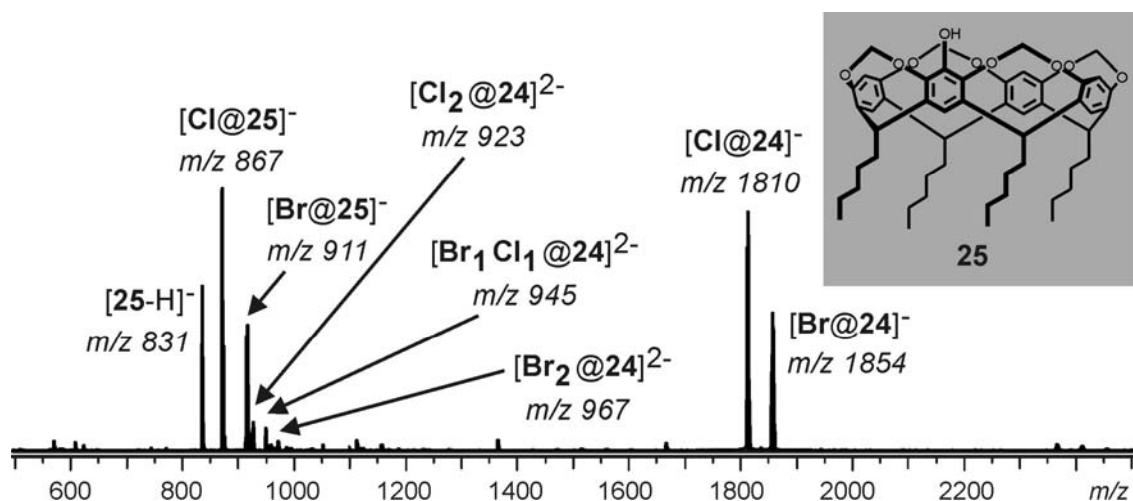


Figure A14: ESI-FTICR mass spectra (ESI⁺) of a solution of **24** + 1 eq. Bu₄NBr + 1 eq. Bu₄NCl (200 μM in acetone); The inset (top right) shows the chemical structure of **25** which is also observable in the spectrum, probably as an impurity.

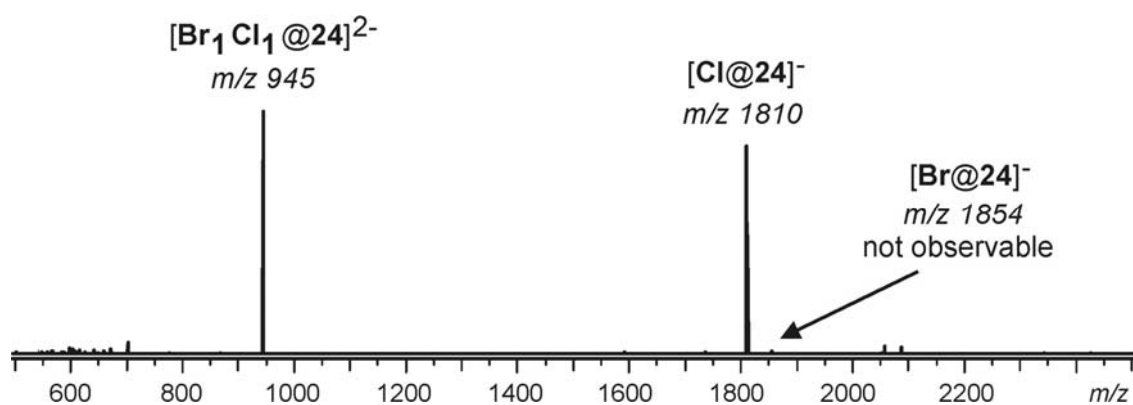


Figure A15: CID mass spectrum with mass-selected, doubly charged heterodimeric "dicavitand"-anion complex [Br₁Cl₁@24]²⁻ (Spray solvent: acetone)

When **24** and the combination of two other anions (for example Cl⁻&I⁻, Br⁻&I⁻, Cl⁻&NO₃⁻ or Cl⁻&PF₆⁻) were used and the corresponding acetone solution was sprayed, no signals for doubly charged ions were observed in the mass spectra apart from [Cl₂@24]²⁻ and [Br₂@24]²⁻, while the corresponding singly charged 1:1 complexes appeared as base peaks.

The instability of doubly charged complexes containing **24** and two discrete anions is probably due to the fact that – in the gas phase – charge repulsion between the two anionic species is larger than the stabilization through binding to the cavitand. Even if complexes such as $[\text{Cl}_1\text{I}_1@24]^{2-}$ were formed in an intermediate stage, it might be more favourable for the whole complex to strip off one anion, generating the singly charged 1:1 complex. Hence, the original idea of comparing the affinity of different anions towards the cavitand host – that is a kind of “gas-phase ranking for anions” – cannot be put into practice using ditopic cavitand **24**.

Gaining a deeper insight into the anion binding properties of **24**, we decided to investigate whether some kind of divalent interaction will be possible with a dianion such as 14^{2-} serving as the guest. ESI-FTICR mass spectra of *solution a* and *solution b* were recorded, but were completely different from what we would expect in case of a divalent interaction between 14^{2-} and **24** (see Table A3). This means that such a divalent host-guest interaction is unlikely to occur. Furthermore, larger assemblies such as 2:2 or 3:3 complexes of 14^{2-} and **24** were also not observed.

	Composition	Mass spectrum expected if divalent interaction prevails	Mass spectrum recorded (with acetone as spray solvent)
Solution a	2 eq. 2 1 eq. 24 1 eq. $\text{Na}_2(\mathbf{14})$	signal for $[\mathbf{14}@24]^{2-}$ should be much more intense than that for $[\mathbf{14}@2_2]^{2-}$	signal for $[\mathbf{14}@24]^{2-}$ is only slightly more intense than that for $[\mathbf{14}@2_2]^{2-}$
Solution b	2 eq. 2 1 eq. 24 2 eq. $\text{Me}_4\text{N}(\mathbf{13})$ 1 eq. $\text{Na}_2(\mathbf{14})$	$[\mathbf{13}@2]^-$ and $[\mathbf{14}@24]^{2-}$ should be the predominant species	$[\mathbf{13}@2]^-$ and $[\mathbf{13}@24]^{2-}$ are the predominant species, the signal for $[\mathbf{14}@24]^{2-}$ only has a very low intensity

Table A3: Testing the divalent interaction – Overview on the mass spectra which were expected and which were actually recorded for the respective solutions

A4 Final Conclusions and Outlook

Mass spectrometric experiments together with theory demonstrate suitably positioned C–H bonds to be able to complex anions, especially if they are polarized by neighboring electronegative heteroatoms. The easy-to-access methylene-bridged resorcinarene cavitands provide exactly the right geometric arrangement of such groups to support anion binding through multiple interactions with up to four converging C–H groups. Particularly remarkable is the fact that already one methylene-bridged cavitand is able to solvate a sulfate dianion well enough to prevent electron autodetachment. It is this experiment which shows that the interaction strength between cavitand host and guest anion can amount to substantial values.^[36]

Not only methylene-bridged cavitands, but also their ethylene-bridged analogues and non-bridged *O*-methyl protected resorcinarenes are capable of binding anions, but with binding strengths being far weaker compared with methylene-bridged cavitands. The reason for that lies in the lower electron deficiency and higher conformational flexibility of the relevant ethylenedioxy and methoxy protons.

In addition, one example for a ditopic methylene-bridged cavitand was also investigated. Apart from one exception, this cavitand was not able to bind two anions simultaneously in the gas phase, probably due to destabilization by charge repulsion. If a large dianion was used as guest, no divalent interaction could be observed.

In conclusion, this study provides new insight into the nature and importance of C–H•••anion interactions. This mode of H-bonding, i.e. hydrogen bonds between an anion and a non-aromatic C–H bond, is very rare and not well studied so far. To the best of our knowledge, the phenomenon that neutral cavitands complex different anions exclusively through this type of weak intermolecular interaction has not been described previously.^[36]

In the future, the study on cavitand-anion interaction, which is now limited to the gas phase, will be extended to the solution and solid state. Although this is a weak intermolecular interaction which could be quite sensitive to solvent effects, there might be appropriate conditions or NMR techniques where it becomes observable in the solution state. Since many weak intermolecular interactions – including anion- π interactions^[48] – have been detected in crystals, future efforts will be directed to obtaining suitable crystals which might prove that this rare C–H•••anion interaction also exists in the solid state.

B. Self-Assembled Metallosupramolecular Helicates: An MS Study

B1 Purpose of the Study and Introduction

B1.1 Helicates in General

More than twenty years ago, Lehn and co-workers introduced the term “helicite” for describing a metal-containing host-guest complex with helical structure.^[49] Since then, following the rise of modern supramolecular chemistry, helicates have attracted continually growing research interest in the related fields. Although the resemblance between helicates and helices in biological systems, e.g. DNA double helix or α -helix in protein structures, is too limited to draw useful conclusions for biomimetic applications, helicates can still serve as an important, all-round system for exploring fundamental supramolecular phenomena such as molecular recognition, self-assembly, self-organization and self-sorting.^[50]

Usually, a helicate is a discrete, i.e. non-polymeric supermolecule and consists of two or more organic ligand strands which are coordinated to two or more metal centers in a way that the metal centers are located on the helical axis.^[50] Helicates are commonly generated in a self-assembly process^[51] in which simple subcomponents spontaneously associate to complex and well-defined supramolecular aggregates by means of non-covalent interactions, while memorizing the intrinsic information of these subcomponents (for example coordination geometries, electronic properties).

Helicates can be classified into the following categories (see Table B1 on next page):

B. Metallosupramolecular Helicates

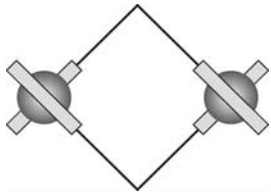
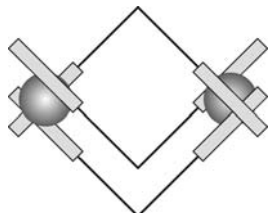
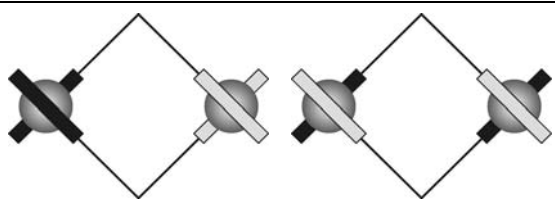
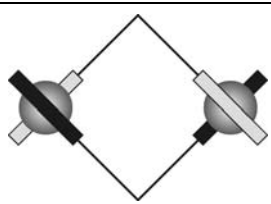
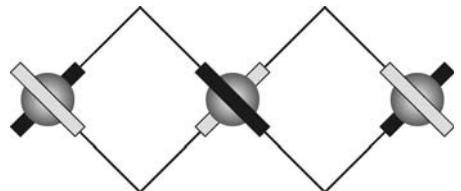
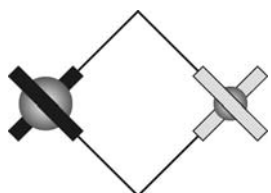
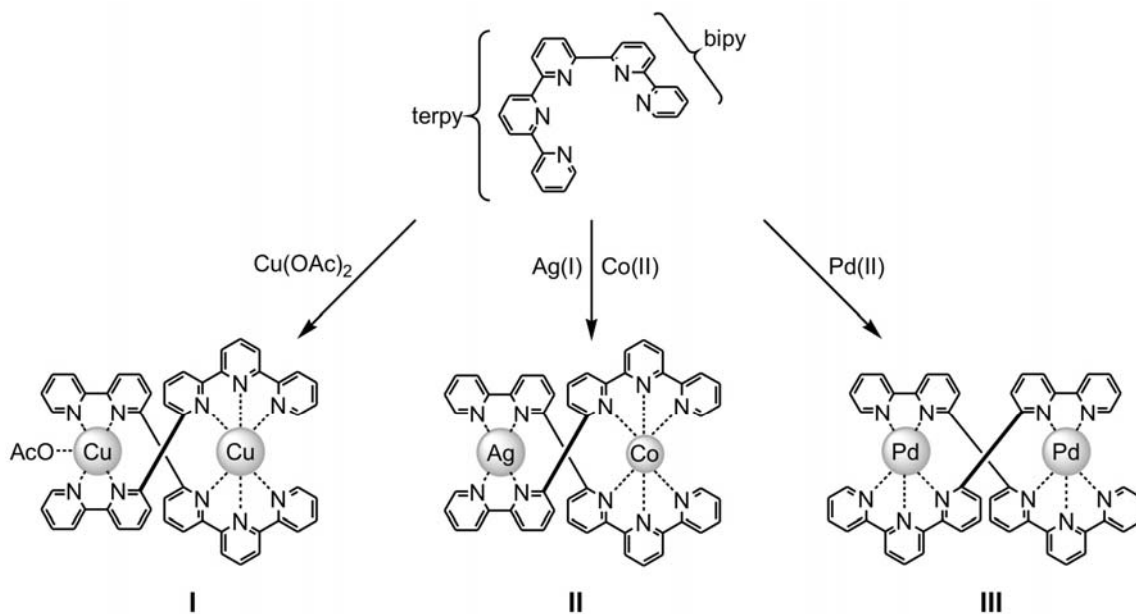
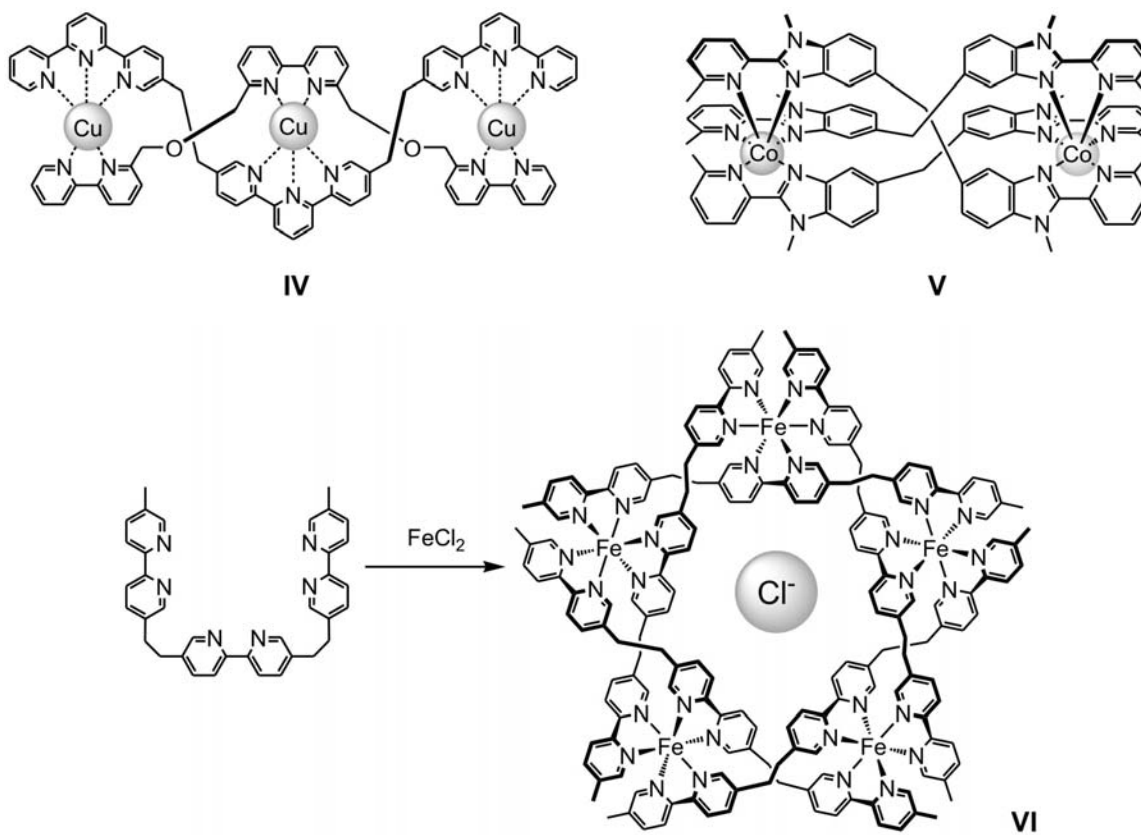
	Criteria for classification	Categories (exemplary)	Cartoon illustrations of the structures	Examples
STRANDS	Number of strands	Double-Stranded		I–IV
		Triple-Stranded		V
	“Topicity” of strands	Homotopic	<i>see all structures listed above</i>	IV/V/VI
		Heterotopic	 (head-to-head) (head-to-tail)	I–III
	Sameness of strands ^[52]	Homostranded (homoleptic)	<i>see all structures listed above</i>	I–III/V/VI
		Heterostranded (heteroleptic)		IV
METAL CENTERS	Number of metal centers	Dinuclear	<i>see all structures listed above</i>	I–III/V
		Trinuclear		IV
	Sameness of metal centers	Homonuclear	<i>see all structures listed above</i>	I/III/IV/V/VI
		Heteronuclear		II

Table B1: Classification of helicates^[50]; Legend for the cartoons: Gray ball represents the metal center, black or light gray sticks represent the binding site of the ligand, black line represents the spacer moiety within the ligand (in the “examples” column, numbers refer to Scheme B1 and B2)



Scheme B1: Examples of double-homostranded, heterotopic helicates **I**^[53] (head-to-head, homodinuclear), **II**^[54] (head-to-head, heterodinuclear) and **III**^[55] (head-to-tail, homodinuclear), self-assembled from a ligand bearing a *terpy* and a 2,2'-*bipy* coordination site

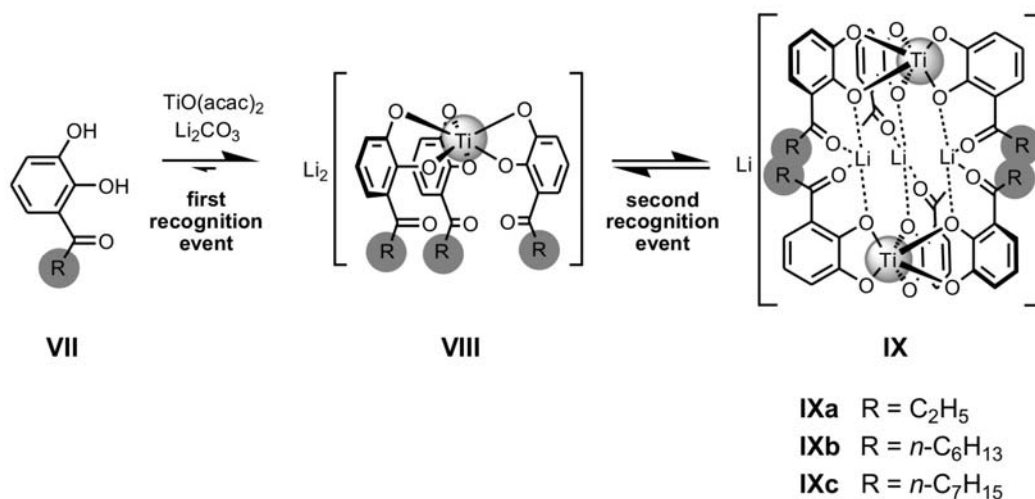


Scheme B2: Example of a double-heterostranded, homotopic and homotrimeric helicate **IV**^[56], of a triple-homostranded, homotopic and homodinuclear helicate **V**^[57], and of a penta-homostranded, homotopic and homopentanuclear helicate **VI**^[58]

B1.2 Helicates Obtained through Hierarchical Self-Assembly

In nature, self-assembly processes often occur on various levels of hierarchy, based on the interplay of quite different binding interactions.^[59] For example, cytoskeletal filamentous actin and cationic lipid complexes are formed via hierarchical self-assembly.^[59a] For supramolecular chemists, this is an elegant and efficient way to generate complexity.^[60]

There are several examples in which helicates were obtained through hierarchical self-assembly. Shannon^[61] and Nitschke^[62] reported the combination of two reversible reactions – imine condensation and metal coordination – in a one-pot hierarchical process to form helicates. Albrecht described the hierarchical, lithium-templated formation of dinuclear helicate-type titanium complexes.^[63] In a first recognition event, three catechol ligands **VII** are coordinated to titanium, generating the mononuclear complex **VIII**, and in a second recognition event, three lithium ions are bound to catechol and carbonyl oxygens, templating the assembly of the triply-bridged dinuclear complex **IX** (Scheme B3, crystal structure see Figure B1). If a set of two catechol ligands bridged by a lithium ion is considered as one single strand, then the final aggregate **IX** can be classified as a triple-homostranded, homotopic, homodinuclear helicate (Table B1). Below, the term “helicate” will therefore be used in its broader sense, including helicate-type complexes such as **IX**.



Scheme B3: Dinuclear titanium helicate **IX** obtained through hierarchical, lithium-templated self-assembly from catechol ligand **VII** (R = alkyl or alkoxy; acac = acetylacetonate)

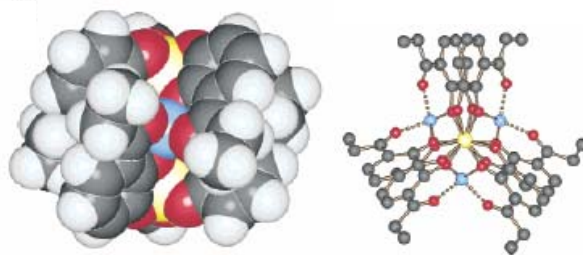
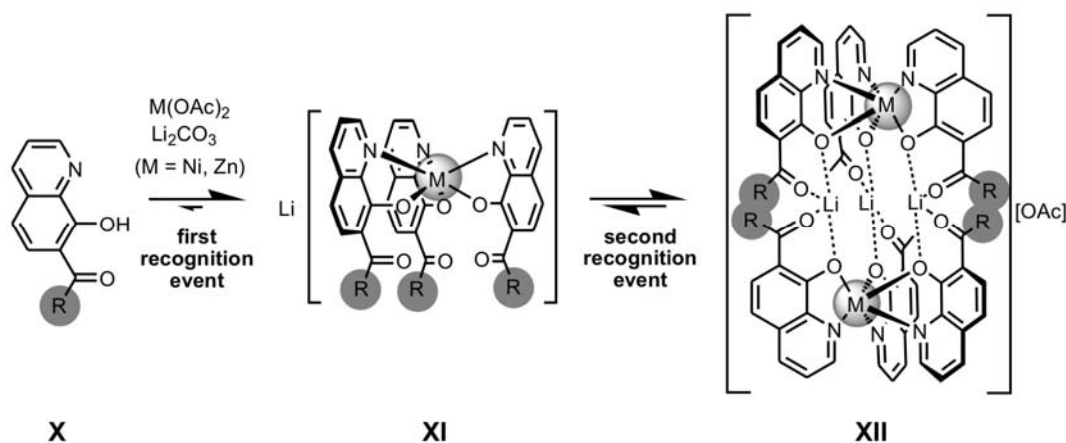


Figure B1:^[63] Crystal structure of **IXa**.

Left: Side view; Right: view along the Ti–Ti axis; Hydrogens are omitted.

When the catecholate ligand **VII** is replaced by quinolinolate ligand **X** and when nickel or zinc is applied as metal centers, an analogous hierarchical self-assembly sequence furnishes dinuclear helicate **XII** via mononuclear complex **XI** (Scheme B4).^[64] The use of a different ligand leads to different charge and electronic properties of the mono- and dinuclear complexes compared to **VIII** and **IX**. In general, the above-mentioned examples demonstrate the versatility of the hierarchical lithium-templated assembly strategy, which is only limited in the sense that the mononuclear complex must have a negative charge to attract lithium ions.



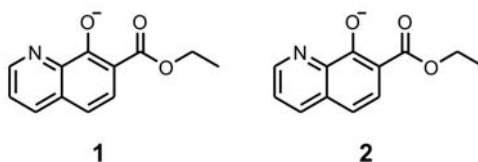
Scheme B4: Dinuclear nickel/zinc helicate **XII** obtained through hierarchical, lithium-templated self-assembly from quinolinolate ligand **X** (R = alkoxy)

B1.3 Advantages of Using Mass Spectrometry for Our Studies

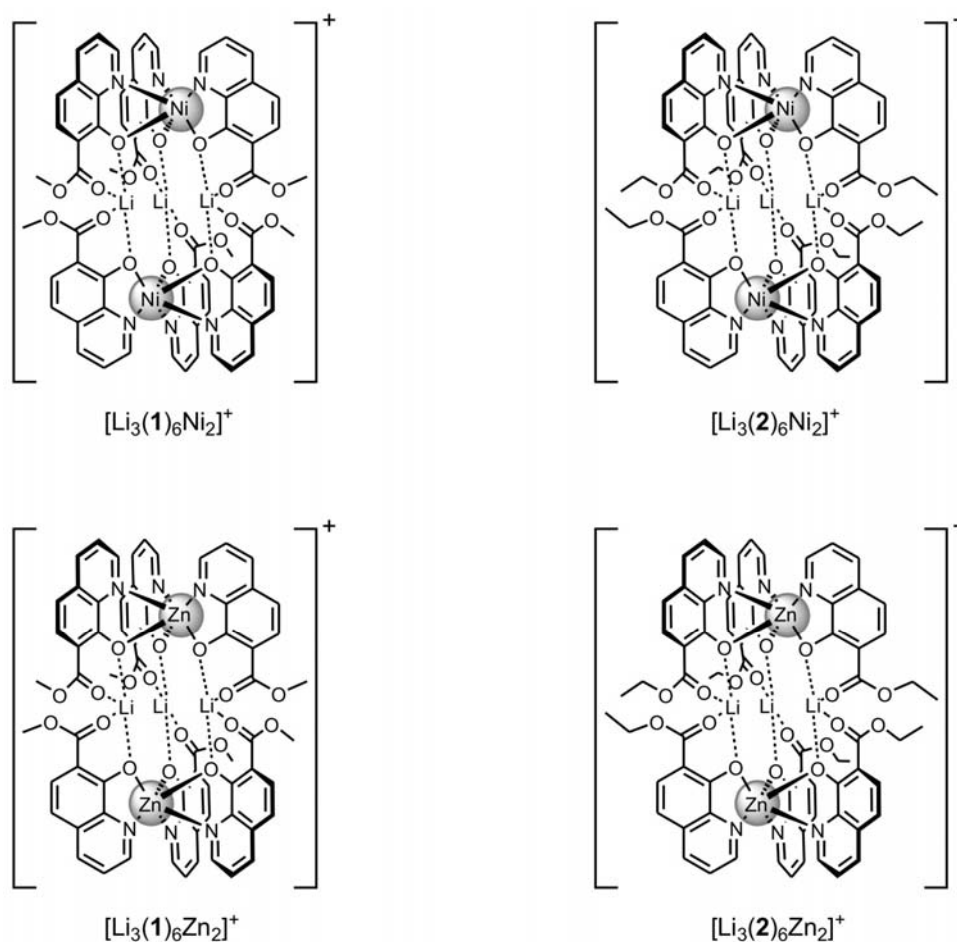
The investigation of metallosupramolecular assemblies such as helicates often relies on X-ray crystallography and NMR spectroscopy (including DOSY-NMR). But these techniques have certain limitations, for example they are not very suitable for studying the gas or solution phase reactivity of the complexes or exchange processes within specific mixtures. In this field, mass spectrometry – especially ESI-FTICR-MS with all its advantages outlined in section A1.3 – has proven to be an outstanding tool for investigating metallosupramolecular aggregates in a way that goes beyond simple analytical characterization.^[65] It is not only possible to study their gas-phase reactivity with tandem MS experiments, but also feasible to follow their solution-phase processes kinetically if these processes comply with the time scale of the MS experiments.^[66] Particularly, the assembly of and ligand exchange within heteroleptic helicates **IX** (Scheme B3, with different R groups) in the solution phase was successfully investigated by recording mass spectra of the corresponding non-equilibrium mixtures after specific time intervals.^[63]

B2 Hierarchically Assembled Helicates – Results and Discussion ^[c]

B2.1 Brief Overview



Scheme B5: Ester-substituted 8-quinolinolate derivatives **1–2** (deprotonated), used as ligands in the lithium-templated hierarchical self-assembly of helicates



Scheme B6: Dinuclear helicates under study, which were assembled using ligands **1–2**

[c] The results of section B2 were obtained in collaboration with Marcel Fiege, Prof. Dr. Markus Albrecht (both at Institut für Organische Chemie, RWTH Aachen, Germany) and Dr. Roland Fröhlich (at Organisch-Chemisches Institut, WWU Münster / University of Münster, Germany). M. Fiege and Prof. Dr. M. Albrecht contributed to the synthesis of the ligands and helicates studied in section B2.

As described in section B1.2, dinuclear helicates **XII** (Schemes B4 and B6) were formed in a lithium-templated hierarchical self-assembly process using for example quinolinolate ligands **1-H** or **2-H** (Scheme B5), a metal acetate and lithium carbonate. The formation of these helicates and the behaviour of mixtures containing different helicates were investigated with the ESI-FTICR-MS technique in section B2.

The counteranion of helicates of the general formula $[\text{Li}_3\text{L}_6\text{M}_2]^+$ (ligand **L** = **1** or **2**; metal **M** = Ni or Zn) is acetate, if not stated otherwise.

B2.2 Homodinuclear Homoleptic Helicates – Kinetic Effects in Their Formation

The self-assembly of the homodinuclear, homoleptic helicate $[\text{Li}_3(\mathbf{1})_6\text{Ni}_2]^+$ (Scheme B6) from its building blocks was tracked over time with ESI-FTICR-MS. At first, three separate methanol solutions, each containing ligand **1**, nickel acetate and lithium carbonate, were prepared at a concentration of 1 mM. In preliminary experiments, this low concentration turned out to be most appropriate to ensure that this self-assembly occurs on a time scale suitable for MS monitoring. In contrast, high concentrations would lead to the instantaneous formation of $[\text{Li}_3(\mathbf{1})_6\text{Ni}_2]^+$ without any intermediates being observable in the MS spectra.

Immediately after mixing the above-mentioned three solutions, the ions $[\text{Li}(\mathbf{1})_2\text{Ni}]^+$, $[(\mathbf{1})_3\text{Ni}_2]^+$, $[\text{Li}(\mathbf{1})_4\text{Ni}_2]^+$, and $[\text{Li}(\mathbf{1})_6\text{Ni}_3]^+$ were observed in the mass spectrum (Figure B2). For all these lithiated ions, the corresponding non-lithiated, sodiated complex is also observable, indicating the stability of these species to be independent of the kind of alkali cation. In the MS spectra recorded in the following days, only the signal intensity for $[\text{Li}_3(\mathbf{1})_6\text{Ni}_2]^+$ increased over time, while all the other ions showed continuously declining intensities. After 12 days, the helicate $[\text{Li}_3(\mathbf{1})_6\text{Ni}_2]^+$ became the predominant species in the mixture for the first time.

An interesting finding is that $[\text{Li}_3(\mathbf{1})_6\text{Ni}_2]^+$ is the only lithiated species in these mass spectra without having a sodiated analogue coming along with it. This demonstrates each of the three lithium ions within $[\text{Li}_3(\mathbf{1})_6\text{Ni}_2]^+$ to be an indispensable part of the complex, i.e. sodium would not fit into the specific positions within the helicate that are occupied by lithium.

These results show that the self-assembly of $[\text{Li}_3(\mathbf{1})_6\text{Ni}_2]^+$ is more a kinetically-controlled process under the conditions of this experiment, while the equilibrium is finally reached after quite long reaction times.

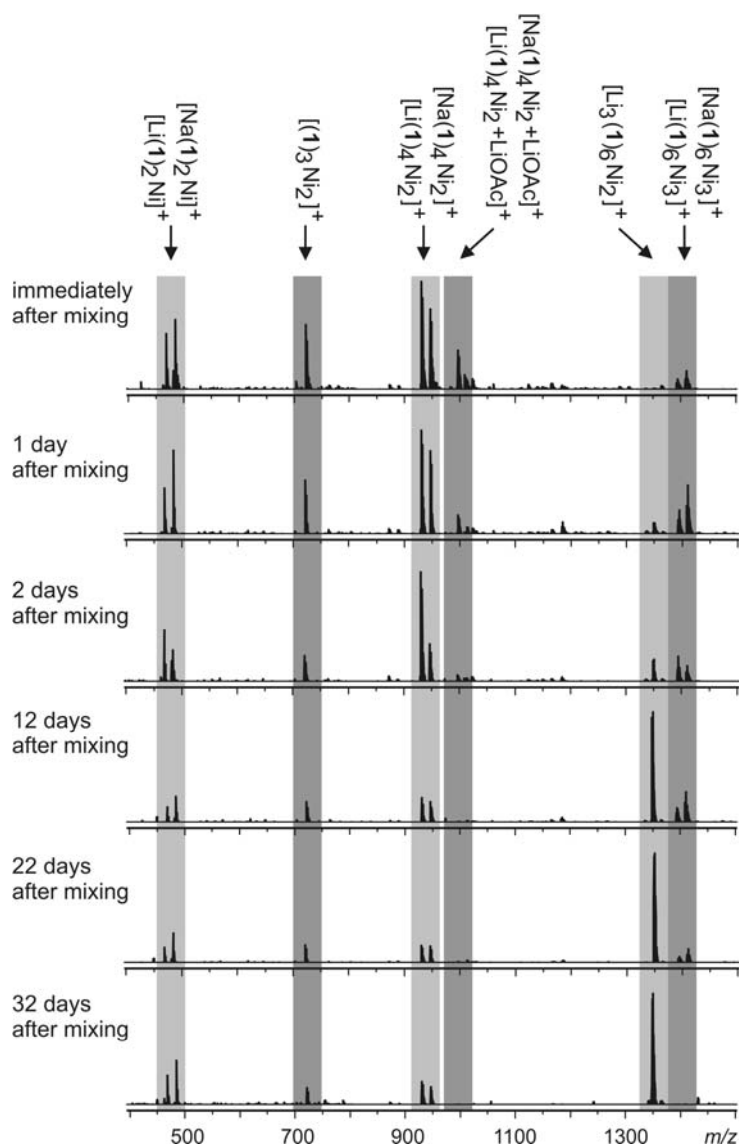


Figure B2: ESI-FTICR mass spectra (ESI^+) of the 6:2:1-mixture of ligand **1**, nickel acetate, and lithium carbonate ($667 \mu\text{M}$ – referring to **1** – in MeOH), recorded at different reaction times without further dilution

B2.3 Mixtures (not) Leading to Heterodinuclear Homoleptic Helicates

After the self-assembly of homodinuclear $[\text{Li}_3(\mathbf{1})_6\text{Ni}_2]^+$ was studied, our next objective is to investigate whether heterodinuclear homoleptic helicates can be generated in a facile approach.

Therefore, we first prepared a 1:1 mixture of $[\text{Li}_3(\mathbf{2})_6\text{Ni}_2]^+$ and zinc(II) acetate in pure THF. The mass spectrum recorded immediately after mixing them only shows $[\text{Li}_3(\mathbf{2})_6\text{Ni}_2]^+$, but the spectrum does not change after the mixture has stood for 40 days at room temperature. This indicates that a Ni/Zn metal exchange in nickel quinolinolate helicates is not possible.

In a second experiment, we tried the same approach the other way round, mixing zinc helicate $[\text{Li}_3(\mathbf{1})_6\text{Zn}_2]^+$ with nickel(II) acetate in an equimolar ratio and using THF as solvent. Four days after that, first signals of $[\text{Li}_3(\mathbf{1})_6\text{Ni}_2]^+$ can be identified in the mass spectrum. During the next days, the equilibrium is gradually shifted to the $[\text{Li}_3(\mathbf{1})_6\text{Ni}_2]^+$ side, until the spectrum only shows $[\text{Li}_3(\mathbf{1})_6\text{Ni}_2]^+$ and hardly any $[\text{Li}_3(\mathbf{1})_6\text{Zn}_2]^+$ after 32 days (Figure B3). The fast exchange of zinc within the $[\text{Li}_3(\mathbf{1})_6\text{Zn}_2]^+$ complex through free nickel cations supports the conclusion that zinc quinolinolate helicates are much more unstable than their nickel analogues.

In the above-mentioned second experiment, a signal for the heterodinuclear helicate $[\text{Li}_3(\mathbf{1})_6\text{ZnNi}]^+$ was expected to be found between the peaks for $[\text{Li}_3(\mathbf{1})_6\text{Ni}_2]^+$ and $[\text{Li}_3(\mathbf{1})_6\text{Zn}_2]^+$. Surprisingly, intensities for $[\text{Li}_3(\mathbf{1})_6\text{ZnNi}]^+$ always remain near the signal-noise-ratio (Figure B3), indicating its formation to be disfavoured. According to our assumption, the reason for this might be a slight difference in the geometries of mononuclear $[\text{Li}(\mathbf{1})_3\text{Zn}]$ and $[\text{Li}(\mathbf{1})_3\text{Ni}]$ units which are the hypothetical precursors of $[\text{Li}_3(\mathbf{1})_6\text{ZnNi}]^+$. In this sense, two of these mononuclear units probably better fit to each other when they are identical.

In conclusion, the formation of heterodinuclear homoleptic helicates is disfavoured in the approach of mixing a zinc quinolinolate helicate with nickel acetate, although metal exchange occurs. Nevertheless, they can be obtained through the approach described in section A2.5.

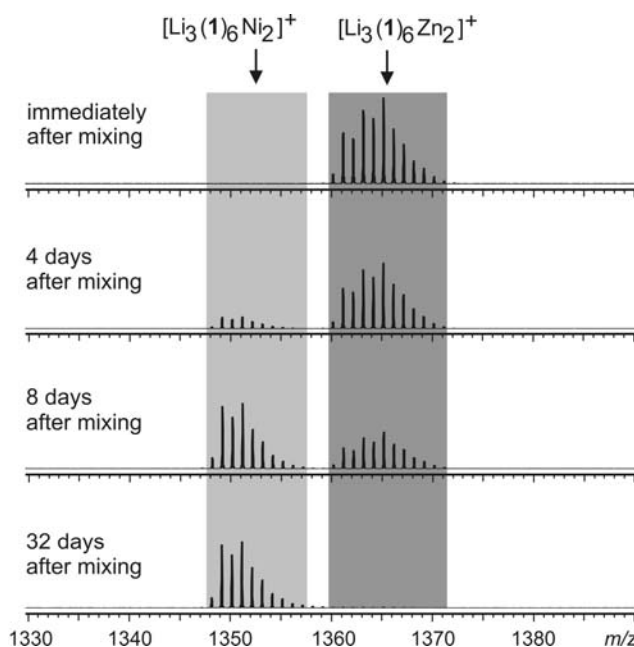


Figure B3: ESI-FTICR mass spectra (ESI⁺) of the 1:1-mixture of $[\text{Li}_3(\mathbf{1})_6\text{Zn}_2]^+$ and nickel(II) acetate (360 μM in THF), recorded at different reaction times (immediately before each measurement, some drops were taken out from the mixture and diluted to approx. 3 μM with THF)

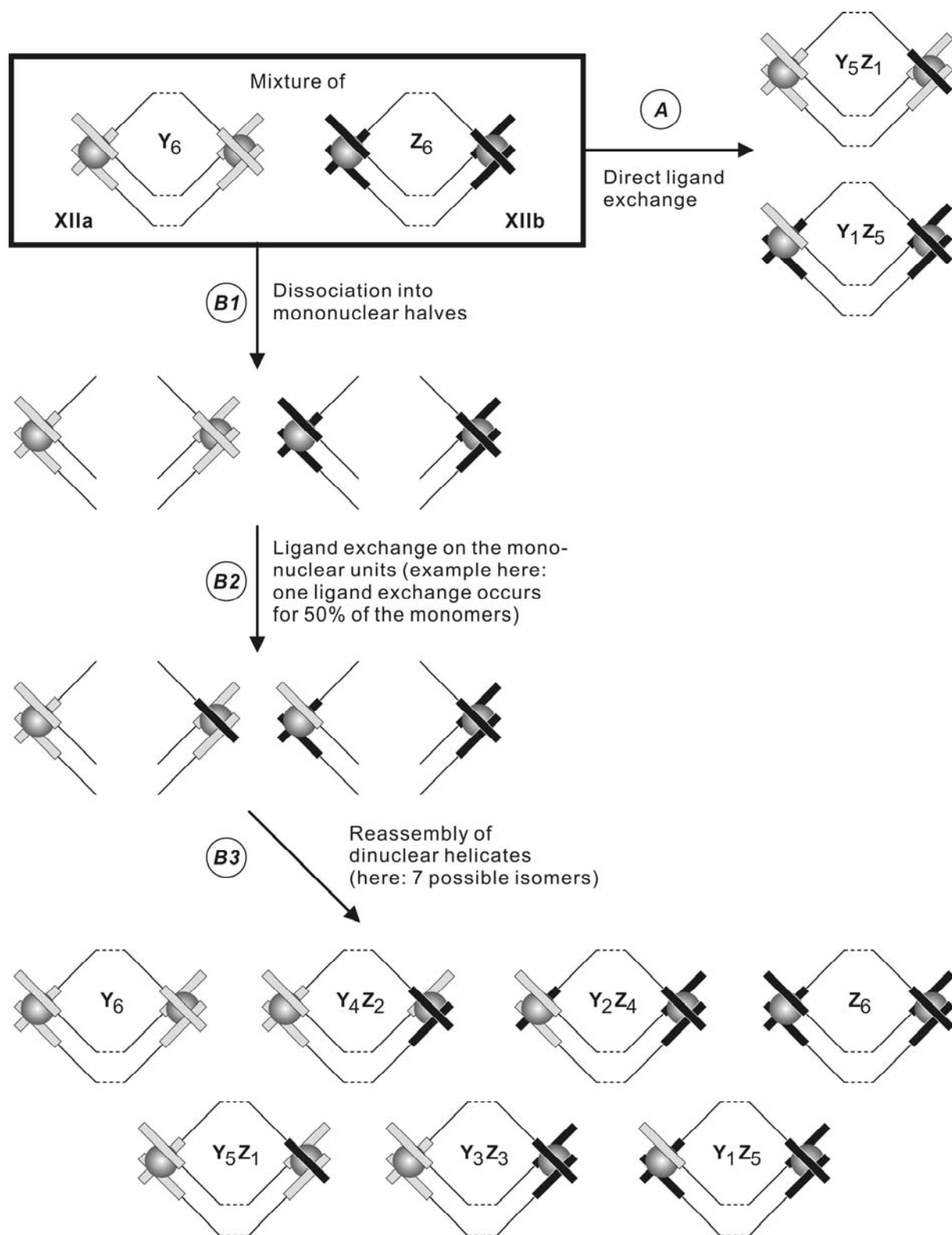


Figure B4: Different pathways – *A* and the *B1–B2–B3* sequence – for ligand exchange in a mixture of dinuclear helicates **XIIIa** and **XIIIb** (Dotted lines denote the bridging lithium cations between the mononuclear units).

If process *B2* is slower than *B1*, the species **Y₆**, **Y₃Z₃** and **Z₆** are preferably formed after process *B3*.

B2.4 Mixtures Leading to Homodinuclear Heteroleptic Helicates (Pathway B)

In a previous ESI-FTICR-MS study,^[63] two dinuclear titanium helicates with different ligands, **IXb** and **IXc** (Scheme B3), were equimolarly mixed using THF or THF/MeOH as solvent. According to the series of mass spectra recorded after specific time intervals, the only observable dynamic process is not the direct ligand exchange between dinuclear helicates (**A**), but a 3-step sequence comprising: dissociation of dinuclear helicates into mononuclear halves (**B1**), ligand exchange on the mononuclear units (**B2**), reassembly to dinuclear helicates (**B3**) (Figure B4). When pure THF is used as solvent, **B1** is much faster than **B2**. However, **B1** is slower than **B2** when a 1:1-mixture of THF/MeOH serves as solvent.

In our present study, analogous experiments were conducted with the 1:1-mixture of $[\text{Li}_3(\mathbf{1})_6\text{Zn}_2]^+$ and $[\text{Li}_3(\mathbf{2})_6\text{Zn}_2]^+$ (Scheme B6) using THF as solvent.^[67] After 20 hours, the mass spectra (Figure B5) revealed $[\text{Li}_3(\mathbf{1})_3(\mathbf{2})_3\text{Zn}_2]^+$ to be the most predominant ion among the heteroleptic species. The similarly high intensity of “ethyl-rich” $[\text{Li}_3(\mathbf{1})_2(\mathbf{2})_4\text{Zn}_2]^+$ in this spectrum has to be relativized in view of the fact that $[\text{Li}_3(\mathbf{2})_6\text{Zn}_2]^+$ has a significantly higher signal intensity than $[\text{Li}_3(\mathbf{1})_6\text{Zn}_2]^+$ in the first two spectra. After 5 days, an approximate statistical distribution of the heteroleptic helicates is achieved. In conclusion, process **A** is here rather insignificant, and **B1** is slower than **B2** (Figure B4). This is comparable to the result obtained with the **IXb/c** mixture using THF/MeOH as solvent (see previous paragraph).

The above-mentioned non-preference for direct ligand exchange (**A**) can be traced back to the fact that ligands are strongly bound within the dinuclear helicate due to additional binding energy of the bridging lithium cations.

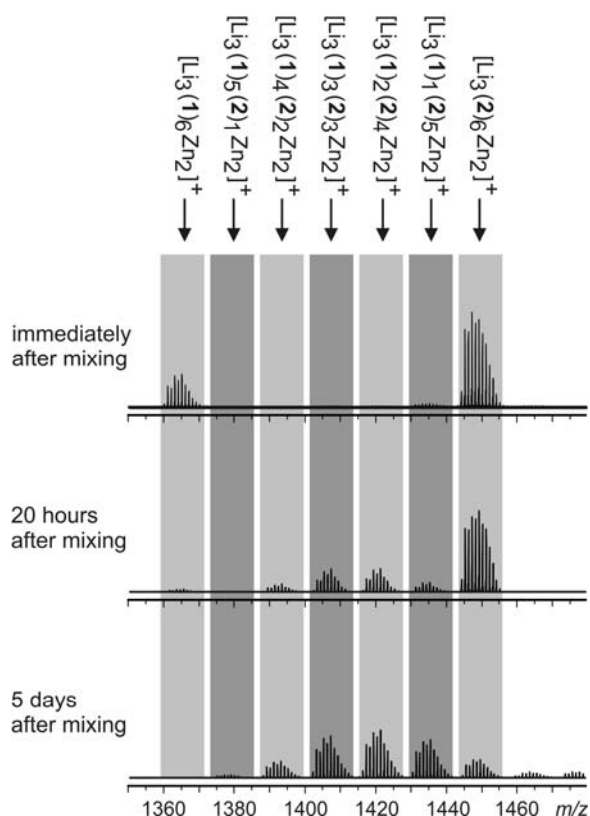


Figure B5: ESI-FTICR mass spectra (ESI^+) of the 1:1-mixture of $[\text{Li}_3(\mathbf{1})_6\text{Zn}_2]^+$ and $[\text{Li}_3(\mathbf{2})_6\text{Zn}_2]^+$ ($4 \mu\text{M}$ in THF) recorded at different reaction times without further dilution

B2.5 Mixtures Leading to Heterodinuclear Heteroleptic Helicates (Pathway A)

Beyond *homodinuclear* heteroleptic helicates studied in section B2.4, the formation of *heterodinuclear* heteroleptic helicates is also of great interest. Therefore, a 1:1-mixture of $[\text{Li}_3(\mathbf{1})_6\text{Zn}_2]^+$ and $[\text{Li}_3(\mathbf{2})_6\text{Ni}_2]^+$ (Scheme B6) in pure THF was subjected to a series of ESI-FTICR-MS measurements (Figure B6), allowing us to monitor ligand as well as metal exchange processes. Both processes are rather slow, and equilibrium is completely reached after 32 days.

As already shown in the first spectrum, nickel-containing ions have much higher signal intensities compared to zinc-containing ions, likely due to different ESI response factors. After four days, homodinuclear heteroleptic nickel helicates appear in the spectrum. Their signal intensities reach high levels after 12 days, whereas heterodinuclear species, particularly $[\text{Li}_3(\mathbf{1})_3(\mathbf{2})_3\text{NiZn}]^+$, are still hardly observable at this stage. This indicates direct ligand exchange A (Figure B4) to occur quickly, in contrast to section B2.4 where sequence **B1–B3** (Figure B4) is clearly dominant.

After reaction times as long as 32 days, heterodinuclear heteroleptic nickel/zinc helicates finally become visible in the spectrum with reasonable signal intensities. The most probable formation mechanism of these heterodinuclear species is considered to be the exchange of intact mononuclear units (**B1–B3**, probably with quite slow **B2** step).

Here, the notable observation that heterodinuclear heteroleptic helicates are generated much slower than their homodinuclear analogues can only be explained if process **A** is assumed to be energetically more favourable than sequence **B1–B3**. Provided that **B1** and **B2** are energetically more or less similar irrespective of whether one metal (section B2.4) or two metals (section B2.5) are present in the helicate mixture, there is only reassembly process **B3** which can make the difference.

Thus, we can conclude that **B3** (as part of sequence **B1–B3**) is rather *disfavoured* while **A** is *favoured* for the formation of *heterodinuclear heteroleptic helicates* compared to the formation of their *homodinuclear analogues*. This is in accord with the result obtained in section B2.3, where the formation of heterodinuclear $[\text{Li}_3(\mathbf{1})_6\text{NiZn}]^+$ is also disfavoured.

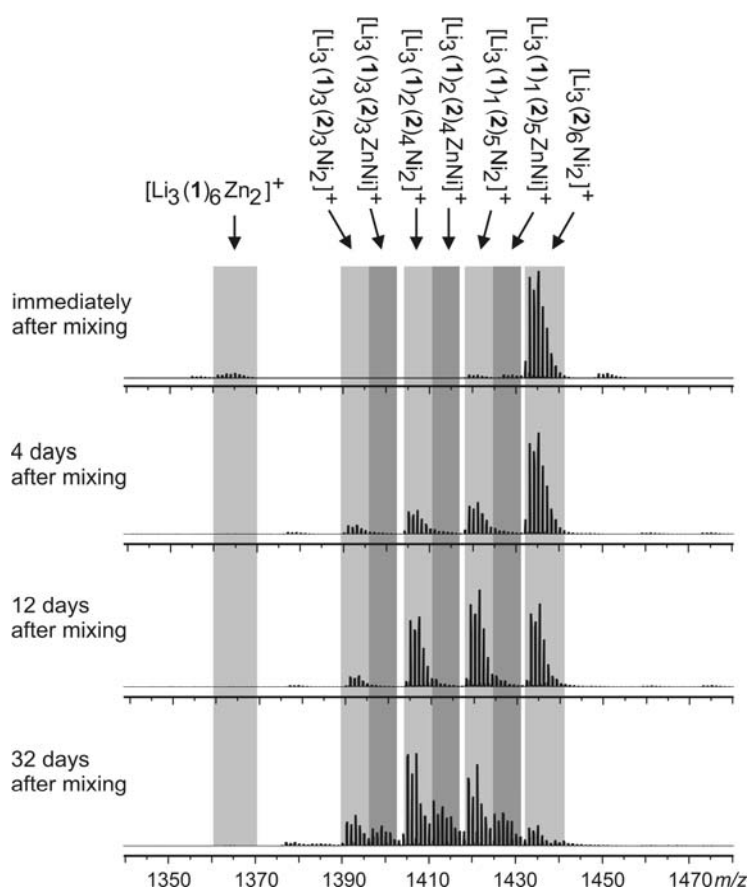
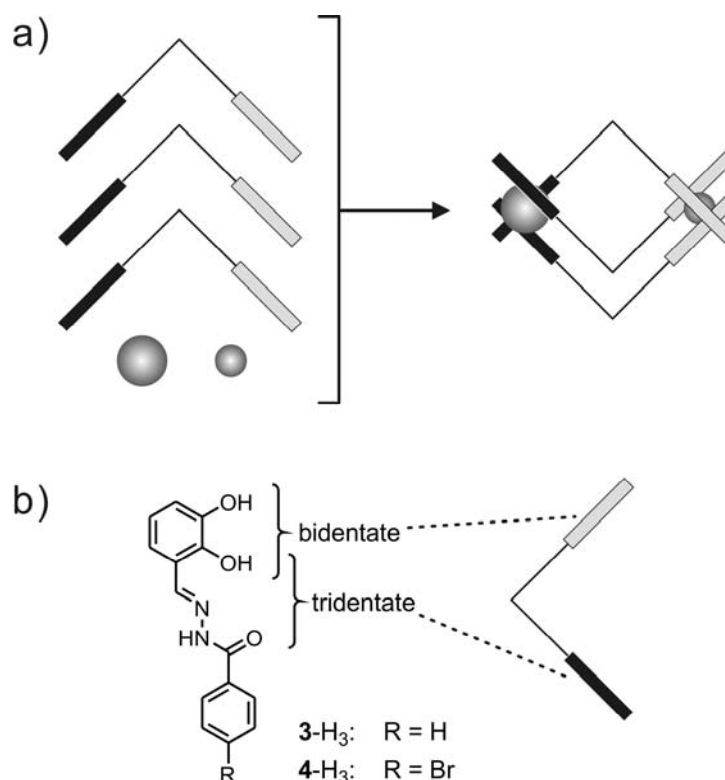


Figure B6: ESI-FTICR mass spectra (ESI^+) of the 1:1-mixture of $[\text{Li}_3(\mathbf{1})_6\text{Zn}_2]^+$ and $[\text{Li}_3(\mathbf{2})_6\text{Ni}_2]^+$ (200 μM in THF), recorded at different reaction times (immediately before each measurement, some drops were taken out from the mixture and diluted to approx. 3 μM with THF)

B3 Heterodinuclear Helicates Assembled from Heteroditopic Ligands – Results and Discussion^[d] [68]

B3.1 Brief Overview

Although a mixture of heterodinuclear helicates can be obtained through combining two readily-assembled helicates as shown in section A2.5, the highly selective generation of these species is quite challenging. Generally, this can be achieved either through the principle of “geometric discrimination”, which uses heteroditopic ligands bearing metal binding sites with different denticity (e.g. bidentate and tridentate),^[69] or through the principle of “electronic discrimination”, which uses heteroditopic ligands bearing electronically different metal binding sites (e.g. 1,2-dithiobenzene/catechol).^[70]



Scheme B7: a) Self-assembly of heterodinuclear helicates from heteroditopic ligands; b) Ligands 3/4-H₃.

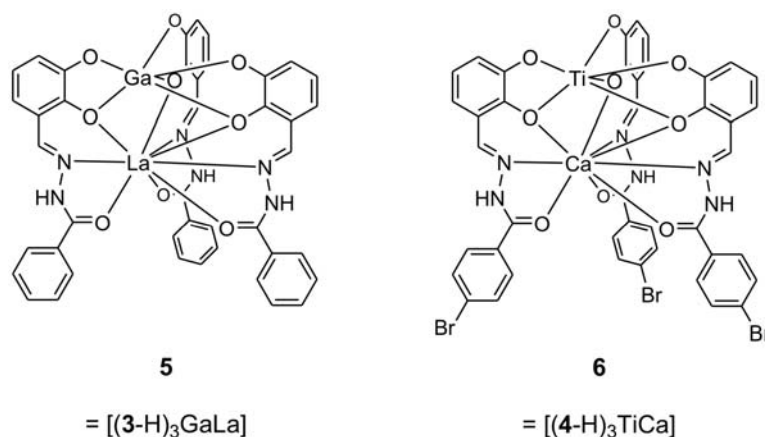
[d] The results of section B3 were obtained in collaboration with Yufeng Liu (at Institut für Organische Chemie, RWTH Aachen, Germany, and at College of Chemistry and Molecular Engineering, Peking University, PR China), Prof. Dr. Markus Albrecht (at Institut für Organische Chemie, RWTH Aachen, Germany) and Dr. Roland Fröhlich (at Organisch-Chemisches Institut, WWU Münster / University of Münster, Germany). Y. Liu and Prof. Dr. M. Albrecht contributed to the synthesis of the ligands and helicates studied in section B3. The results of section B3 were published in ref. [68].

In the present study, readily available heteroditopic ligands **3/4-H₃** (Scheme B7) obtained through condensation of 2,3-dihydroxybenzaldehyde and acylhydrazide^[71] are used for the assembly of various heterodinuclear helicates, following the above-mentioned principle of “geometric discrimination”.

B3.2 MS Characterization of the Reaction Product of a Ga-La-Helicate

5 (Scheme B8) is a gallium(III) lanthanum(III) helicate based on ligand **3**. In a preliminary study, ¹H-NMR spectra of **5** were recorded in the solvent [D₆]DMSO. The spectra unambiguously show that **5** has one set of signals which is clearly different to the shifts observed for ligand **3-H₃** alone. The structure of **5**, where each of the three hydrazone NH positions of the ligand **3-H₃** is singly protonated, was also confirmed by X-ray crystallographic studies. Upon addition of KOH to **5**, a new set of ¹H-NMR signals was found, in which the signal of hydrazone NH vanished (indicating deprotonation), and signals of catecholate aryl protons and CH=N protons underwent a highfield shift. The question of which species is represented by this new signal set may be answered by MS characterization.

Negative ESI-MS using methanol as solvent (Figure B7) shows *full deprotonation* of the ligand **3-H₃** with concomitant formation of a heterotrinnuclear species [(**3**)₄Ga₂La]³⁻ and its potassium methanolate adducts (*m/z* = 1368.9 [K₂(**3**)₄Ga₂La]⁻, 1438.9 [K₂(**3**)₄Ga₂La]⁻ · KOCH₃ and 1508.9 [K₂(**3**)₄Ga₂La]⁻ · 2KOCH₃). The exact structure of this trinnuclear species is yet unknown. In addition, [K₂(**3**)₃GaLa]⁻ is observed at *m/z* = 1044.9 as a peak with low intensity.



Scheme B8: Structures of the heterodinuclear helicates **5** and **6**.

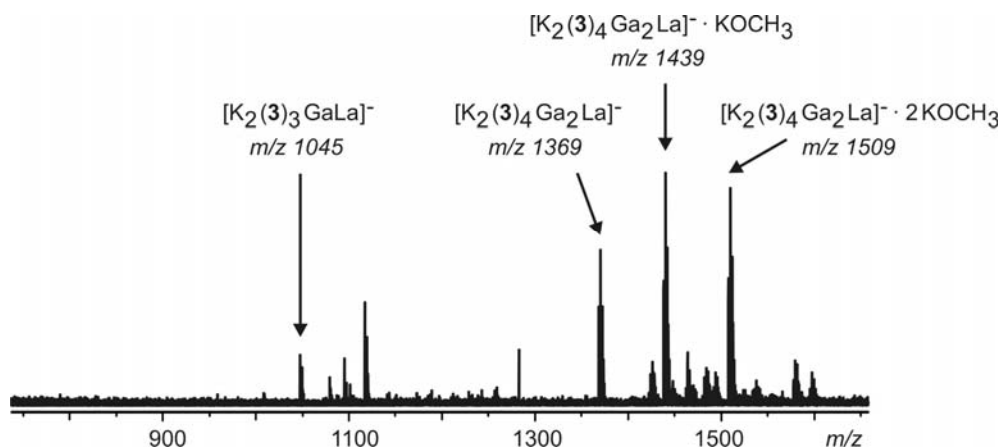


Figure B7: ESI-FTICR mass spectrum (ESI^-) of the reaction product of **5** with KOH (in MeOH)

B3.3 MS Characterization of a Ti-Ca-Helicate

6 is a titanium(IV) calcium(II) helicate based on ligand **4**. X-ray crystallography reveals the structure of **6** to be as shown in Scheme B8, with an unusual ninefold coordination at the Ca(II) ion. Negative ESI-MS from methanol (Figure B8) also confirms this structure of **6** ($m/z = 1084.8 [4_1(4-H)_2 TiCa]^-$).

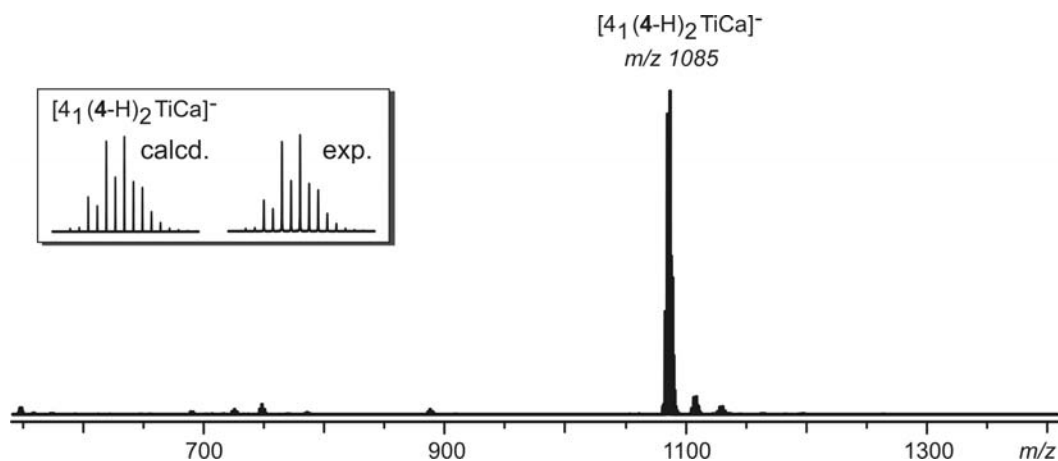


Figure B8: ESI-FTICR mass spectrum (ESI^-) of **6** (in MeOH)

B4 Final Conclusions and Outlook

From section B2, in which ESI-FTICR-MS investigations of formation and exchange processes in hierarchically self-assembled dinuclear quinolinolate helicates **XII** (Schemes B4 and B6) were described, we can draw the following conclusions:

- The self-assembly of homodinuclear homoleptic $[\text{Li}_3(\mathbf{1})_6\text{Ni}_2]^+$ is rather a kinetically-controlled process.
- The formation of heterodinuclear homoleptic helicates is disfavoured in the approach of mixing $[\text{Li}_3(\mathbf{1})_6\text{Zn}_2]^+$ with nickel acetate, although metal exchange takes place.
- The formation of homodinuclear heteroleptic helicates in the approach of mixing $[\text{Li}_3(\mathbf{1})_6\text{Zn}_2]^+$ and $[\text{Li}_3(\mathbf{2})_6\text{Zn}_2]^+$ preferably proceeds via the pathway **B1-B2-B3**, with **B1** being slower than **B2**, while process **A** is disfavoured (pathways see Figure B4).
- The formation of heterodinuclear heteroleptic helicate in the approach of mixing $[\text{Li}_3(\mathbf{1})_6\text{Zn}_2]^+$ and $[\text{Li}_3(\mathbf{2})_6\text{Ni}_2]^+$ preferably proceeds via the pathway **A**, whereas the sequence **B1-B2-B3**, particularly process **B3**, is probably disfavoured (pathways see Figure B4). Direct exchange of quinolinolate ligands (pathway **A**) is an interesting mechanistic scenario which has not been observed in the previous ligand exchange study on titanium triscatecholate helicates^[63].

In conclusion, the MS study on quinolinolate helicates has provided new insight into metal and ligand exchange processes. Furthermore, the finding that homodinuclear helicates are formed rather than heterodinuclear Ni/Zn helicates in corresponding mixtures (see b, d in previous paragraph) indicates that the geometries of mononuclear $[\text{LiL}_3\text{Zn}]$ and $[\text{LiL}_3\text{Ni}]$ (L = ligand **1** or **2**) units might be slightly different.

In section B3, the MS characterization of heterodinuclear helicates assembled from heteroditopic ligands confirmed the structure of **6** (Scheme B8) and revealed the existence of heterotrimeric species $[(\mathbf{3})_4\text{Ga}_2\text{La}]^{3-}$ which only contains fully deprotonated ligands.

In the future, the MS study on quinolinolate helicates will be extended to systems containing other metals and ligands. These ligands will for example bear higher functionalized side chains, enabling interactions with other molecular species and probably leading to novel properties of the corresponding mixtures. Combinations of other metals might provide deeper insight into the unusual behaviour of mixtures leading to heterodinuclear helicates.

In forthcoming MS studies on heterodinuclear helicates assembled from heteroditopic ligands, the formation of these helicates and also exchange processes in their mixtures will be investigated.

C. Multimacrocylic Hosts as Precursors for Multiply Interlocked Systems: A Study on Modular Synthesis ^[e] [72]

C1 Purpose of the Study and Introduction

In nature, complex architectures are assembled using a limited set of well-selected modules - for example twenty amino acids, four nucleosides and a series of monomeric carbohydrates - from which a sheer infinite variety of protein structures, nucleic acids, and linear or branched carbohydrate oligo- and polymers can be generated. This modular strategy is highly efficient in that it reduces the number of the required building blocks to a minimum, without restricting the structural diversity of the end products. However, biopolymers are not only diverse in structures, but also in function. The implementation of functions like catalysis, information storage, or cell-cell communication has been realized in living organisms. However, it requires more than just a modular approach to structurally diverse architectures. Nature's approach also makes structures programmable and optimizable. The quite complex scaffolds of, for example, a large protein allow evolution to optimize by adjusting the structures gradually in small steps. These great achievements found in nature are a particularly stimulating source of inspiration to many chemists nowadays.

A realization of a similar modular strategy for the generation of structurally diverse, more complex artificial architectures is still a challenge. In the field of supramolecular chemistry, the application of this approach requires the design of modules which need to fulfill the following criteria: **(i)** The number of building blocks should be limited. **(ii)** They should be synthetically accessible through inexpensive syntheses that provide high yields of the desired building blocks. **(iii)** A kind of chemistry needs to be identified or developed with which these units can be easily and flexibly combined into numerous supramolecular architectures with desired structures and functions – either through covalent or non-covalent bonding. Self-

[e] The results of section C were obtained in collaboration with Bilge Baytekin, Boris Brusilowskij, Dr. Jens Illigen, Lena Kaufmann (all members of the research group of Prof. Dr. Christoph A. Schalley at the Institut für Chemie und Biochemie, Freie Universität Berlin / Free University of Berlin), Jenni Ranta, Dr. Juhani Huuskonen, Dr. Luca Russo, Prof. Dr. Kari Rissanen (all at Nanoscience Center, Department of Chemistry, University of Jyväskylä, Finland). B. Baytekin, B. Brusilowskij, Dr. J. Illigen, L. Kaufmann, J. Ranta, and the author of this thesis contributed to the synthesis of the compounds described in section C. Dr. J. Huuskonen, Dr. L. Russo, and Prof. Dr. K. Rissanen contributed to the x-ray analysis of the crystal structures described in section C. The results of section C were published in ref. [72].

assembly^[73] may well be helpful in reducing the synthetic efforts. Supramolecular chemists so far often followed the strategy to identify a goal, e.g. binding a guest molecule by a host through molecular recognition, followed by the design of a specific molecule which might fulfill the task. This molecule has then been evaluated and quite often turned out to be less than perfectly suited. A detailed analysis may then lead to a new design concept, which requires the synthesis of a new host through, by and large, a completely new synthetic route. This approach of finding one individual synthetic pathway for each target molecule is reasonable and often preferred, when the number of targets is small. The modular route is a more process-oriented way of chemical thinking and provides much higher adaptability, if a part of the specific target molecule design needs to be modified at a later stage. The modular approach has been explicitly described for various supramolecular assemblies, e.g. receptors and capsules;^[74] mechanically interlocked compounds,^[75] such as rotaxanes or catenanes; metal-porphyrin complexes;^[76] and artificial double helices.^[77]

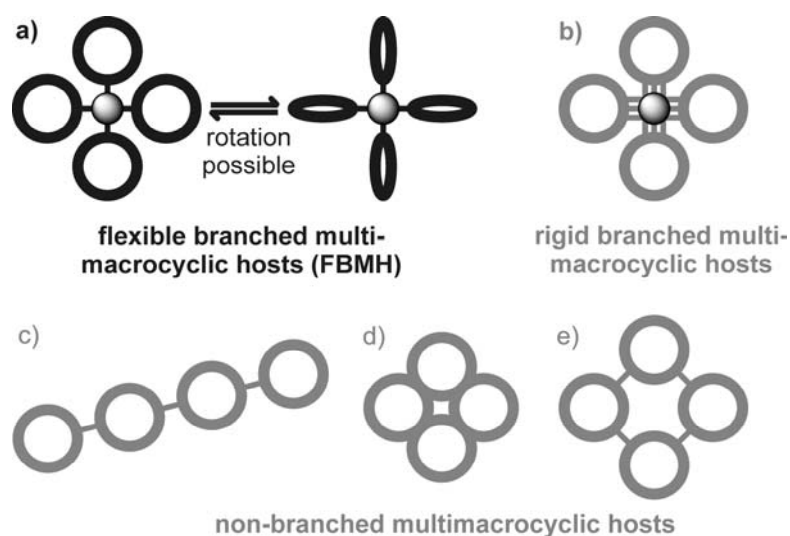


Figure C1: Generic structures of branched multimacroyclic hosts that (a) are connected to a common core through single bonds and can thus freely rotate or (b) are rigidified through multiple connections to the core. (c) to (e) Examples for oligo-macrocycles that are not connected to a common core. Here we focus on group (a).

As one of the fundamental scaffolds in supramolecular chemistry, macrocyclic molecules have been widely used not only for the binding of small guest molecules,^[78] but also for the fabrication of mechanically-interlocked architectures such as rotaxanes or catenanes.^[79] In recent years, assemblies consisting of several (at least two) host macrocycles linked to one

single core,^[80] which are shown in Figure C1a,b and which we decide to simply call “branched multimacrocylic hosts”, have attracted increasing interest among supramolecular researchers. The reason for this is the versatility of these hosts which can: **(i)** either interact with mono-^[80a] or multivalent^[80e] guests without threading, or **(ii)** contain mono-^[80c-d] or multivalent^[80b] guests threaded into them. In this section C, we focus on hosts which open the gate to **multiply mechanically-interlocked architectures (MIA)**. Among these hosts, we further distinguish **flexible branched multimacrocylic hosts (FBMHs)**, in which each of the bonds between macrocycle and core can rotate freely, from their rigid counterparts (e.g. triptycene-^[80d] or triphenylene-based platforms^[80b]), in which this rotation mode is disabled. Compared to the inflexible hosts, FBMHs have the advantages that **(i)** they can better adapt to the structures of multivalent guests, **(ii)** they provide more possibilities for self-assembly, and **(iii)** one single FBMH can serve as precursor for quite different MIAs (rotaxane-like as well as catenane-like MIAs), inherently complying with the modular philosophy of “few modules leading to many targets”.

FBMHs with this precursor function, which are rarely known as such,^[80b] have not been obtained in great structural diversity through a modular approach so far. Here, we describe the synthesis and characterization of a family of easily accessible, tetralactam-based FBMHs in which amide coupling, cross-coupling reactions and metal templates are applied to combine the well-selected modules. We demonstrate that a broad structural variety is accessible, which encompasses covalently linked FBMHs as well as some examples for non-covalently linked analogues that are complexed to a metal core through rather weak coordinative bonds. On the other hand, chromophore-centered FBMHs are presented which relate to future functions through their photochemical properties. From some of the macrocyclic precursors, rotaxanes have been made either substituted with a chromophore or with a metal binding site. As a proof of principle, the metal-coordination approach is applied to a rotaxane.

C2 Results and Discussion

C2.1 Brief Overview

Our FBMHs are based on the well-known Hunter-Vögtle tetralactam macrocycle (“TLM”), which was reported by Hunter^[81] and Vögtle et al.^[82] Since these macrocycles provide four converging hydrogen bonds for interaction with guests,^[83] they have been frequently applied in templated, high-yield syntheses of mechanically-interlocked molecules such as (pseudo)-rotaxanes and catenanes.^[84,85] Another advantage is that TLMs provide high chemical stability against many reaction conditions.

We aim to functionalize the macrocycles with a broad selection of different groups. Two pathways can be imagined (Figure C2): One possibility is to introduce the functional group – for example the metal-coordinating site mentioned in Figure C2 – before macrocyclization. We call this route the pre-macrocyclization pathway. In an earlier study,^[86] we reported bisquinoline-bearing macrocycles, catenanes, and rotaxanes that were synthesized according to this route. The alternative is to first perform the macrocyclization step followed by attachment of the desired functional group. This so-called post-macrocyclization pathway^[87] has the advantage that functionalization can start from a common macrocyclic intermediate. A variety of functional groups can thus be introduced after the macrocyclization step – an approach which saves a significant amount of synthetic effort.

On the post-macrocyclization route to our FBMHs, a crucial key step is the connection of the macrocycles to a common core. In order to limit the flexibility in these target molecules to the rotation around the macrocycle–core bond, cross coupling reactions were chosen to realize this key step.

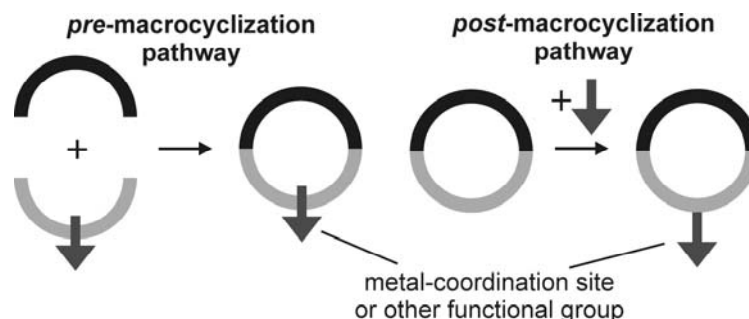
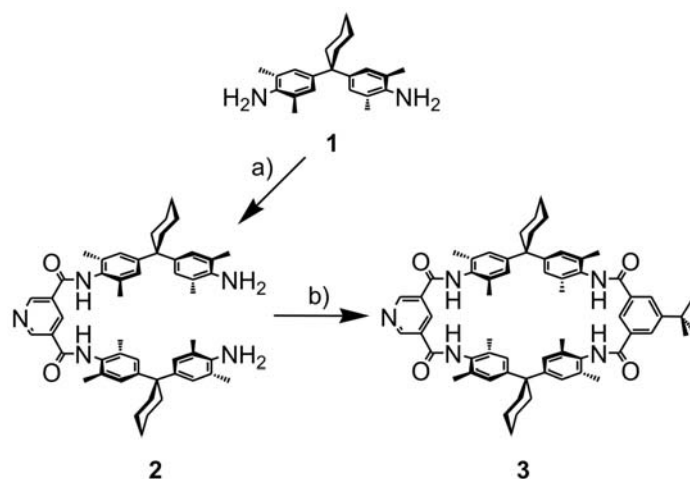


Figure C2: The pre- versus post-macrocyclization pathway used to arrive at macrocycles bearing specific ligand functions, for example, the pyridine moiety (indicated by the dark gray arrow). Note that for the pre-macrocyclization pathway, the ligand function is incorporated into the macrocycle.

C2.2 Synthesis of a Tetralactam Macrocycle via the Pre-Macrocyclization Pathway

As illustrated in Scheme C1, the pyridine-containing TLM **3** is accessible by well-known literature procedures in two steps starting from Hunter's diamine **1**.^[81] The pyridine nitrogen is in an exo-cyclic position and thus can be utilized for metal coordination, by which several of these macrocycles can finally be connected (see below). The pyridine is incorporated into the corresponding building block before macrocyclization. The advantage of this strategy is that the synthetic route is analogous to that of other well-known TLMs and thus benefits from the experience that is available in the chemical literature. However, the reaction conditions still need to be significantly modified in the crucial and yield-determining macrocyclization step due to solubility problems with the intermediate extended diamine **2**. This optimization is quite time-consuming and such problems will likely be encountered when other functional groups are attached to or incorporated in the building blocks. To our experience, small structural changes in the building blocks may significantly alter the macrocyclization yields. This makes the pre-macrocyclization pathway less flexible with respect to a toolbox approach. Consequently, the pre-macrocyclization pathway is quite limited.



Scheme C1: Synthesis of tetralactam macrocycle **3**: **a)** pyridine-3,5-dicarbonyl dichloride, NEt₃, CH₂Cl₂, RT, 2 d, 64%; **b)** 5-tert-butylisophthaloyl dichloride, pyridine, NEt₃, CH₂Cl₂, high dilution, 40°C, 2 d, 41%.

C2.3 Crystal Structure of Macrocycle **3**

X-ray quality crystals of **3**^[88] were grown after four weeks at the interface of a biphasic system comprising a dichloromethane solution of **3** and an acidic (pH = 4) aqueous solution of K₂PtCl₄. Conformational isomorphism^[89] is observed in the crystal structure: The unit cell contains one macrocycle in its “*all-in*” conformation **3A**, in which all four amide protons converge into the macrocyclic cavity, and two macrocycles as the “*two-in-two-out*” conformer **3B**, in which the amide protons pointing into the macrocycle alternate with those pointing out of it (see arrows in Figures C3a,b). The presence of two different conformations of the macrocycle in the crystal indicates that both conformations are (a) energetically not too distant from each other and (b) can interconvert without being hampered by a high barrier. This is in excellent agreement with a previous theoretical study,^[83a] which predicted both features for similar macrocycles. The reason why both conformers appear in the solid state presumably lies in crystal packing. In particular, intermolecular hydrogen bonds connect the macrocycles and generate an infinite ribbon (Figures C3c,d). In this ribbon, two macrocycles **3B** connect two molecules in conformation **3A**. The latter macrocycle is disordered in the crystal with respect to the positions of the pyridine and the *t*-butyl group. Either one of the two possible orientations can occur. The N–O distances of the intermolecular N–H•••O=C hydrogen bonds are 2.808 and 2.852 Å. In the crystal structure, the hydrogen-bonded assembly of one **3A** and two **3B** molecules serves as a non-covalent “monomer unit” for the twisted-ribbon-like, hydrogen-bonded polymer, in which two parallel strands of **3B** are interconnected by **3A** (Figure C3d).

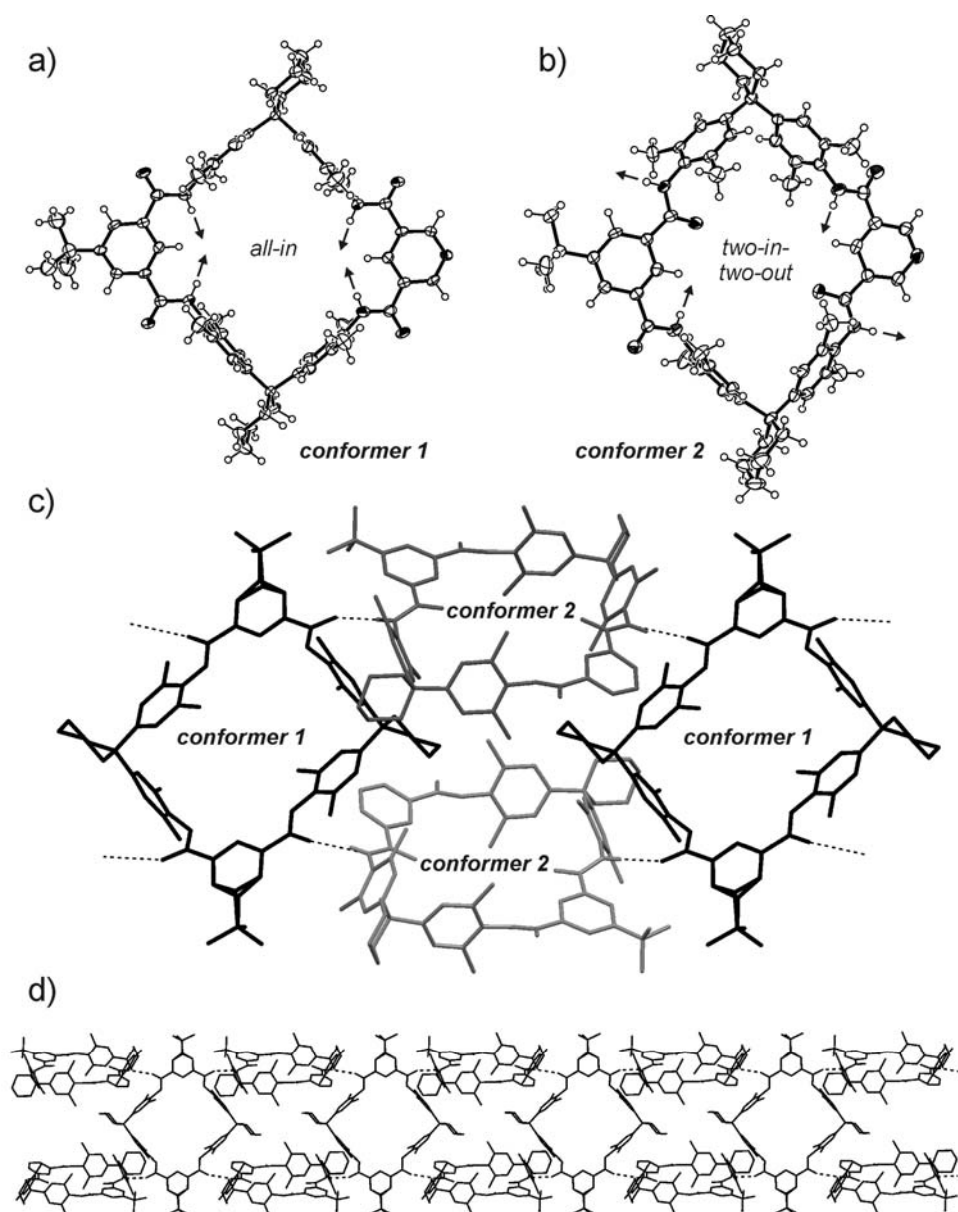


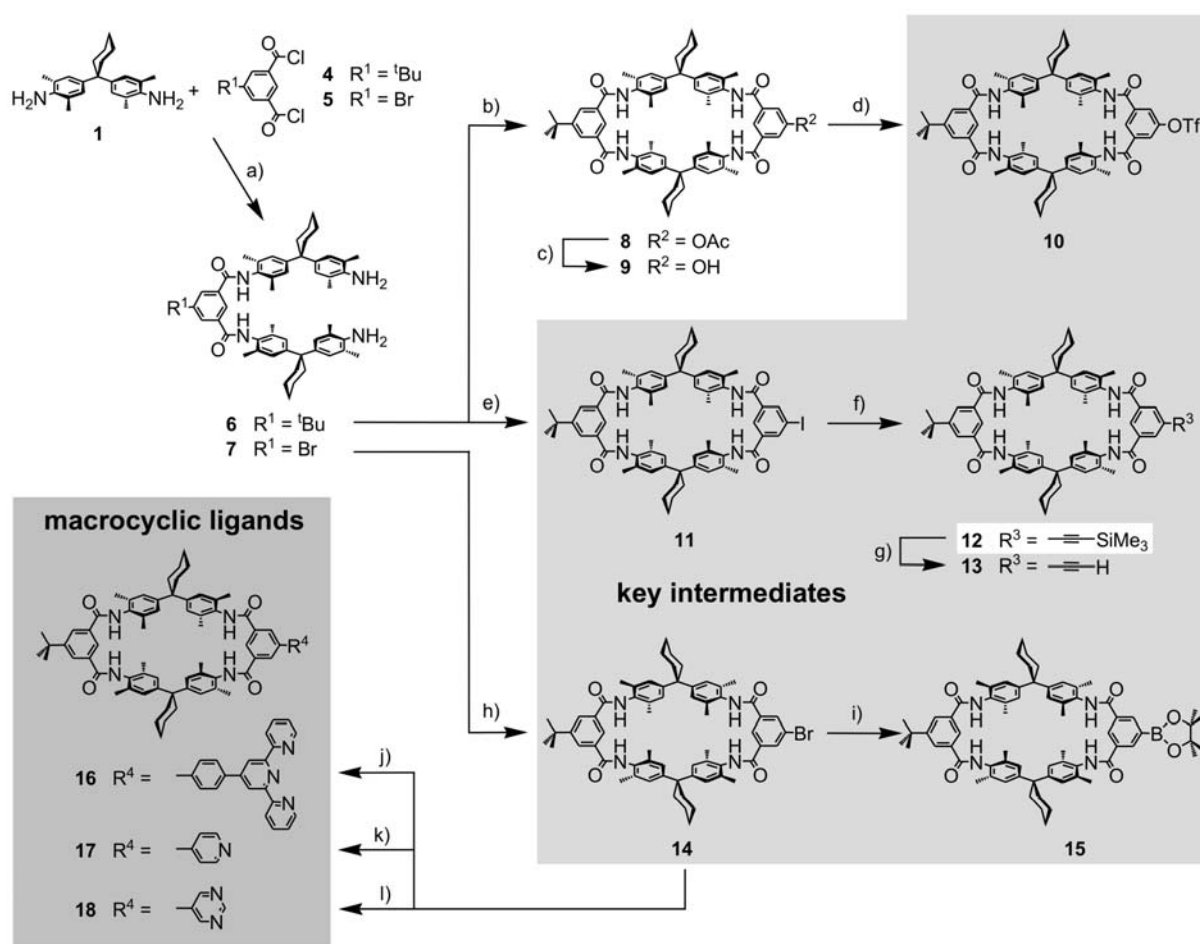
Figure C3: Crystal structure of **3**: **a**) ORTEP plot of all-in conformer **3A** (conformer 1), **b**) ORTEP plot of two-in-two-out conformer **3B** (conformer 2) (both conformers shown with 50% probability ellipsoids); **c**) Intermolecular hydrogen bonds (dashed) between **3A** (black) and **3B** (dark gray, gray) (hydrogen atoms omitted for clarity, except for the amide protons involved in hydrogen bonding); **d**) Visualization of the infinite molecular “chain” in form of a twisted-ribbon-like, hydrogen-bonded polymer (all hydrogen atoms omitted).

C2.4 Synthesis of Key Intermediates and Synthesis of Macrocylic Ligands via the Post-Macrocyclization Pathway

To avoid the above-mentioned potential weaknesses of the pre-macrocyclization pathway, we explored the post-macrocyclization route to macrocylic ligands. In order to be able to make use of the large potential of cross-coupling reactions, a series of key intermediates have been prepared that are already equipped with the functional groups needed for cross-coupling reactions (Scheme C2). From the hydroxy-substituted macrocycle **9**, the triflate **10** can easily be obtained with good yields. Similarly, the iodo- and bromo-substituted analogues **11** and **14** are obtained, when the extended diamine **6** is reacted under high-dilution conditions with the corresponding isophthaloyl dichloride. Two more cross-coupling precursors are available from the halogenated macrocycles: A Sonogashira coupling^[90] followed by deprotection of the trimethyl silyl group with potassium hydroxide provides acetylene-substituted **13** which may serve as a precursor in a second Sonogashira coupling. Besides this, it can also be employed in Glaser-Hay coupling reactions^[91] (see below) or potentially in Huisgen-Sharpless-Meldal click chemistry^[92] (not described here). From **14**, the pinacolato boronate-substituted macrocycle **15** is easily available through Miyaura borylation^[93] and may – besides the two halogenated macrocycles **11** and **14** – serve as another key intermediate for Suzuki cross-coupling reactions.^[94] The scope of the cross-coupling reactions mentioned here can certainly be extended beyond the scope of the present study. Just to mention one example, which has not been explored in our study, boronates such as **15** may also be used in Chan-Lam^[95] couplings. Consequently, the set of key intermediates **10–15** represents a very versatile and flexible, but at the same time compact basis for further functionalization of the TLMs. This toolkit can be used for a broad spectrum of cross-coupling reactions with a vast range of coupling agents and is characterized – in accord with the principles of modular approach – by its easy accessibility, great flexibility and high adaptability.

A quick view at the cyclization yields again reveals them to depend much on the substituent: While **3** and **8** are obtained in similar yields of 41% and 43%, respectively, the yields are significantly lower in the case of the halogenated analogues **11** (15%) and **14** (20%). The sometimes quite drastic effects might be rationalized not only by invoking different distributions of macrocycle and undesired oligomeric side products. Another major product usually found in substantial amounts is the corresponding catenane. It consists of two identical macrocycles that become intertwined during the macrocyclization by a hydrogen-bond-mediated template effect. This hydrogen-bonding pattern is rather sensitive to structural

changes in the macrocycle structures.^[83] Some of the catenanes have been isolated and fully characterized in the course of the present study. However, we refrain from describing them in detail here, since they unfortunately turned out to be rather unreactive in cross-coupling reactions.



Scheme C2: Synthesis of key intermediates and macrocyclic ligands: **a)** NEt₃, CH₂Cl₂, RT, 1 d, 64% (**6**) or 74% (**7**); **b)** 5-acetoxyisophthaloyl dichloride, NEt₃, CH₂Cl₂, high dilution, RT, 1 d, 43%; **c)** KOH, dioxane, H₂O, reflux, 8 h, 95%; **d)** Tf₂O, pyridine, CH₂Cl₂, -25°C, 2 h, 87%; **e)** 5-iodoisophthaloyl dichloride, NEt₃, CH₂Cl₂, high dilution, RT, 1 d, 15%; **f)** trimethylsilyl acetylene, CuI, Pd(PPh₃)₂Cl₂, NEt₃, DMF, RT, 15 h, 41%; **g)** KOH, MeOH/CH₂Cl₂, RT, 75%; **h)** 5-*tert*-butylisophthaloyl dichloride, NEt₃, CH₂Cl₂, high dilution, RT, 1 d, 20%; **i)** B₂pin₂, Pd(dppf)Cl₂, KOAc, DMSO, 80°C, 6 h, 82%; **j)** 4-(2,2';6',2'')-terpyridine-4'-yl)phenyl-B(pin), Pd(PPh₃)₄, Cs₂CO₃, toluene/DMF, 120°C, 2 d, 66%; **k)** (pyridine-4-yl)B(pin), Pd(PPh₃)₄, Cs₂CO₃, toluene/DMF, 120°C, 2 d, 83%; **l)** (pyrimidine-5-yl)B(pin), Pd(PPh₃)₄, Cs₂CO₃, toluene/DMF, 120°C, 2 d, 83%. (pin = pinacolato; dppf = 1,1'-bis(diphenylphosphino)-ferrocene).

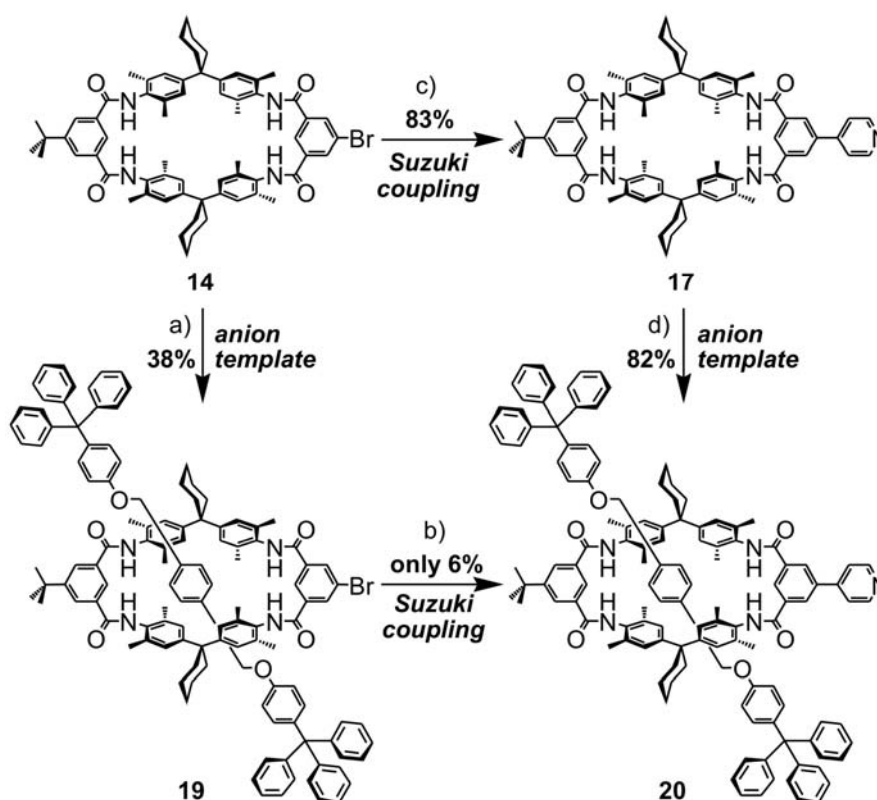
The first Suzuki cross-coupling reactions have been successfully performed with bromo-substituted **14** and the pinacol boronates of phenyl terpyridine, pyridine, and pyrimidine as shown in Scheme C2. This approach turned out to be much more fruitful as compared to the second possible variant, i.e. Suzuki cross-coupling of **15** with the corresponding halogenated heterocycles.^[96] The products **16 - 18** of these coupling reactions all carry heterocycles that can coordinate to transition-metal ions. This set of molecules can thus be connected to each other through the use of metal ions with their wide variety of coordination geometries.

C2.5 Rotaxane Synthesis

Scheme C3 shows attempts to synthesize rotaxanes with ether axles from some of the macrocycles following the anion-mediated template developed by Vögtle et al.^[97] Again, two different routes were explored. In order to shift the macrocycle functionalization step to an as late state of the synthesis as possible, we first attempted to generate the rotaxane **19** from bromo-substituted TLM **14**. Then, **19** may serve as a precursor for the attachment of a variety of different functional groups such as the pyridine finally yielding rotaxane **20**. This approach would have another, practical advantage. Some of the macrocycles cause solubility problems. As soon as the axle is present, the resulting rotaxanes are usually well soluble, since the interactions of macrocycles with each other in the crystal are disturbed by the stoppers protruding on both sides. Consequently, **19** would help to circumvent solubility problems. From the Suzuki coupling of the pinacol boronate of pyridine with **19** only a disappointingly low yield of approximately 6% of rotaxane **20** has been obtained. The rotaxane can easily be identified by mass spectrometry^[98] as well as its ¹H NMR spectrum. Axle protons that are located inside the cavity of the macrocycle experience a significant upfield shift of up to $\Delta\delta = 1.8$ ppm^[99] due to the anisotropy of the aromatic rings incorporated in the Hunter diamines.

One of the major side products of this reaction is the free axle. This finding may help to identify the reason for the low yield: Since the tritylphenol stoppers efficiently prevent deslipping of the axle even at elevated temperatures,^[100] such a process certainly is not the reason for this finding. Most likely, the cross-coupling catalyst activates the benzyl ether bond and causes it to open and close reversibly. Once it is cleaved, the mechanical bond is released and most of the rotaxane is thus destroyed.

In the second approach, the order of the two steps is reversed. The pyridine is attached first to macrocycle **14** furnishing **17** in an acceptable isolated yield of 83%. Rotaxane synthesis with **17** then provided rotaxane **20** with 82%. Thus, following this approach is by far superior as compared to the first strategy – at least when aiming at rotaxanes with ether axes. These experiments provide some insights into some limitations which may occur. However, these limitations are not grave, if one considers that the TLMs can also serve as wheels for rotaxanes with more stable amide axes^[85] that can certainly be expected to survive the conditions of the cross-coupling reactions.



Scheme C3: Synthesis of pyridyl rotaxane **20** using two different routes: **a)** α,α' -dibromo-*p*-xylene, 4-tritylphenol, dibenzo[18]crown-6, K_2CO_3 , CH_2Cl_2 , RT, 7 d, 38%; **b)** (pyridin-4-yl)B(pin), $Pd(PPh_3)_4$, Cs_2CO_3 , toluene/DMF, $120^\circ C$, 2 d, 6%; **c)** (pyridin-4-yl)B(pin), $Pd(PPh_3)_4$, Cs_2CO_3 , toluene/DMF, $120^\circ C$, 2 d, 83%; **d)** α,α' -dibromo-*p*-xylene, 4-tritylphenol, dibenzo[18]crown-6, K_2CO_3 , CH_2Cl_2 , RT, 7 d, 82%. (pin = pinacolato)

C2.6 Synthesis of Covalently Linked, Cross-Coupled Macrocycle Dimers and Trimers

In principle, the key intermediates described above can be converted into covalently linked FBMHs in two ways by (a) coupling two or more macrocycles to a common core or by (b) homo- or heterocoupling of two or more of the key intermediates directly to each other, thus simultaneously building the joint core. According to the first alternative, the divalent benzene-centered FBMH **22** (Scheme C4) has been afforded through a standard Suzuki coupling of bromo-substituted macrocycle **14** with diborylated benzene **21**, a readily available core component. The use of the brominated macrocycle requires elevated temperatures (around 120°C), but the yield of 90% is quite high. In a similar manner, the trivalent benzene-centered FBMH **24** could be synthesized in a Sonogashira reaction between readily available triethynylbenzene **25** and iodomacrocycle **11**. No separate core component is required for the Glaser-Hay homocoupling of two acetylene-substituted macrocycles **13** to the butadiyne-spacer dimer **25**. This reaction is an example for the second pathway described above.

The butadiyne product itself represents a functional group, which permits further functionalization: In a preliminary experiment, we reacted a few mg of **25** with $\text{Na}_2\text{S}^{[101]}$ and analyzed the raw product by mass spectrometry. In a quite clean ESI mass spectrum (Figure C4), minor amounts of reactant **25** are observed together with the product **26** (Scheme C4) which corresponds to the by far dominating signal. Such a transformation induces a change in the geometry of the tether connecting the two macrocycles.

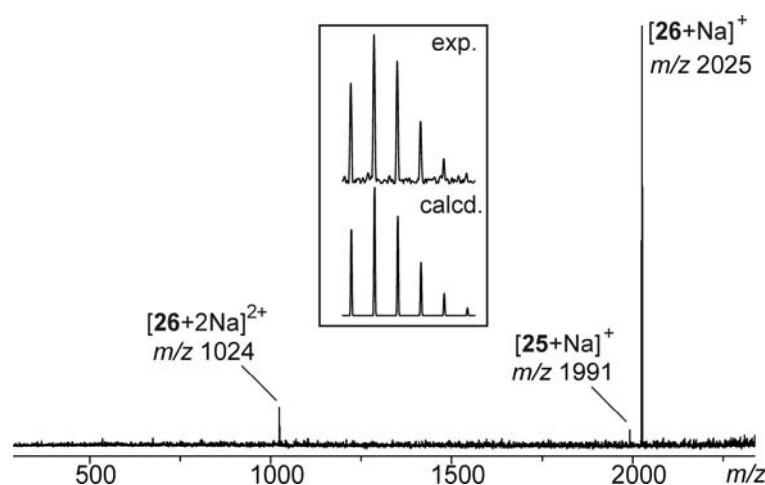
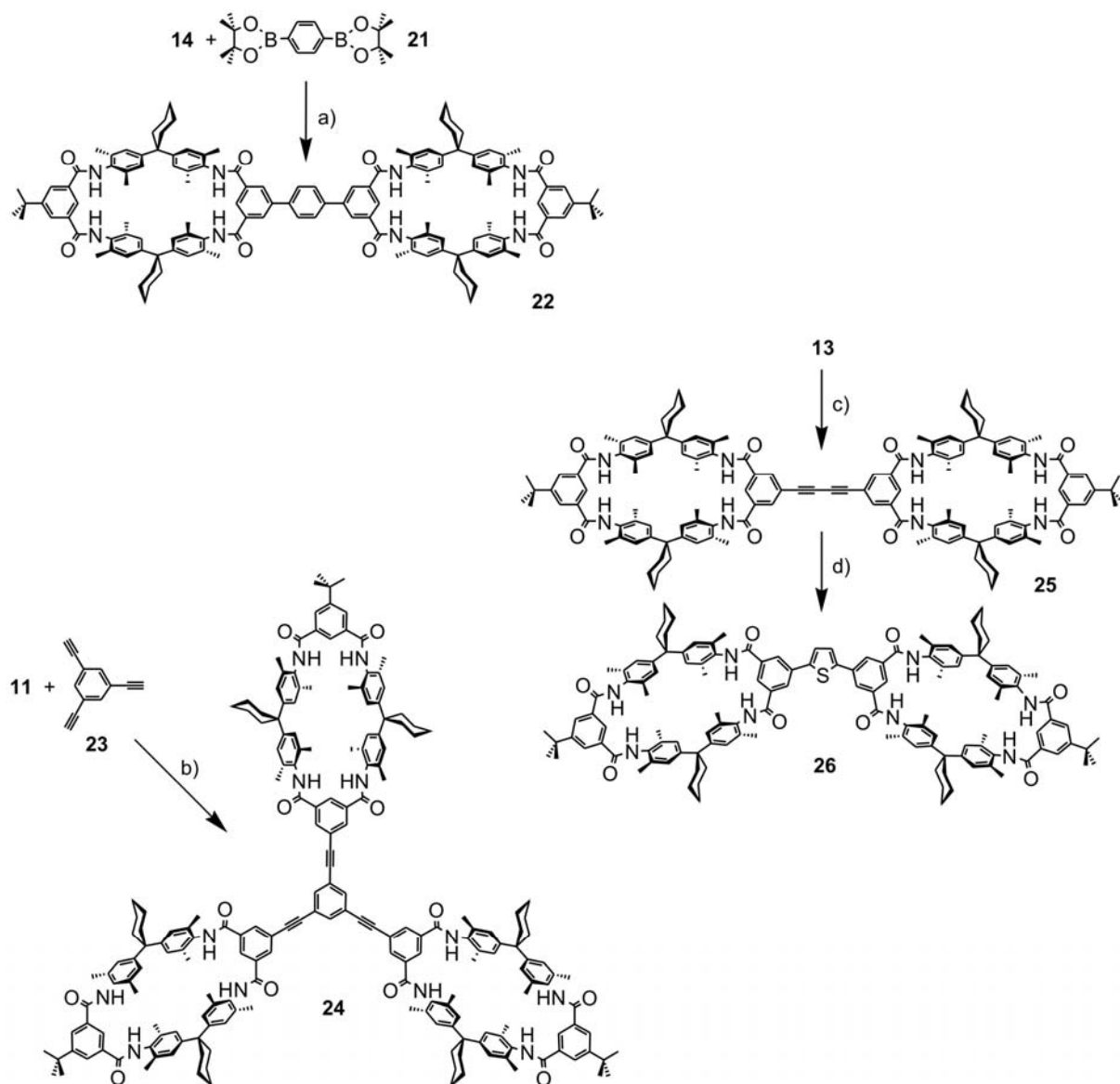


Figure C4: ESI-FTICR mass spectrum (ESI^{+}) of the raw product obtained from the reaction of **25** with $\text{Na}_2\text{S}\cdot(\text{H}_2\text{O})_x$ yielding thiophene-centered **26**.

These three examples of different coupling reactions, i.e. the Suzuki, the Sonogashira, and the Glaser-Hay reactions, together with the possibility to post-functionalize the butadiyne spacer may suffice to provide evidence for the utility of our toolbox concept. In the following, we now apply the concept to chromophore-substituted macrocycles and metal-coordination.



Scheme C4: Synthesis of FBMHs **22**, **24**, and **25**: a) Pd(PPh₃)₄, Cs₂CO₃, toluene, DMF, 120°C, 1 d, 90%;

b) CuI, PPh₃, Pd(PPh₃)₂Cl₂, NEt₃, DMF, RT, 40 h, 40%; c) CuCl, O₂, DMF, RT, 12 h, 26%;

d) Na₂S•(H₂O)_x, THF, 3 d, 60°C. (pin = pinacolato)

C2.7 Synthesis of Chromophore-Substituted Macrocycles

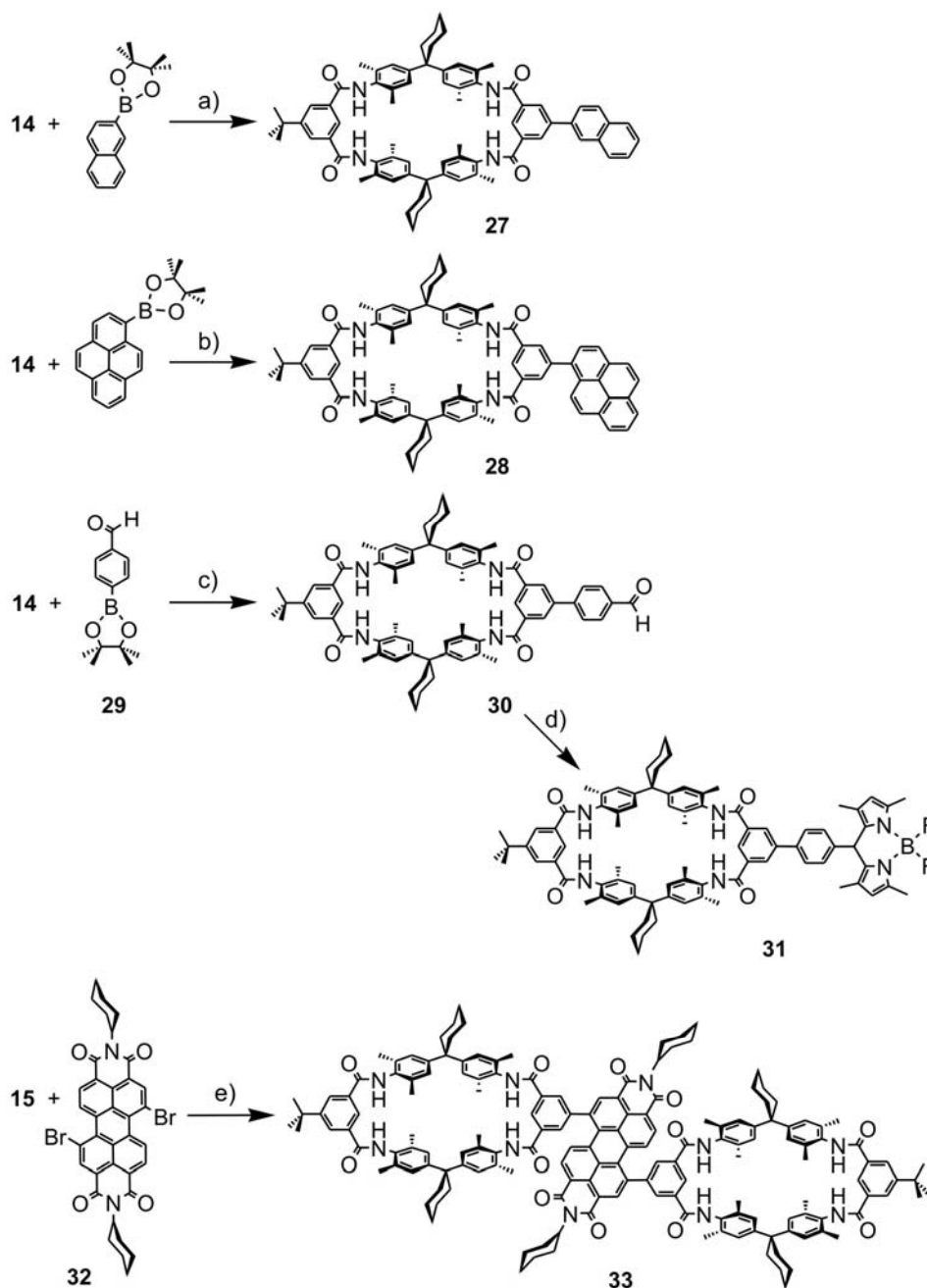
Scheme C5 shows the syntheses of chromophore-substituted macrocycles starting with either the bromo-substituted macrocycle **14** or the borylated analogue **15**. All cross-coupling reactions applied here are Suzuki reactions. A naphthyl group is easily coupled in good yields to one of the isophthalic acid moieties of the macrocycle providing easy access to **27**. Since pyrene boronic acid is commercially available, we initially attempted to use the triflate-substituted macrocycle **10** together with pyrene boronic acid in an analogous Suzuki coupling. Indeed, **28** could be isolated from that reaction, but only with a disappointingly low yield of 19%. Consequently, the procedure, which had been successful for naphthyl-attachment, has been applied and provided **28** in 87% yield.

BODIPY (BOron DIPYrrromethene) dyes are interesting chromophores because of their easy preparation, narrow absorption and emission bands, and high quantum yields which is of great importance for energy transfer and sensing processes.^[102] Thus, it seemed attractive to add a BODIPY-substituted macrocycle to the series of chromophore-substituted compounds presented here. Again, a Suzuki cross-coupling reaction can be used to synthesize the aldehyde precursor **30** from which the target compound **31** is available in a three-step one-pot reaction.^[103] The aldehyde is first converted into the corresponding dipyrromethane by acid-catalyzed reaction with 2,4-dimethyl pyrrole. The dipyrromethane is oxidized to the dipyrromethene with *p*-chloranil without workup of the intermediate. Finally, addition of $\text{BF}_3 \cdot \text{Et}_2\text{O}$ provides the desired product in 62% overall yield.

The last compound in the series of chromophore-substituted macrocycles, **33**, bears a perylene as the core connecting two macrocycles. It can most easily be prepared from the borylated macrocycle **15** and the dibromo perylene **32**. With 45%, the yield is somewhat lower than that for the other Suzuki reactions described so far which can be attributed to the rather low solubility of the mono-substituted intermediate.

The UV/VIS spectra for the latter three compounds **28**, **31**, and **33** shown in Figure C5 display the typical absorbance patterns of the photoactive groups in the host macrocycles. Up to 300 nm lies the absorbance of the phenyl rings within the macrocycle body (typical range is around 200 nm). In the case of pyrene and perylene macrocycles, absorbance maxima in the visible range are 348 nm and 548 nm respectively. The former maximum is not affected, when the solvent was changed from CH_2Cl_2 to acetonitrile whereas the latter shifts by about 10 nm which is again expected from the solvatochromic behaviour of 1,7-substituted perylene

dyes.^[104] The BODIPY macrocycle has the highest extinction coefficient ($67.200 \text{ M}^{-1} \text{ cm}^{-1}$ at 498 nm) with the typical sharp peak shape.



Scheme C5: Synthesis of chromophore-substituted macrocycles **27**, **28**, and **31** and FBMH **33**.

All coupling reactions are performed under standard Suzuki conditions ($\text{Pd}(\text{PPh}_3)_4$, Cs_2CO_3 , toluene, DMF, 120°C , 1 d) with the following yields: **a)** 76%; **b)** 87%; **c)** 84%; **e)** 45%.

The BODIPY-substituted macrocycle **31** was synthesized from **30** in a one-pot reaction with **d)** i) 2,4-dimethyl pyrrole, trifluoro acetic acid (cat.), ii) *p*-chloranil, iii) $\text{BF}_3 \cdot \text{Et}_2\text{O}$, 62%.

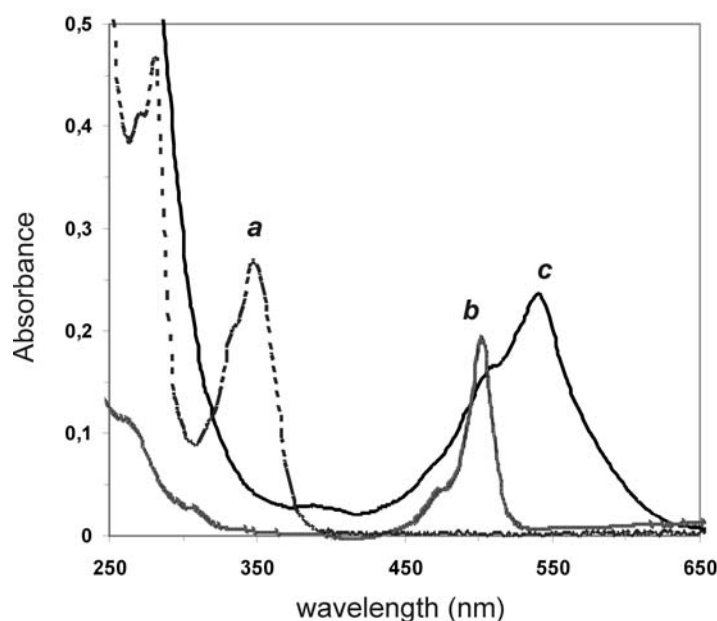
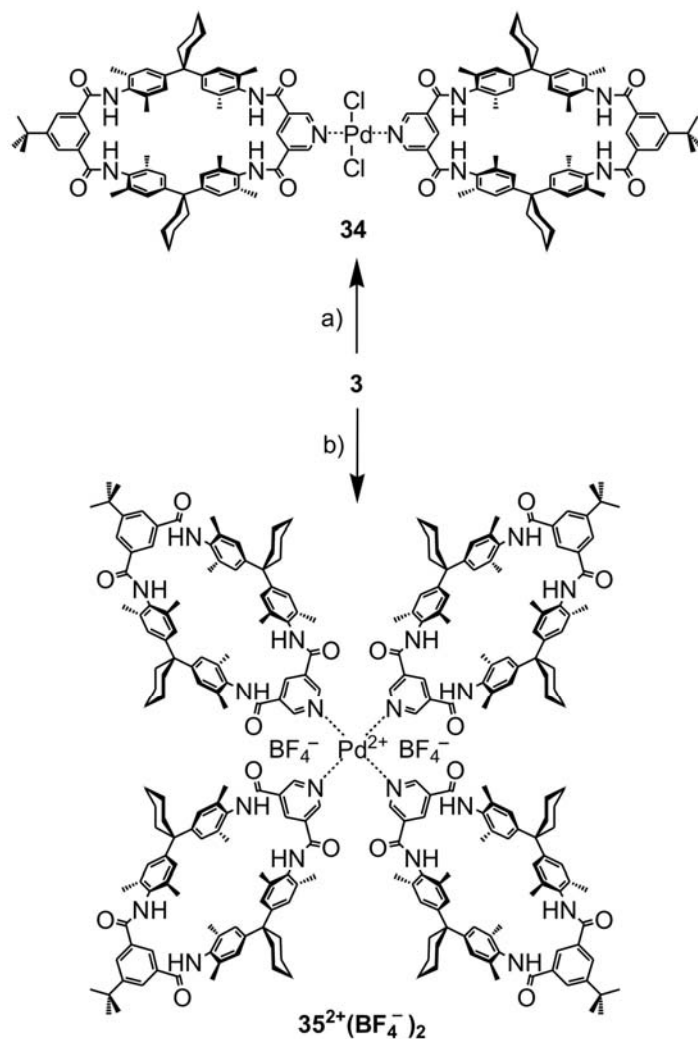


Figure C5: UV-spectra of **a)** pyrene macrocycle **28** ($1 \cdot 10^{-6}$ M; multiplied by 10), **b)** BODIPY macrocycle **31** ($5 \cdot 10^{-6}$ M), and **c)** FBMH **33** ($1.6 \cdot 10^{-5}$ M) in CH_2Cl_2 .

C2.8 Self-Assembly of Macrocylic Ligands to Metal-Centered FBMHs – Pyridine Coordination

Metal-directed self-assembly^[105] is a powerful approach to complex supramolecular structures with controllable, predefined sizes and geometries. It reduces the synthetic effort significantly which would be required for the generation of a similarly complex covalent molecule. Other advantages of metal coordination complexes are the variety of coordination geometries available, the quite large range of accessible binding energies allowing for weakly bound complexes that form reversible bonds as well as for kinetically quite inert coordination.

Macrocylics **3**, **16–18** have been equipped with different metal coordination sites. Two of these ligands, **3** and **17**, carry monodentate pyridine moieties pointing away from the macrocylics' cavities. Depending on the choice of the central metal complex, different number of macrocylics can be combined in different orientations. In this study, we have investigated the coordination to different d^8 -metal centers: *trans*- PdCl_2 , $(\text{CH}_3\text{CN})_4\text{Pd}(\text{BF}_4)_2$, and $(\text{dppp})\text{Pt}(\text{CF}_3\text{SO}_3)_2$. These metal centers provide access to quite different complex geometries.

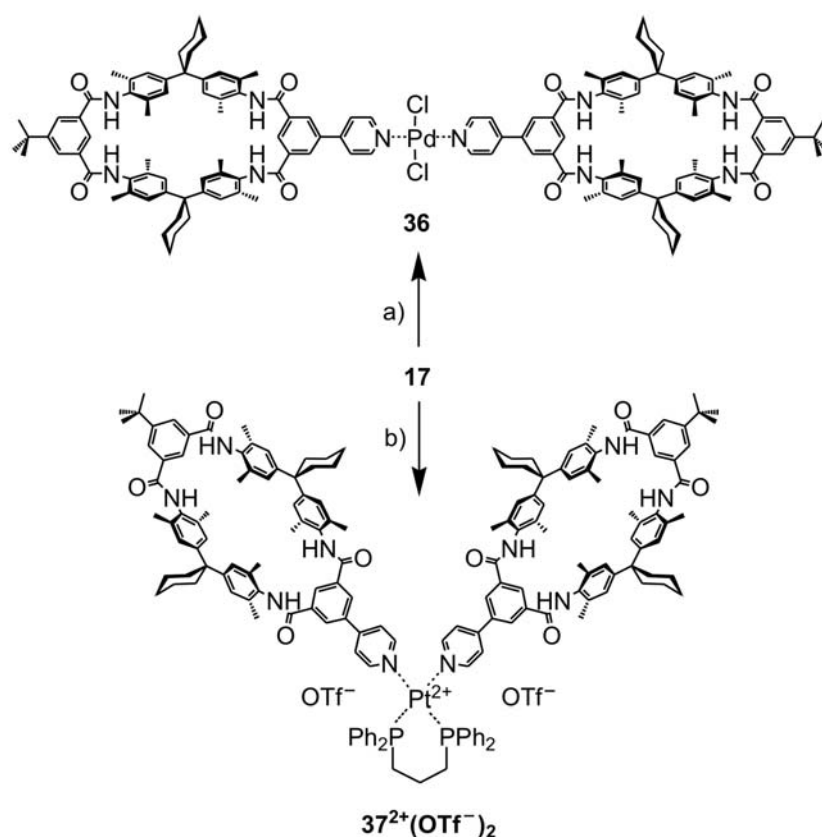


Scheme C6: Self-assembly of **34** and **35²⁺(BF₄⁻)₂**: **a)** PdCl₂(PhCN)₂, CH₂Cl₂, RT, 9 h, 49%;
b) [Pd(MeCN)₄](BF₄)₂, CDCl₃/CD₃CN, RT, 1 d, then cooling, 3 d, 33%.

When **3** was reacted with PdCl₂(PhCN)₂, which has two trans-oriented coordination sites blocked with chloride, divalent Pd-centered FBMH **34** precipitated as a pale yellow solid (Scheme C6). Analogously, FBMH **36** (Scheme C7) was obtained from macrocyclic ligand **17** which bears a peripheral pyridine attached to one of the isophthalic acid moieties. Furthermore, the tetravalent Pd-centered FBMH **35²⁺** was afforded as the tetrafluoroborate salt upon addition of [Pd(MeCN)₄](BF₄)₂ to **3**. By utilizing the *cis*-blocked platinum corner (dppp)Pt(OTf)₂, a reagent applied for the assembly of metallocsupramolecular squares^[106], we were able to obtain divalent Pt-centered FBMH **37²⁺** in which the macrocyclic parts are nearly perpendicular to each other. Since the pyridine rings prefer to coordinate to the metal in an orientation almost perpendicular to the plane defined by the four donor atoms around the

metal center, **3** and **17** result in different orientations of the macrocycles in the complex. In **35**²⁺, for example, the four macrocycles likely form a propeller-shaped arrangement with the cavities opening towards the neighbours. The analogous complex prepared from **17** would result in an arrangement, in which the pyridines obtain their preferred perpendicular orientation, while – due to the aryl-aryl bond – the macrocycles are in a more or less flat arrangement with their cavities opening to above and below the complex. Due to the larger macrocycle-metal distance, the rings can likely rotate without substantial rotation barriers caused by steric congestion.

The formation of metal-centered FBMHs is confirmed by ESI-MS spectra as well as by ¹H NMR spectra, in which the ortho pyridine protons show downfield shifts due to metal coordination. The (dppp)Pt(II) complex in **37**²⁺ has the particular advantage that the Pt-P coupling constants are very sensitive to the coordination of the two pyridines. The coupling constant in **37**²⁺ is ¹J(Pt-P) = 3023 Hz, while it is ¹J(Pt-P) = 3650 Hz in the (dppp)Pt(CF₃SO₃)₂ precursor, thus clearly indicating the coordination of the pyridine rings.



Scheme C7: Self-assembly of **36** and **37**²⁺(OTf⁻)₂: a) PdCl₂(PhCN)₂, CH₂Cl₂, RT, 16 h, then 40°C, 1h, 44%;
b) Pt(dppp)(OTf)₂, DMF, 10 min, quantitative. (dppp = 1,3-bis(diphenylphosphino)propane)

C2.9 Crystal Structure of Metal-Centered FBMH **34**

When **34** was dissolved in approximately a 2:1:1 mixture of 1,4-dioxane, dichloromethane, and methanol and the solution was left to stand in a parafilm-closed test tube for two months, pale-brown needle-like single-crystals of **34**^[107] were obtained. According to X-ray crystal structure analysis, two molecules of **3** are bound to the Pd center through their pyridine moieties, forming the expected square-planar *trans*-Pd-complex (Figure C4a). Since each corner of the unit cell, which is the crystallographic inversion center in the $P\bar{1}$ space group, is occupied by a Pd atom, **34** is a perfectly centro-symmetric molecule in the solid state. Compared to the crystal structure of **3**, the striking difference is that all macrocycles are arranged in the “all-in” conformation, indicating **34** to be a suitable host for the formation of multiply interlocked architectures (MIAs). A highly interesting feature of the crystal packing

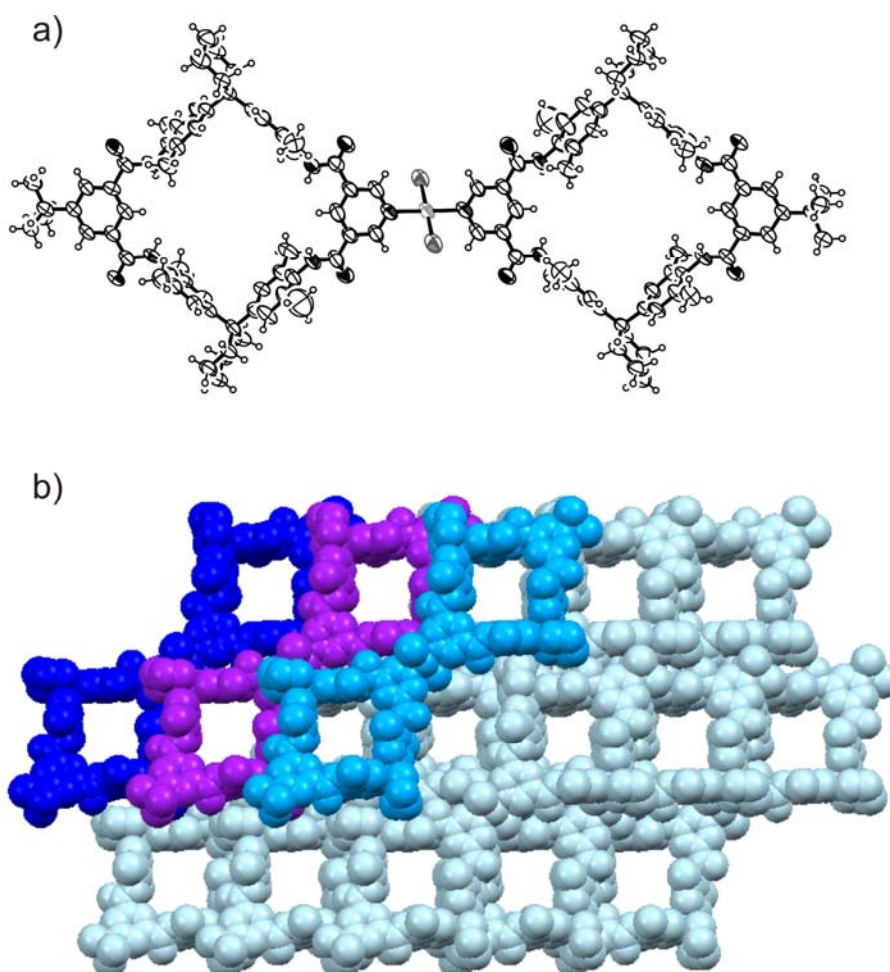
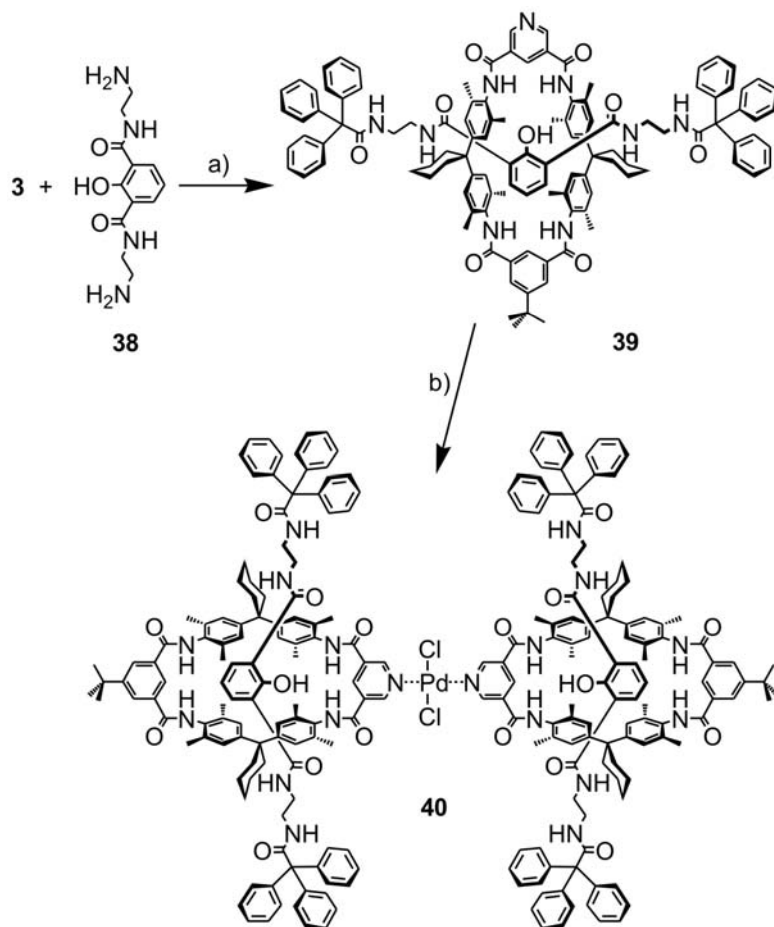


Figure C6: Crystal structure of **34** (solvent molecules are omitted for clarity): **a)** ORTEP plot (shown with 50% probability ellipsoids). **b)** Crystal packing, space-filling view along the diagonal between the crystallographic axes a and $-c$, showing the infinite channels.

is the existence of infinite channels passing through the macrocyclic cavities (Figure C4b). The channels, which are filled with quite disordered solvent molecules in the crystal, might be an interesting structural element for applications going beyond the use for MIA formation.

C2.10 Synthesis and Molecular Modeling of MIA 40

As a proof-of-principle for the formation of multiply interlocked architectures through metal coordination, rotaxane **39** has been synthesized and subsequently coordinated to a *trans*-PdCl₂ center. The rotaxane can easily be made through our previously published anion template procedure.^[84c] Axle center-piece **38** is deprotonated at the phenolic hydroxy group. The anion can – supported by one of the carbonyl groups – then form rather strong hydrogen bonds with TLM **3**. The axle center piece is fixed inside the wheel in an orientation which ensures that triphenyl acetyl stoppers are attached to the two amino groups from opposite sides of the macrocycle. The axle is thus trapped in the cavity; a rotaxane forms. The mechanically interlocked structure of the rotaxane can be identified from strong upfield shifts of the ¹H NMR signals of those protons that are located in the macrocycle cavity. For **39**, the methylene spacers between the stoppers and the central phenol are affected most ($\Delta\delta = 0.9 - 1.0$ ppm; see analytical data below). The threaded topology can also be determined from tandem MS experiments. In these experiments, fragmentations are induced by collisions of the mass-selected rotaxane ions with a collision gas (Ar) in an FTICR mass spectrometer. Mass-selected **39** was thus subjected to this experiment. The same experiment was then conducted under exactly the same conditions with a 1:1-mixture of macrocycle **3** and the free, stoppered axle. During ionization these two components form a non-interlocked, hydrogen-bonded complex with the same *m/z* as **39**. The two MS/MS spectra differ much: The MS/MS spectrum of **39** still shows the rotaxane ion as the base peak while the free axle appears as a fragment with approximately 30% relative intensity accompanied by axle fragments. In the same experiment conducted with the hydrogen bonded complex, all parent ions have dissociated and the free axle is the only fragment visible. This indicates that it is energetically much easier to dissociate the hydrogen bonded complex than to fragment the rotaxane, in which a covalent bond needs to be broken in order to release the mechanical bond. We have reported similar experiments on an analogous rotaxane before with a similar outcome.^[84c,98] Consequently, the rotaxane has unambiguously formed.



Scheme C8: Synthesis of rotaxane **39** and assembly of MIA **40**: **a)** *t*-butylimino-tris(dimethylamino)-phosphorane (P_1 base), NEt_3 , triphenylacetyl chloride, CH_2Cl_2 , RT, 3 d, 14%;
b) $\text{PdCl}_2(\text{PhCN})_2$, CH_2Cl_2 , RT, 1 d, then cooling, 7 d, 11%.

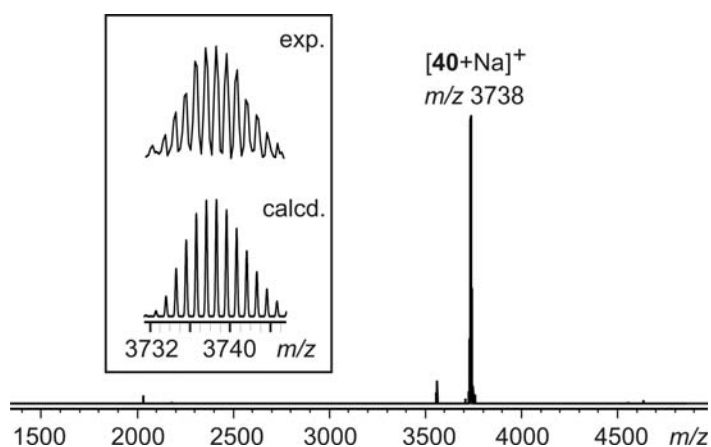


Figure C7: ESI-FTICR mass spectrum (ESI^+) of MIA **40**.

Subsequently, **39** was reacted with $\text{PdCl}_2(\text{PhCN})_2$ affording MIA **40** through metal-directed self-assembly. In the ESI-FTICR mass spectrum of **40**, the only intense ion observed is the sodium adduct of **40**, showing the quite high stability of this rotaxane dimer (Figure C7). The characteristic isotope pattern confirms the presence of the PdCl_2 unit. Compared to **39**, a downfield shift of the ortho pyridine protons was found in the ^1H NMR spectrum of **40**. For getting an idea of the structure of **40**, molecular modeling calculations were performed with the augmented MM2 force field implemented in the CAChe 5.0 program^[108]. Figure C8 shows one example out of many possible low-energy conformations of **40**.

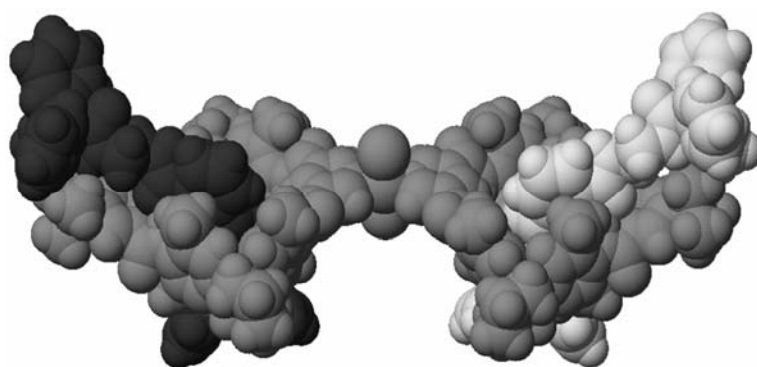


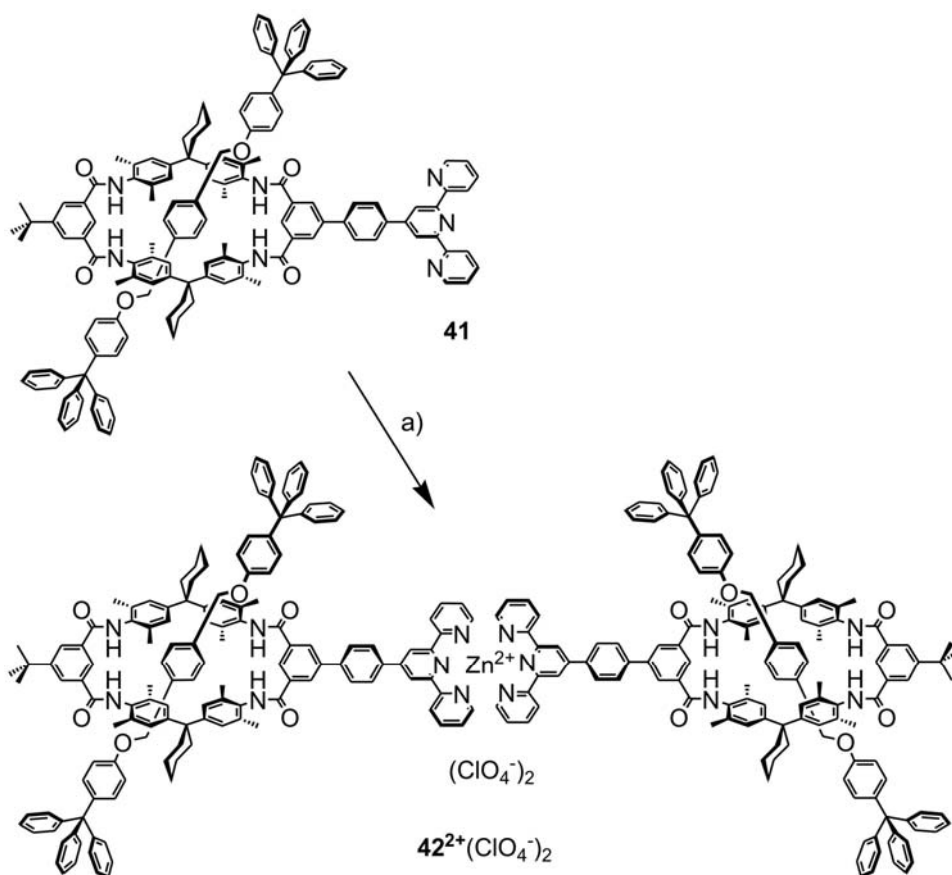
Figure C8: Space-filling representation of one example out of many possible low-energy conformations of MIA **40** calculated at MM2 level (dark gray: FBMH part of the MIA; black and light gray: axle components).

C2.11 Self-Assembly of Macrocyclic Ligands to Metal-Centered FBMHs – Terpyridine Coordination

From terpyridine-substituted macrocycle **16**, rotaxane **41** (Scheme C9) was synthesized by the same procedure as that used for **19**. Again, rotaxane synthesis is successful, if carried out after the cross-coupling of the terpyridine moiety to the bromo-macrocycle **14**. Figure C9 (top) shows the aromatic region of the ^1H NMR spectrum of **41**. The threaded topology of the rotaxane can easily be determined from the unusual upfield shifts of the protons located at the axle center-piece (labeled *a*, *b*, and *c*). They experience the anisotropy of the macrocycle's aromatic rings. In comparison to the signals of the free axle, proton *a* shifts by approximately 1.7 ppm to higher field.

When half an equivalent of zinc perchlorate is added to the solution of rotaxane **41**, a ^1H NMR spectrum is obtained which contains only one set of well-resolved signals and thus indicates that only one complex, i.e. the Zn(II)-bridged dimer of the rotaxane, is almost

quantitatively formed. Most of the signals in the aromatic region are shifted to some extent upon complexation of the rotaxane to the metal ion.



Scheme C9: Synthesis of the dimeric Zn(II) complex 42^{2+} of rotaxane **41**. a) $\text{Zn}(\text{ClO}_4)_2 \cdot 6\text{H}_2\text{O}$, CDCl_3 , r.t., quant.

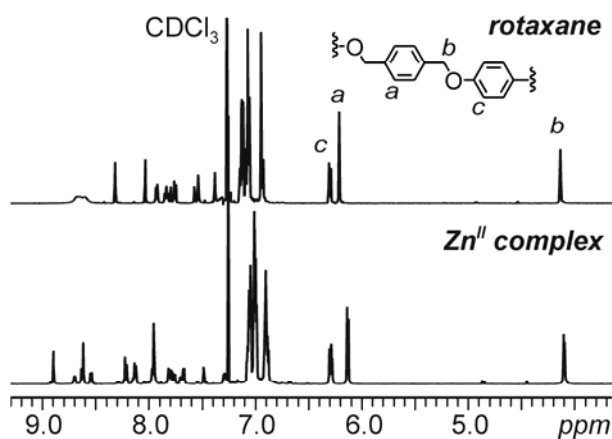


Figure C9: Top: Partial ¹H NMR spectrum of rotaxane **41** synthesized from terpyridine-substituted macrocycle **16**. Unusual upfield shifts of the protons *a*, *b*, and *c* of the axle centerpiece indicate rotaxane formation. Bottom: Partial ¹H NMR spectrum of the dimeric Zn(II) complex 42^{2+} of the rotaxane. The appearance of one set of sharp signals at positions shifted relative to those observed for the rotaxane indicates quantitative complex formation.

C3 Final Conclusions and Outlook

In this study, we have developed a toolbox of building blocks on the basis of tetralactam macrocycles for the supramolecular assembly of more complex, multiply interlocked architectures. We can draw the following conclusions:

(a) A quite limited set of five key intermediates, i.e. macrocycles that bear substituents suitable for cross-coupling reactions, serves as the basis for quite different purposes. Simple organic spacers can be used to connect several macrocycles around a common core providing access to multivalent host molecules. Photoactive groups can be attached and may have potential for future energy-transfer studies. Metal-binding sites are easily coupled to the macrocycles which can then coordinate to a metal center serving as a non-covalent core. Consequently, a large variety of different structures is now available based on the small set of key intermediates.

(b) Different key intermediates open the opportunity to use almost any kind of cross-coupling reaction. Iodinated, brominated, and borylated macrocycles have proven to be excellent precursors for Suzuki cross-coupling reactions. Iodinated and alkinylated derivatives can be utilized in Glaser-Hay or Sonogashira reactions. Even the tosylated macrocycle reacted in coupling reactions, however with unsatisfactory yields. This variety of different reactions increases the range of accessible structures drastically.

(c) Although only shown for one example, some of the cross-coupling products can be converted into different functional groups after the cross-coupling reaction, again providing access to different geometries.

(d) Rotaxanes can be made from almost all macrocycles reported in this study – maybe with the exception of the borylated macrocycle **15**, which we did not test in the threading reaction. As a proof of principle, we synthesized two types of rotaxanes, one of which bears benzyl ether axles, the other one an amide axle. The benzyl ethers do not survive a Suzuki coupling due to the Lewis acidity of the catalyst. This finding points to a limitation of our approach which however can be circumvented by the use of other, more stable axles.

(e) The formation of metal complexes has been demonstrated up to a tetravalent complex of the pyridine macrocycle.

The present toolbox-approach to macrocyclic and interlocked molecules is thus extremely versatile in several different aspects and opens a new playground for supramolecular synthesis which can rely on a large set of different structures accessible from our five key intermediates. The synthetic approach is a convergent one, since more complex substituents that are to be

coupled to the macrocycles can be prepared independently from macrocycle synthesis and then be coupled to it afterwards.

D. Conformationally Flexible Tetralactam Macrocycles: An X-ray Study^[f] [109]

D1 Purpose of the Study and Introduction

Since their first preparation more than a decade ago, Hunter's tetralactam macrocycles ("TLM")^[82a,110] have gained more and more importance in supramolecular chemistry, as they are widely used not only as hosts for small guest molecules,^[110,111] but also as ring components in mechanically interlocked architectures such as pseudorotaxanes,^[84b] rotaxanes,^[84a,c,d,100b] and catenanes.^[82a,86,112] These easily accessible, chemically stable macrocycles bear four amide groups capable to form hydrogen-bonding patterns on which guest binding and templated syntheses of catenanes and rotaxanes are based.

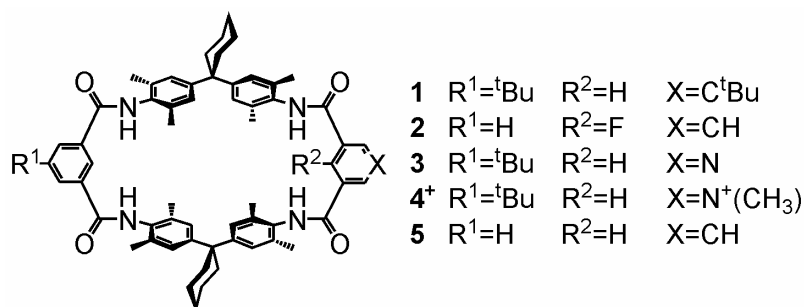
According to theoretical calculations,^[83a,113] TLMs exhibit a certain degree of conformational flexibility in that the amide groups and the *m*-xylene rings can quite easily be rotated. This essential structural feature certainly contributes to enhancing their versatility as building blocks in supramolecular chemistry, because they keep their overall shape, but can nevertheless adapt to the special steric requirements of their binding partners. One can safely assume that the secondary amide groups in the TLMs are *trans*-configured. Rotation about the amide C–N bond is thus unfavorable. Theory predicts a barrier lower than 30 kJ/mol for rotation of the *whole* amide group from an A_{in} (amide group with NH converging into the cavity) into an A_{out} (amide NH pointing away from the cavity) conformation. Consequently, an *all-in*, a *3-in-1-out*, and two different *2-in-2-out*^[114] conformations are predicted to be accessible within an energy range of approx. 8 kJ/mol.^[113] Significant strain is however generated when both amides of the same isophthalamide adopt the A_{out} conformation so that for example a *1-in-3-out* conformation is unfavorable in energy. In the following, three aspects are discussed based on X-ray crystal structures of TLMs **1** – **5** (Scheme D1): **(i)** The conformational freedom of the amide groups, **(ii)** the effects of the presence of guests on the

[f] The results of section D were obtained in collaboration with Dr. Martin Nieger (at Laboratory of Inorganic Chemistry, Department of Chemistry, University of Helsinki, Finland), Dr. Jörg Daniels (at Institut für Anorganische Chemie, Universität Bonn / University of Bonn, Germany), Dr. Thorsten Felder (member of the research group of Prof. Dr. Christoph A. Schalley at the Institut für Chemie und Biochemie, Freie Universität Berlin / Free University of Berlin), Dr. Iordan Kossev, Prof. Dr. Moritz Sokolowski (both at Institut für Physikalische und Theoretische Chemie, Universität Bonn / University of Bonn, Germany), Dr. Thomas Schmidt and Prof. Dr. Fritz Vögtle (both at Kekulé-Institut für Organische Chemie und Biochemie, Universität Bonn / University of Bonn, Germany). The results of section D were published in ref. [109].

cavity shape and the orientation of *m*-xylene rings, and (iii) intermolecular hydrogen bond formation in the crystals.

D2 Results and Discussion

X-ray quality crystals^[115] of TLMs **4**⁺ and **5** (Scheme D1) were obtained in different ways: **4**⁺ was crystallized by slow evaporation of CDCl₃, whereas needle-like crystals of **5** were obtained through gradient vacuum sublimation at 1•10⁻⁵ mbar and a sublimation temperature of 600-630 K.^[116] For comparison, we include the previously published crystal structures of **1**,^[117] **2**,^[118,119] and the crystal structure of **3** described in section C2.3. Note that TLM **3** is an exceptional case, since two different conformers (**3A**, **3B**) coexist in the crystal structure in a 1 : 2 ratio.



Scheme D1: Chemical structures of TLMs **1**–**5**.

The first aspect to be discussed concerns the amide conformations in the solid state (Figure D1). The *all-in* conformer is observed for TLMs **1**, **3A**, and **5**, while **2** and **3B** adopt the *2-in-2-out* and **4**⁺ the *3-in-1-out* conformation. According to calculations,^[83a,113] the *all-in* conformation is the slightly more favorable one and enables the formation of two bifurcated hydrogen bonds for guest binding within the TLM's cavity. Thus, this conformation was not only found in the crystal structures of **1** and **3A**, in which solvent molecules and Cl⁻ anions are hydrogen-bonded to the four A_{in} protons. It is also observed in crystal structures of TLM-containing [2]rotaxanes^[84c,120] and [2]pseudorotaxanes,^[84b] in which the axle is hydrogen-bonded to the TLM part in the same manner. In contrast, the less common *3-in-1-out*

conformer has one “inverted” amide group A_{out} which can serve both as hydrogen-bond donor for the exterior and as acceptor for the interior of the cavity. The latter is essential for TLM-containing [2]catenanes which form an interesting network of six hydrogen bonds between the two wheels. This pattern is not only observed in the crystal structures^[112,121] of the final catenanes, but also is believed to play a pivotal role in their templated synthesis.^[113] TLM **4**⁺ is still unique in being the only TLM displaying a *3-in-1-out* conformation in the solid state so far without being incorporated in a catenane. A second A_{out} group is present in the *2-in-2-out* conformation, which has been observed in the solid state structures of **2**^[118] and **3** (conformer **3B**). This conformation is less effective for guest binding, but facilitates the formation of *intermolecular* hydrogen-bond networks (for *intermolecular* hydrogen bonding distances, see Table D1). The solid-state structures of **1** – **5** thus ideally confirm theoretical predictions. The *all-in*, the *3-in-1-out*, and the *2-in-2-out* conformations all exist in the crystals and thus must be quite close in energy and connected through rather low barriers for amide group rotation.

Although the conformations of the amide groups affect the cavity shape by slightly distorting its rhomboid form, an overall open cavity is still retained, as long as the *m*-xylene moieties are more or less perpendicular to the overall plane of the macrocycle. In almost all crystal structures of TLMs known so far, guests such as solvent molecules or anions are present inside the cavity. The *m*-xylene rings accommodate the guests by adopting tilt angles relative to the macrocycle plane^[122] between 56° and 90° (Table D2). This is for example true for **1** and **2** which both host two ethyl acetate molecules in their cavities (Figure D1a,b). Chloride anions are the guests in the crystal of **3** implying that at least some of the TLM pyridine rings are protonated. Also for **3A** and **3B**, the tilt angles are within the above range. The only exception is the crystal of TLM **5**. This crystal was obtained by sublimation of the macrocycle and thus is - in contrast to all other examples - entirely free of solvent and guest molecules. In **5**, the two *m*-xylene rings X1 are nearly coplanar with the macrocycle plane with tilt angles as low as 4.6° (Figure D1f, Table D2). This causes the open macrocyclic cavity to be partly closed. We call this structure the “closed-doors” conformation. A comparison of the space-filling representations of the structures of **1** and **5** (insets, Figure D1) shows the differences between the open and the closed cavity. The “closed-doors” conformation of **5** might be advantageous in that it allows a more compact packing, but it is unsuitable for hosting guests. The marked differences in the tilt angles of the *m*-xylene rings depend on the presence of guest molecules and thus confirm that the macrocycle is quite easily able to adapt to the guest molecule's shape.

(to be continued after Figure D4)

TLM	Donor–H…Acceptor (D–H…A)	d(D–H)	d(H…A)	d(D–A)	∠(DHA)
2 ^[a]	N1–H1…O1	0.89	2.13	3.01	171.5°
3 ^[a]	N1B–H1B…O1A ^[b]	0.88	1.99	2.85	166.7°
	N2B–H2B…O2A ^[b]	0.88	1.98	2.81	157.0°
4 ⁺	N4–H4…I1 [−]	0.88	2.93	3.77	159.4°
	C1–H1…O1	0.98	2.36	3.10	131.2°
	C3–H3…O3	0.98	2.49	3.21	129.4°
	C1–H1…O2	0.98	2.49	3.28	138.1°
	C2–H2…O2	0.95	2.16	3.03	151.8°
5 ^[a]	N1–H1…O1	0.89	2.09	2.97	177.1°
	N2–H2…O1	0.86	2.37	3.21	167.5°

Table D1: Intermolecular hydrogen bonds for **2–5** between the atoms labeled in Figure D1 (the patterns are depicted in Figure D2). Hydrogen bonds with d(H…A) more than 2.5 Å (except for amide-iodine interaction) are not listed in the Table.

Footnote for Table D1: [a] Symmetry transformations used to generate equivalent atoms: $-x + 1, -y + 1, -z + 1$.

[b] "A" and "B" denote the two crystallographically independent molecules found in the crystal of **3**.

TLM	Angles between macrocycle plane and <i>m</i> -xylene planes ^[a]				Angles between macrocycle plane and amide planes ^[b]			
1	60.4	60.4	83.1	83.1	16.7 (<i>A</i> _{in})	16.7 (<i>A</i> _{in})	30.7 (<i>A</i> _{in})	30.7 (<i>A</i> _{in})
2	68.8	68.8	75.0	75.0	32.6 (<i>A</i> _{in})	32.6 (<i>A</i> _{in})	44.4 (<i>A</i> _{out})	44.4 (<i>A</i> _{out})
3A ^[c]	82.9	82.9	85.9	85.9	11.5 (<i>A</i> _{in})	11.5 (<i>A</i> _{in})	24.7 (<i>A</i> _{in})	24.7 (<i>A</i> _{in})
3B ^[c]	56.2	64.4	70.6	86.2	11.0 (<i>A</i> _{out})	16.2 (<i>A</i> _{in})	16.5 (<i>A</i> _{out})	25.4 (<i>A</i> _{in})
4 ⁺	77.9	80.8	82.5	87.9	8.1 (<i>A</i> _{out})	27.1 (<i>A</i> _{in})	27.4 (<i>A</i> _{in})	36.4 (<i>A</i> _{in})
5	4.6	4.6	88.7	88.7	22.8 (<i>A</i> _{in})	22.8 (<i>A</i> _{in})	50.3 (<i>A</i> _{in})	50.3 (<i>A</i> _{in})
∅ ^[d]	71.9				24.2 (<i>A</i> _{in}) 21.6 (<i>A</i> _{out})			

Table D2: Tilt angles relative to the macrocycle plane for **1–5**, given in degrees (°).

Footnote for Table D2: [a] The “*m*-xylene plane” is defined by the least-squares fit plane through all the six aromatic carbons of the corresponding *m*-xylene ring. [b] The “amide plane” is defined by the least-squares fit plane through the four atoms H–N–C=O of the corresponding amide group. [c] "A" and "B" denote the two crystallographically independent molecules found in the crystal of **3**. [d] Average value from the dataset of ten TLMs or TLM-containing compounds (X-ray structures of TLMs **1–5** and CCDC-182/213, CCDC-161428, CCDC-253084, CCDC-687762).

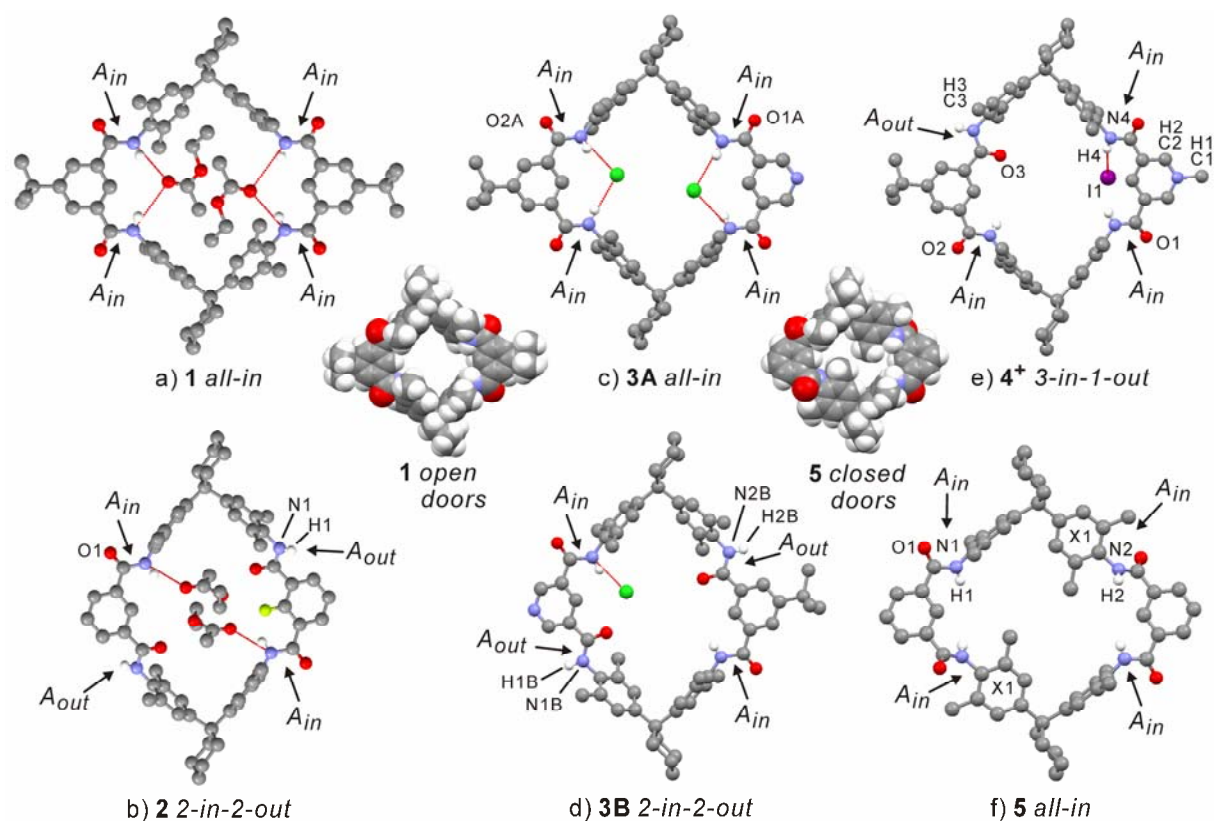


Figure D1: X-ray crystal structures of: a) **1**, b) **2**, c) **3A**, d) **3B**, e) **4⁺**, and f) **5**, all shown in ball-and-stick representation. Hydrogen bonds to guest molecules or anions are shown as red, dotted lines. Color code: C grey, Cl green, F yellow, H white, I purple, N blue, O red. H atoms (except amide protons), and other solvents or anions that are not hydrogen-bonded to the TLMs are omitted for clarity. The two insets display the space-filling plots for **1** and **5**, highlighting the "open doors" and "closed doors" conformations.

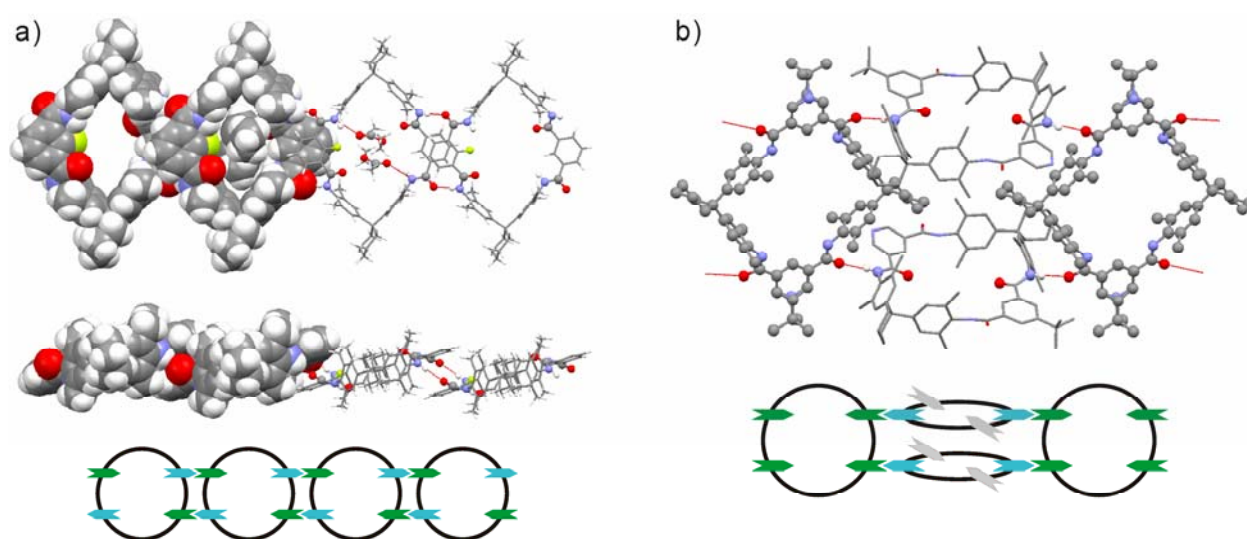


Figure D2: Hydrogen-bonding patterns of a) **2**, b) **3**, shown in a combination of stick, ball-and-stick and space-filling representation (H atoms except for the amide protons are omitted for **3**). For clarity, a cartoon illustrates the patterns in which amide groups are involved. Hydrogen bonds appear as red dotted lines.

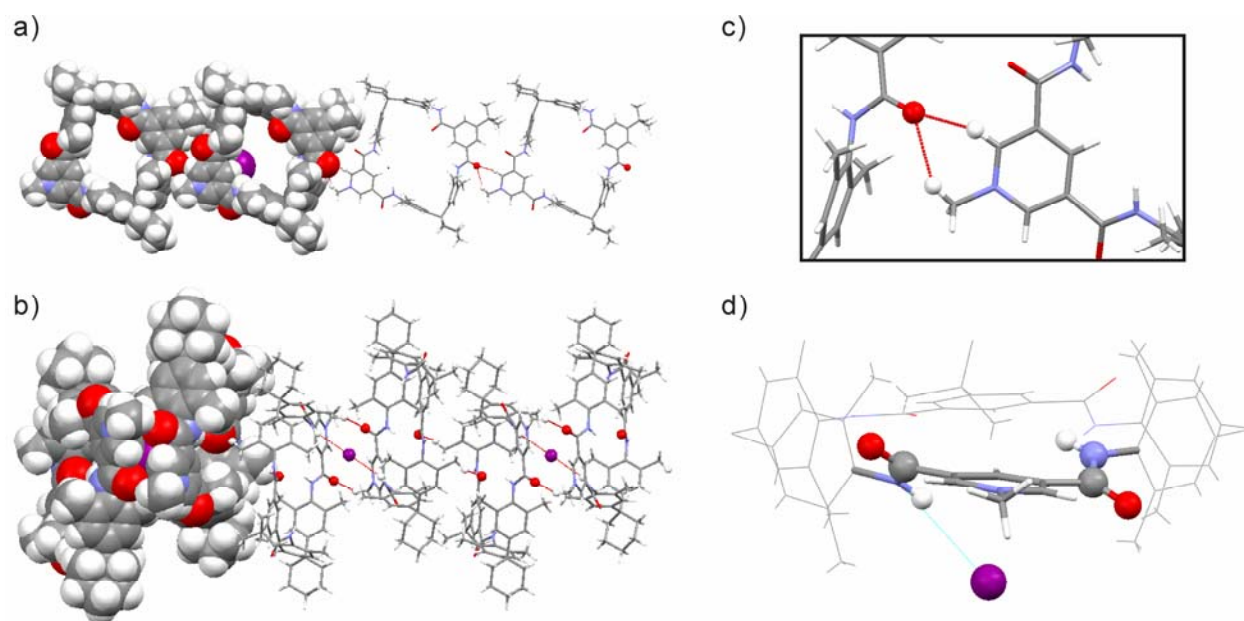


Figure D3: Hydrogen-bonding pattern of 4^+ , **a)** view along crystallographic axis c , **b)** view along crystallographic axis b , shown in a combination of stick, ball-and-stick and space-filling representation, with hydrogen bonds appearing as red dotted lines. **c)** Enlarged view of the bifurcated C–H \cdots O=C hydrogen bond of 4^+ . **d)** View parallel to the macrocycle plane of 4^+ showing the two A_{in} groups pointing into different hemispheres which are separated by the macrocycle plane.

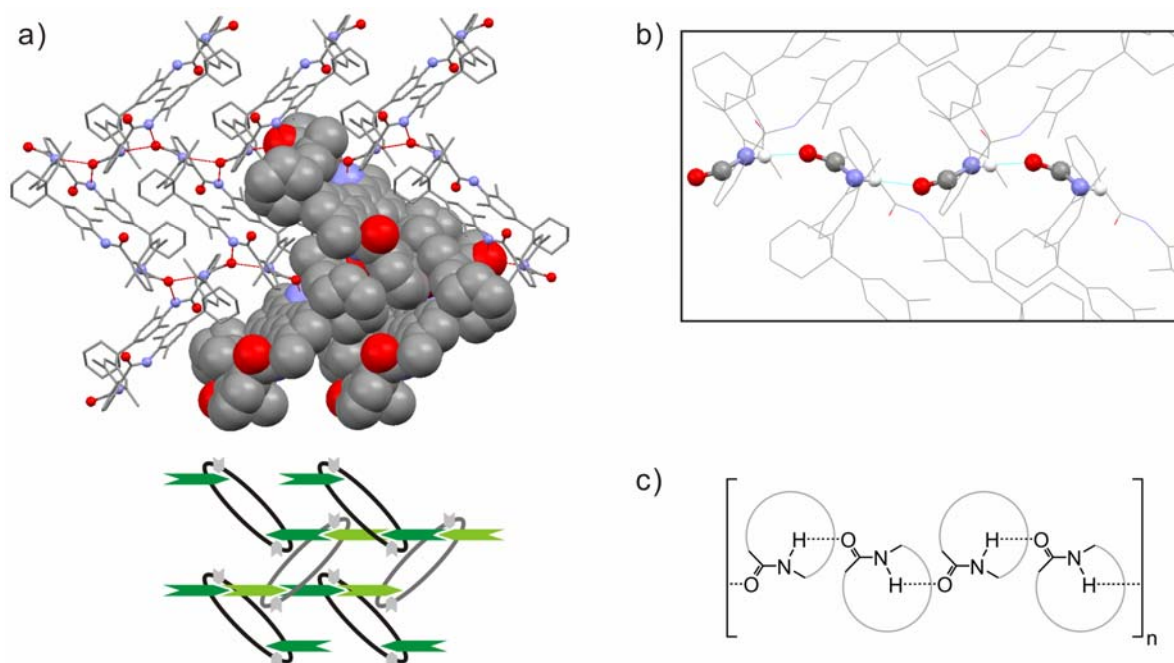


Figure D4: **a)** Hydrogen-bonding pattern of 5 , shown in a combination of stick, ball-and-stick and space-filling representation (all H atoms omitted). For clarity, a cartoon illustrates the patterns in which amide groups are involved. **b)** Enlarged view of the amide catemer motif in 5 . **c)** Schematic representation of this catemer motif.

The reason for the realization of different amide conformations are specific *intermolecular* hydrogen-bonding patterns (for H-bond lengths, see Table D1). The binding energy liberated upon the formation of intermolecular hydrogen bonds counterbalances the small energy differences between the different conformations. We will not discuss **1** here, since no intermolecular hydrogen bonds are found in the crystal. The *all-in* conformation merely results in the binding of two ethyl acetate molecules inside the cavity.

Besides the formation of one hydrogen bond to each of the two ethyl acetate guest molecules inside the cavity, the *2-in-2-out* conformer in the crystal of **2** forms a pair of intermolecular N–H•••O=C hydrogen bonds between the two symmetry-equivalent A_{out} protons H1 and A_{in} oxygen atoms O1 of the two neighboring molecules. Each TLM molecule **2** is thus connected with the next neighbors through a total of four hydrogen bonds and becomes a self-complementary building block, which assembles to a hydrogen-bonded homopolymer with the shape of an infinite ladder (Figure D2a). To allow this H-bonding pattern to form, the isophthaloyl units of two adjacent molecules are stacked upon each other and the amide groups of **2** must be significantly tilted out of the overall macrocycle plane. The deviation from coplanarity of 44.4° ^[123] is unusually large for TLMs (Table D2). Quite interestingly, the same hydrogen-bonding motif has been observed recently for monolayers of **5** on Au(111) surfaces by ultrahigh-vacuum scanning tunneling microscopy (UHV-STM). The solid-state structure of **2** thus nicely supports the structural model which was based on the STM images and theoretical calculations of TLM trimers.^[116] Variations of this pattern have been observed by STM: Two different types of domains have been observed in the monolayer of **5** - one, in which infinite ladders of macrocycles cover the surface and one, in which trimers of **5** exist forming the same H-bonding pattern as that found in the crystal of **2**.^[116]

In contrast to **2**, the *2-in-2-out* conformation of **3** (**3B**) coexists with the corresponding *all-in* conformation (**3A**)^[124] in the solid state in a 2:1 ratio. This results in a quite different hydrogen-bonding pattern: The two conformers are interconnected by intermolecular N–H•••O=C bonds between all A_{out} protons of **3B** and all A_{in} oxygens of **3A**, thus forming a hydrogen-bonded “copolymer”, again as an infinite ladder (Figure D2b). Furthermore, the A_{in} protons of **3A** and **3B** interact with chloride anions.

In the X-ray crystal structure of **4**⁺, all solvent molecules and half of the counteranions cannot be fully resolved because they are disordered. The other half of the iodide anions can be located within the crystal lattice. Each of these iodide anions (I1 in Figure D1e) is connected to two TLMs through weak hydrogen bonds to their A_{in} proton H4 (Figure D3b). The intermolecular hydrogen-bonding pattern is quite unusual in that four C–H•••O=C

interactions are observed (Figure D3a,c): **(i)** between the A_{in} oxygen O1 and the pyridinium methyl proton H1 of the adjacent macrocycle, **(ii)** between the A_{out} oxygen O3 and the *m*-xylyl methyl proton H3, **(iii)** between the A_{in} oxygen O2 and the pyridinium methyl proton H1, and **(iv)** between O2 and the *ortho*-pyridinium proton H2. Together with the N–H•••I[−] interactions, the first two hydrogen bonds build up an infinite zigzag stack of TLM 4^+ molecules (Figure D3b), while the last two interactions constitute a bifurcated hydrogen bond leading to the assembly of an infinite chain within the crystal structure (Figure D3a). In addition, the fourth hydrogen bond is an exceptionally short C–H•••O=C hydrogen bond (Table D1: $d(\text{H}\cdots\text{O}) = 2.16 \text{ \AA}$, $d(\text{C}–\text{O}) = 3.03 \text{ \AA}$).^[125] Together with the D–H•••A angle of 151.8° , one can assume this bond to be comparably strong. N–H•••O=C interactions are absent in the solid-state structure of 4^+ . In particular, the seemingly predestined A_{out} proton H3 does not form any hydrogen bonds to adjacent TLMs as in **2** thus indicating that the C–H•••O=C bonds energetically compensate the lack of N–H•••O=C interactions.

A further remarkable finding in the X-ray crystal structure of 4^+ is the “divergence” of the two A_{in} groups bound to the pyridinium moiety. The proton of one A_{in} group points to the iodine on the lower side, while the proton of the other A_{in} group points to the upper side. Hence, they point into different hemispheres which are separated by the macrocycle plane (Figure D3d). This is unique because two A_{in} groups of the same isophthaloyl unit normally point into the same hemisphere, as observed in all the other crystal structures of TLMs. The absence of rather strong H-acceptors (such as carbonyl oxygen in ethyl acetate, or chloride) in the interior of the cavity could be a possible reason for this unusual conformational property of the amides.

In the crystal structure of **5**, the *all-in* conformation combined with the “closed-doors” conformation leads to a very interesting hydrogen-bonding motif: The H1 proton (Figure D1f) of the O1=CN1H1 amide group forms an intermolecular hydrogen bond to oxygen O1, which is part of the same amide group in the adjacent TLM (Figure D4a). The TLMs are arranged in a herringbone pattern with an angle of approximately 90° between them. In this manner, a quite remarkable catemer motif $[\text{O}=\text{C}–\text{N}–\text{H}\cdots\text{O}=\text{C}–\text{N}–\text{H}\cdots]_\infty$ is obtained (Figure D4b,c).^[126] Here, the catemer motif is unprecedented in that the secondary amide group involved is an integral (and not peripheral) part of a macrocycle. This infinite chain of hydrogen bonds runs through the crystal along the “spine” of the herringbone motif - in marked contrast to the ladders observed for **2** and **3**, in which the hydrogen bonds are oriented more or less parallel with the ladder axis. Furthermore, this interaction is supported by a somewhat longer and thus likely weaker N–H•••O=C bond between amide proton H2 and the same O1 oxygen atom. As

a consequence of the hydrogen bonds, two of the four amide groups exhibit an unusually high deviation (50.3°) from coplanarity with the macrocycle plane, which is – to the best of our knowledge – the largest out-of-plane angle observed so far for TLMs in the solid state (Table D2).

The quite compact, intermolecular hydrogen bonding patterns observed for **2** and **5** certainly depend on the TLMs' conformational properties. Nevertheless, they are also determined by the substituents attached in the TLM periphery. For example, if R_1 (Scheme D1) in **2** would be a *tert*-butyl group instead of a hydrogen, the overlapping pattern of the isophthaloyl units would likely be distorted and the structure observed for unsubstituted **2** might not form. Probably, the fact that a *tert*-butyl substituent disturbs such hydrogen-bonding patterns contributes significantly to the much higher solubility of *tert*-butyl substituted TLMs in unpolar solvents.

D3 Final Conclusions and Outlook

The detailed analysis of the solid-state structures of **1** – **5** uncovered several quite remarkable features of the TLMs under study. Although the overall macrocycle scaffold is quite rigid, it can easily adapt to the space requirements of guest inside the cavity because of the almost free rotatability of the amide groups and the *m*-xylene rings. The TLM conformation changes significantly into the "closed-doors" structure, when no guest is present. Together with the peripheral substituents, the conformational properties lead to a variety of interesting intermolecular hydrogen-bonding patterns. For instance, **5** reveals a notable catemer motif, whereas **4**⁺ exhibits several C–H \cdots O=C interactions including a remarkably short one. Our findings do not only provide support for previous theoretical predictions and STM experiments, but will also be advantageous for crystal engineering. A more profound understanding of the rigidity/flexibility balance in TLMs will also help in the design of templated syntheses of supramolecular assemblies involving TLMs.

E. Experimental Section

E1 Instruments for NMR spectroscopy

¹H NMR: AMX300 (300 MHz), AMX400 (400 MHz), AMX500/DRX500 (500 MHz) instruments

¹³C-NMR: AMX300 (75 MHz), AMX400 (100 MHz), AMX500/DRX500 (125 MHz) instruments

The supplier of all NMR instruments mentioned in this section is Bruker BioSpin GmbH, Am Silberstreifen, 76287 Rheinstetten, Germany.

All chemical shifts are reported in ppm with solvent signals taken as internal standards; coupling constants are given in Hertz (Hz).

E2 Instruments and General Settings for Mass Spectrometry

Mass spectra were recorded using a Bruker APEX IV Fourier-transform ion-cyclotron-resonance (FT-ICR) mass spectrometer with an Apollo ESI ion source equipped with an off-axis 70° spray needle. The supplier of this instrument is Bruker Daltonik GmbH, Fahrenheitstr. 4, 28359 Bremen.

Generally, the samples were dissolved in polar solvents (usually acetone or methanol) and sprayed into the ion source using a Cole-Parmer Instruments (Series 74900) syringe pump at flow rates around 2–5 $\mu\text{L}/\text{min}$. The ion transfer into the first of three differential pump stages occurred through a glass capillary with an inner diameter of 0.5 mm and nickel coatings at both ends. For each measurement, 4 to 120 scans were averaged to improve the signal-to-noise ratio.

Typically, the following ionization parameters were used:

a) General settings for ESI negative mode:

Gas settings of the Apollo ESI source:

Normal pressure settings: nebulizing gas 25–30 psi and drying gas 15 psi; Low pressure settings: nebulizing gas < 10 psi and drying gas 20–25 psi; drying gas temperature: 150–200°C.

Vacuum lens voltages of the Apollo ESI source:

capillary: 4.5 kV; end plate: 4.0 kV; capexit: -30 to -400 V; 1st skimmer: -20 V; 2nd skimmer: -10 V; offset: -1.5 V; RF amplitude 500 V; trap -15 V; extract 15 V.

Ion transfer and cell parameters of APEX IV FTICR-MS mass spectrometer:

Hexapole accumulation: 0.7–10.0 sec; beam steering parameter XDFL: -20 V; beam steering parameter YDFL: 0 V; voltage gradient at the cell entrance (DEV2): -3 V, attenuation level of excitation (excite / PL3): 3.6–5.8 dB.

b) General settings for ESI positive mode:

Gas settings of the Apollo ESI source:

Normal pressure settings: nebulizing gas 25–30 psi and drying gas 15 psi; Low pressure settings: nebulizing gas < 10 psi and drying gas 20–25 psi; drying gas temperature: 150–200°C.

Vacuum lens voltages of the Apollo ESI source:

capillary: -4.6 kV; end plate: -4.0 kV; capexit: 120 to 400 V; 1st skimmer: 15–20 V; 2nd skimmer: 7–10 V; offset: 1.9 V; RF amplitude 550 V; trap 18 V; extract -9 V.

Ion transfer and cell parameters of APEX IV FTICR-MS mass spectrometer:

Hexapole accumulation: 0.7–10.0 sec; beam steering parameter XDFL: 5 V; beam steering parameter YDFL: 0 V; voltage gradient at the cell entrance (DEV2): 13 V, attenuation level of excitation (excite / PL3): 3.6–5.8 dB.

c) Settings for MS/MS experiments:

For MS/MS experiments, the whole isotope patterns of the ion of interest were isolated by applying correlated sweeps, followed by high resolution isolation shots to remove the higher isotopes. After isolation, argon was introduced into the ICR cell as the collision gas through a pulsed valve at a pressure of approx. 10^{-8} mbar. The ions were accelerated by a standard excitation protocol and detected after a 2 sec pumping delay. A sequence of several different spectra was recorded at different excitation pulse attenuations in order to get at least a rough and qualitative idea of the effects of different collision energies on the fragmentation patterns.

Typical parameter settings for the CID experiments are:

attenuation level of correlated sweep (CorrSweep / PL4): 15–18 dB; attenuation level of correlated shots (CorrShot / PL7): 43–50 dB; attenuation level of ion activation (activation/PL9): 54–62 dB; collision gas: argon 4.6; pulsed valve opening duration: 0.015–0.03 sec; pumping delay: 2 sec.

E3 Chemicals and Miscellaneous

Reagents and deuterated solvents were purchased from Sigma-Aldrich, Fluka, Riedel-de Haën, Merck, Lancaster, ABCR, Acros Organics and used as received. Solvents such as dichloromethane and ethyl acetate were dried and distilled prior to use by usual laboratory methods.

Thin-layer chromatography (TLC) was carried out on TLC plates pre-coated with silica gel 60 F₂₅₄ from Merck. Silica gel (0.04–0.063, 0.63–0.100 mm; Merck) were used for column chromatography.

Melting points were determined using an instrument, which was assembled by the electronics facility of the Chemistry Institutes of the University of Bonn, and were not corrected.

E4 Abbreviations

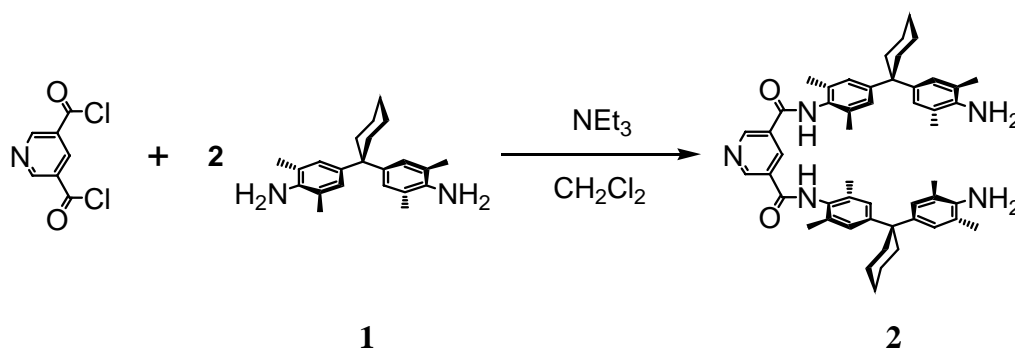
Å	Ångström, equals 10^{-10} meter (unit)
Ac	acetyl
acac	acetylacetonate
A _{in}	amide group (of a tetralactam macrocycle) with NH converging into the cavity
A _{out}	amide group (of a tetralactam macrocycle) with NH pointing away from the cavity
Ar	aryl
bipy	bipyridine
Boc	<i>tert</i> -butyloxycarbonyl
BODIPY	boron dipyrromethene
br	broad (NMR signals)
Bu	<i>n</i> -butyl
^t Bu	<i>tert</i> -butyl
C _q	quarternary carbon
calcd	calculated
CCDC	Cambridge Crystallographic Data Centre
CID	collision-induced dissociation
Cy	cyclohexane, cyclohexyl
d	doublet (NMR signals)

deg.	degree
D _n	n times deuterated
dppf	1,1'-bis(diphenylphosphino)ferrocene
dppp	1,3-bis(diphenylphosphino)propane
δ	chemical shift [ppm]
dB	decibel
DMF	<i>N,N</i> -dimethyl formamide
DMSO	dimethyl sulfoxide
EtOAc	ethyl acetate
ESI	electrospray ionization
ESI ⁻	electrospray ionization, negative mode
ESI ⁺	electrospray ionization, positive mode
exp	experimental
EWG	electron-withdrawing group
FBMH	flexible branched multimacrocylic host
FT	Fourier transform
h	hour (unit)
HR	high resolution
Hz	hertz (unit)
ICR	ion cyclotron resonance
J	joule (unit)
J	NMR coupling constant (NMR signals)
K	Kelvin (unit)
k	kilo- (standard prefix for units, denotes factor 10 ³)
kJ	kilojoule, equals 10 ³ joule (unit)
kV	kilovolt, equals 10 ³ volt (unit)
L	liter (unit)
L	ligand (in chemical formula)
M	molecular ion
M	moles per liter (unit)
M	mega- (standard prefix for units, denotes factor 10 ⁶)
M	metal (in chemical formula)
m	milli- (standard prefix for units, denotes factor 10 ⁻³)
MeOH	methanol

MHz	megahertz, equals 10^6 hertz (unit)
MIA	multiply interlocked architecture
min	minute (unit)
mM	millimole per liter, equals 10^{-3} mole per liter (unit)
mol	mole (unit)
m.p.	melting points
MS	mass spectrometry, mass spectrometric
m/z	mass-to-charge ratio
μ	micro- (standard prefix for units, denotes factor 10^{-6})
μ M	micromole per liter, equals 10^{-6} mole per liter (unit)
n	nano- (standard prefix for units, denotes factor 10^{-9})
nm	nanometer, equals 10^{-9} meter (unit)
NMR	nuclear magnetic resonance
Ph	phenyl
pin	pinacolato
psi	pounds per square inch (1 psi = 14,7 atm = 1.489.478 Pa)
py	pyridine, pyridyl
m	multiplet (NMR signals)
ref.	reference
R_f	retention factor
s	singlet (NMR signals)
s	second
sec	second
t	triplet (NMR signals)
terpy	2,2';6',2''-terpyridine
tert	tertiary
THF	tetrahydrofurane
TLC	thin layer chromatography
TLM	tetralactam macrocycle
V	volt (unit)

E5 Synthetic Procedures

*N*³,*N*⁵-bis(4-(1-(4-amino-3,5-dimethylphenyl)cyclohexyl)-2,6-dimethylphenyl)pyridine-3,5-dicarboxamide (compound **2** from section C) [72]



At room temperature, a solution of pyridine-3,5-dicarbonyl dichloride (1.0 g, 5.0 mmol) in CH₂Cl₂ (150 mL) was slowly added over 5 h to a solution of **1** (10.2 g, 31.6 mmol) in CH₂Cl₂ (50 mL) and NEt₃ (2 mL). The mixture was left stirring at room temperature for 48 h. The solvents were then evaporated and the product was isolated by column chromatography (silica gel, CH₂Cl₂/EtOAc = 1/2) as a white solid (2.5 g, 3.2 mmol, 64%).

R_f 0.4 (CH₂Cl₂/EtOAc = 1/2)

C₅₁H₆₁N₅O₂ 776.06 g/mol

M.p. >200°C

¹H-NMR (400 MHz, CDCl₃, 298 K)

δ [ppm] = 1.43-1.53 (m, 20H; CH₂), 2.13-2.16 (m, 24H; CH₃), 6.83 (s, 4H; Ar-H), 6.99 (s, 4H; Ar-H), 7.57 (s, 2H; NH), 8.70-8.71 (m, 1H; Ar-H(py)), 9.17 (d, ⁴J(H,H)=2.0 Hz, 1H; Ar-H(py)).

¹³C-NMR (100 MHz, CDCl₃, 298 K)

δ [ppm] = 18.2 (CH₃), 19.0 (CH₃), 23.2 (CH₂), 26.7 (CH₂), 37.4 (CH₂), 45.2 (C_q), 121.7 (Ar-C_q), 127.3 (Ar-CH), 127.4 (Ar-CH), 130.4 (Ar-C_q), 130.6 (Ar-C_q), 134.3 (Ar-C_q), 134.8 (Ar-CH), 137.7 (Ar-C_q), 140.4 (Ar-C_q), 149.5 (Ar-C_q), 150.9 (Ar-CH), 163.4 (C=O).

NMR file 11x4a037

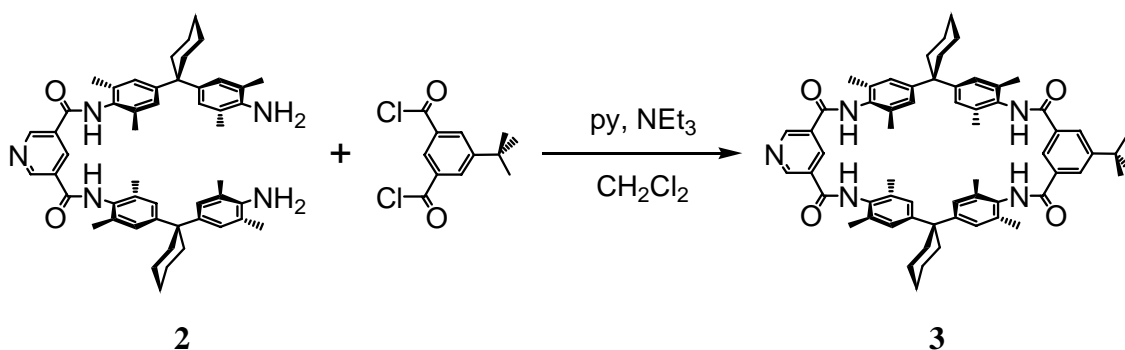
FT-ICR-MS (ESI⁺, from MeOH)

m/z (%): 798 (49) [M+Na]⁺, 776 (100) [M+H]⁺.

HR-MS (ESI⁻, from MeOH)

m/z calcd for C₅₁H₆₀N₅O₂⁻: 774.4752 [M-H]⁻; found: 774.4792 (Δ = 5.2 ppm).

23⁵-tert-butyl-7³,7⁵,13²,13⁶,20³,20⁵,26³,26⁵-octamethyl-8,10⁵,12,21,25-pentaaza-7,13,20,26(1,4),10,23(1,3)-hexabenzendispiro[5.7.5¹⁴.7⁶]hexacosaphane-9,11,22,24-tetrone (compound **3** from sections C, D)^[72,127,128]



A suspension which was obtained from adding **2** (2.44 g, 3.1 mmol) into a solvent mixture of 500 mL CH₂Cl₂, 10 mL pyridine and 0.3 mL NEt₃ was stirred in an ultrasonic bath for 1 h to afford a clear, light green solution. This solution and a solution of 5-*tert*-butylisophthaloyl dichloride (0.77 g, 3.0 mmol) was simultaneously added over 24 h into a flask with 2000 mL refluxing CH₂Cl₂ using an automatic solvent pump. The reaction mixture was refluxed for another 24 h. The solvents were then evaporated off and the residue was purified by column chromatography (silica gel, CH₂Cl₂/EtOAc/pyridine 50:50:3). The solid obtained from the purification was taken up in toluene, and the solvent was evaporated off. This was done two more times. The product was again purified by column chromatography (silica gel, CH₂Cl₂/EtOAc/MeOH = 14/2/1) to afford **3** (0.93 g, 1.0 mmol, 31%) as a white solid.

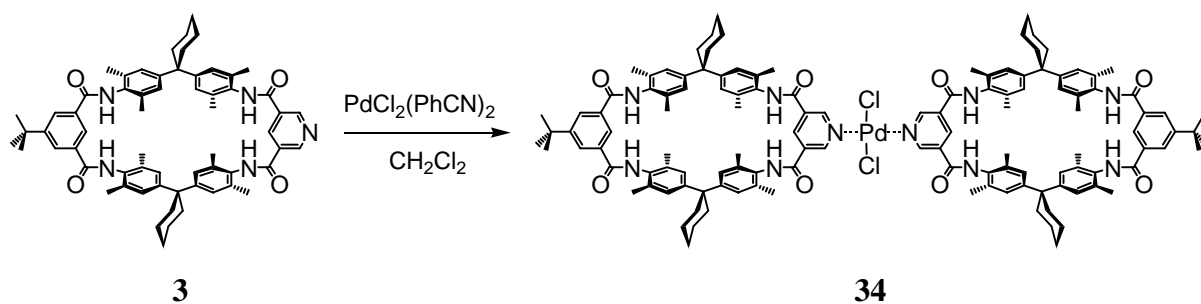
R_f 0.54 (CH₂Cl₂/EtOAc/MeOH = 14/2/1)

C₆₃H₇₁N₅O₄ 962.27 g/mol

M.p. >200°C

- ¹H-NMR** (400 MHz, CDCl₃/CD₃OD = 5/1, 298 K)
 δ [ppm] = 1.24 (s, 9H; ^tBu-CH₃), 1.34-1.35 (br, 4H; CH₂), 1.47 (br, 8H; CH₂), 1.99 / 2.00 (s, 24H; Ar-CH₃), 2.16 (br, 8H; CH₂), 6.81 / 6.82 (s, 8H; Ar-H), 7.97 (br, 1H; Ar-H), 8.01 (d, ⁴J(H,H)=1.4 Hz, 2H; Ar-H), 8.74 (br, 1H; Ar-H (py)), 9.07 (d, ⁴J(H,H)=1.9 Hz; Ar-H(py)).
- ¹³C-NMR** (75 MHz, CDCl₃/CD₃OD = 5/1, 298 K)
 δ [ppm] = 18.3 (Ar-CH₃), 22.8 (CH₂), 26.2 (CH₂), 30.9 (^tBu-CH₃), 35.0 (CH₂), 35.1 (^tBu-C_q), 45.0 (C_q), 123.8 (Ar-CH), 126.1 (Ar-CH), 126.2 (Ar-CH), 128.3 (Ar-C_q), 130.7 (Ar-C_q), 130.7 (Ar-C_q), 131.3 (Ar-C_q), 134.0 (Ar-CH), 134.7 (Ar-C_q), 134.9 (Ar-C_q), 137.0 (Ar-C_q), 147.8 (Ar-C_q), 148.2 (Ar-CH), 149.5 (Ar-CH), 153.2 (Ar-C_q), 163.6 (C=O), 166.9 (C=O).
- NMR file** 13x4b012.06
- FT-ICR-MS** (ESI⁻, from MeOH)
m/z (%): 996 (2) [*M*+Cl]⁻, 960 (100) [*M*-H]⁻.
- HR-MS** (ESI⁻, from MeOH)
m/z calcd for C₆₃H₇₀N₅O₄⁻: 960.5433 [*M*-H]⁻; found: 960.5396 (Δ = 3.9 ppm).

Bis{23⁵-*tert*-butyl-7³,7⁵,13²,13⁶,20³,20⁵,26³,26⁵-octamethyl-8,10⁵,12,21,25-pentaaza-7,13,20,26(1,4),10,23(1,3)-hexabenzendispiro[5.7.5¹⁴.7⁶]hexacosaphane-9,11,22,24-tetrone}palladium(II)chloride (compound **34** from section C) ^[72,127,129]



Under argon atmosphere, a solution of **3** (25.9 mg; 0.027 mmol) in 6 mL CH₂Cl₂ was slowly added to a solution of bis(benzonitrile)palladium(II)chloride (4.8 mg; 0.013 mmol) in 2 mL

CH₂Cl₂. After 9 hours of stirring, a pale yellow precipitation was filtered and dried, yielding 13.5 mg (0.006 mmol; 49%) of the product.

C₁₂₆H₁₄₂Cl₂N₁₀O₈Pd 2101.86 g/mol

M.p. >200°C

¹H-NMR (400 MHz, CDCl₃/CD₃OD = 5/1, 298 K)
δ [ppm] = 1.31 (s, 18H; ^tBu-CH₃), 1.43 (br, 8H; Cy-CH₂), 1.55 (br, 16H; Cy-CH₂), 2.06 (br, 48H; Ar-CH₃), 2.24 (br, 16H; Cy-CH₂), 6.88-6.89 (m, 16H; Ar-H), 8.03 (br, 2H; Ar-H), 8.08 (br, 4H; Ar-H), 8.64 (br, 2H; Ar-H (py)), 9.38 (br, 4H; Ar-H(py)).

¹³C-NMR (125 MHz, CDCl₃/CD₃OD = 5/1, 298 K)
δ [ppm] = 18.4 (Ar-CH₃), 22.9 (CH₂), 26.3 (CH₂), 31.0 (^tBu-CH₃), 35.0 (CH₂), 35.2 (^tBu-C_q), 45.1 (C_q), 123.8 (Ar-CH), 126.1 (Ar-CH), 126.3 (Ar-CH), 128.3 (Ar-CH), 130.8 (Ar-C_q), 131.3 (Ar-C_q), 131.7 (Ar-C_q), 134.0 (Ar-C_q), 134.8 (Ar-C_q), 135.0 (Ar-C_q), 137.7 (Ar-CH), 147.9 (Ar-C_q), 148.3 (Ar-C_q), 153.3 (Ar-C_q), 154.4 (Ar-CH), 162.1 (C=O), 166.8 (C=O).

NMR file 16x4b005.07 (¹H-NMR), 16x5m003.07 (¹³C-NMR)

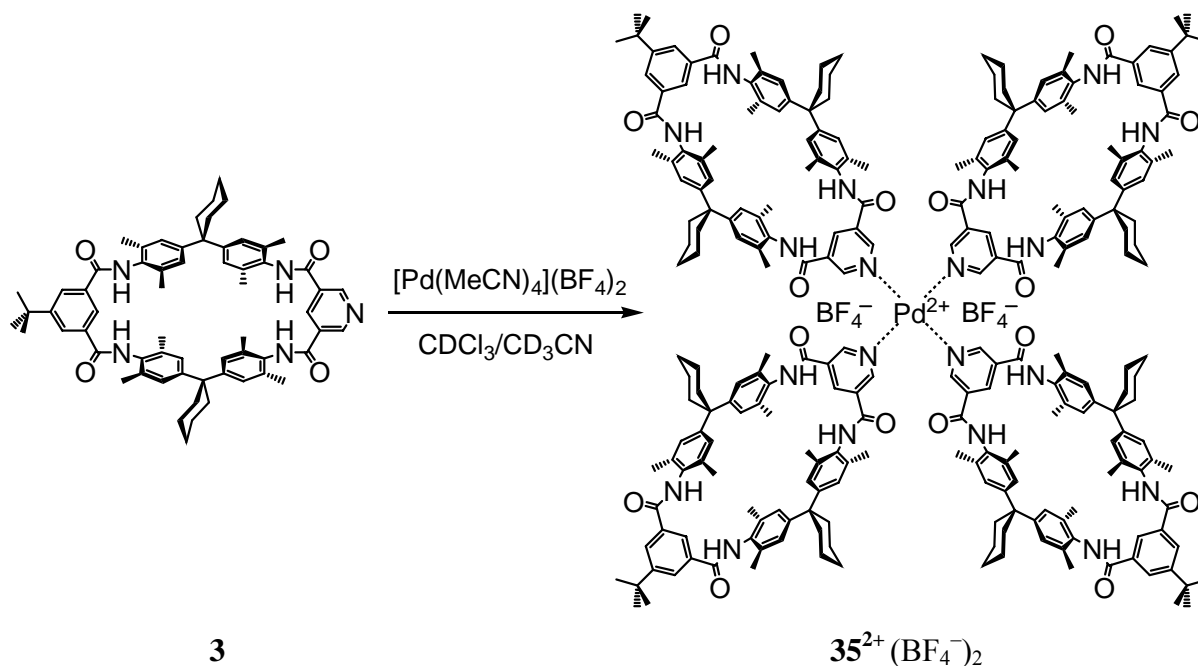
FT-ICR-MS (ESI⁺, from acetone)

m/z (%): 2138 (60) [M+K]⁺, 2122 (100) [M+Na]⁺.

HR-MS (ESI⁻, from acetone)

m/z: calcd for C₁₂₆H₁₄₁Cl₂N₁₀O₈Pd: 2099.9382 [M-H]⁻; found: 2099.9416 (Δ = 1.6 ppm).

Tetrakis{23⁵-*tert*-butyl-7³,7⁵,13²,13⁶,20³,20⁵,26³,26⁵-octamethyl-8,10⁵,12,21,25-pentaaza-7,13,20,26(1,4),10,23(1,3)-hexabenzendispiro[5.7.5¹⁴.7⁶]hexacosaphane-9,11,22,24-tetrone}palladium(II)tetrafluoroborate (compound **35²⁺** (BF₄⁻)₂ from section C) [72,127,130]



A solution of macrocycle **3** (27.3 mg; 0.028 mmol) was dissolved in 500 μl deuterated chloroform. Under argon atmosphere, a solution of tetrakis(acetonitrile)palladium(II)-tetrafluoroborate (2.6 mg; 0.006 mmol) in 60 μl deuterated acetonitrile was slowly added. After 400 μl deuterated chloroform was added to the mixture, it was stirred for a day and then stored in the refrigerator. After 3 days, a white precipitation was obtained which was filtered, yielding 9 mg (0.002 mmol; 33%) of the product.

C₂₅₈H₃₀₄B₂F₈N₂₀O₁₆Pd 4221.33 g/mol

M.p. > 200°C

¹H-NMR (500 MHz, CDCl₃/CD₃OD = 5/1, 298 K)
 δ [ppm] = 1.31 (s, 36H; ^tBu-CH₃), 1.43 (br, 16H; Cy-CH₂), 1.55 (br, 32H; Cy-CH₂), 2.00–2.06 (br, 96H; Ar-CH₃), 2.22 (br, 32H; Cy-CH₂), 6.85–6.90 (m, 32H; Ar-H), 8.00 (br, 4H; Ar-H), 8.08 (d, ⁴J = 1.6 Hz, 8H; Ar-H), 8.55 (br, 4H; Ar-H (py)), 9.71 (d, ⁴J = 1.7 Hz, 8H; Ar-H(py)).

¹³C-NMR (125 MHz, CDCl₃/CD₃OD = 5/1, 298 K)
 δ [ppm] = 18.4–18.5 (Ar-CH₃), 22.9 (CH₂), 26.3 (CH₂), 31.0 (^tBu-CH₃), 35.1 (^tBu-C_q), 35.2 (CH₂), 45.1 (C_q), 123.6 (Ar-CH), 126.2 (Ar-CH),

126.4 (Ar-CH), 128.3 (Ar-CH), 128.5 (Ar-CH), 130.4 (Ar-C_q), 131.3 (Ar-C_q), 134.1 (Ar-C_q), 134.6 (Ar-C_q), 134.8 (Ar-C_q), 134.9 (Ar-C_q), 147.9 (Ar-C_q), 148.5 (Ar-C_q), 152.2 (Ar-CH), 153.4 (Ar-C_q), 162.1 (C=O), 166.8 (C=O).

NMR file 17x5m002.07

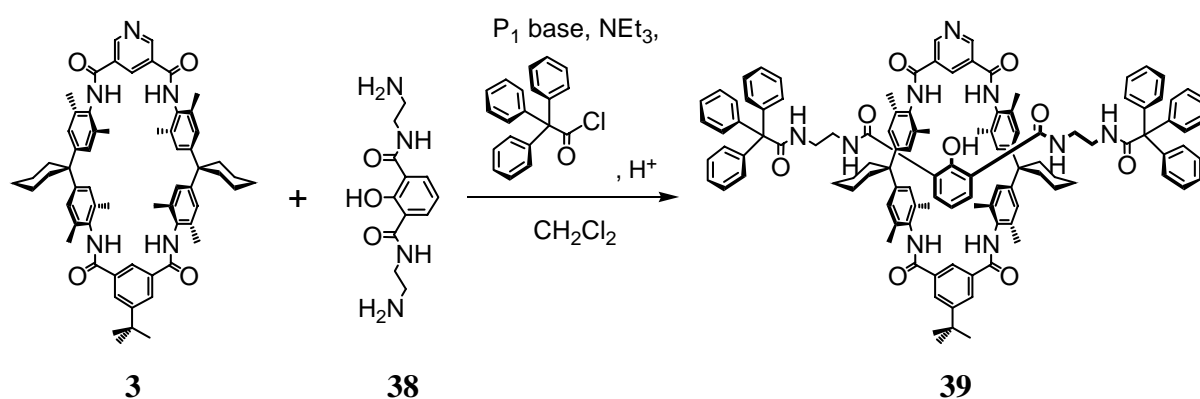
FT-ICR-MS (ESI⁺, from acetone)

m/z (%): 4014 (33) [*M*+acetate]⁺, 3051 (100) [*M*-macrocycle+acetate]⁺.

HR-MS (ESI⁺, from acetone)

m/z: calcd for C₂₅₄H₂₈₇N₂₀O₁₈Pd⁺: 4010.1222 [*M*+acetate]⁺; found: 4010.1530 (Δ = 7.7 ppm).

[2][[2-Hydroxy-*N,N'*-bis-(2-(2,2,2-triphenyl-acetyl-amino)-ethyl)-isophthalamide]-rotaxa-[23⁵-*tert*-butyl-7³,7⁵,13²,13⁶,20³,20⁵,26³,26⁵-octamethyl-8,10⁵,12,21,25-pentaaza-7,13,20,26(1,4),10,23(1,3)-hexabenzendispiro[5.7.5¹⁴.7⁶]hexacosaphane-9,11,22,24-tetrone]] (compound **39** from section C) ^[72,127,131,132]

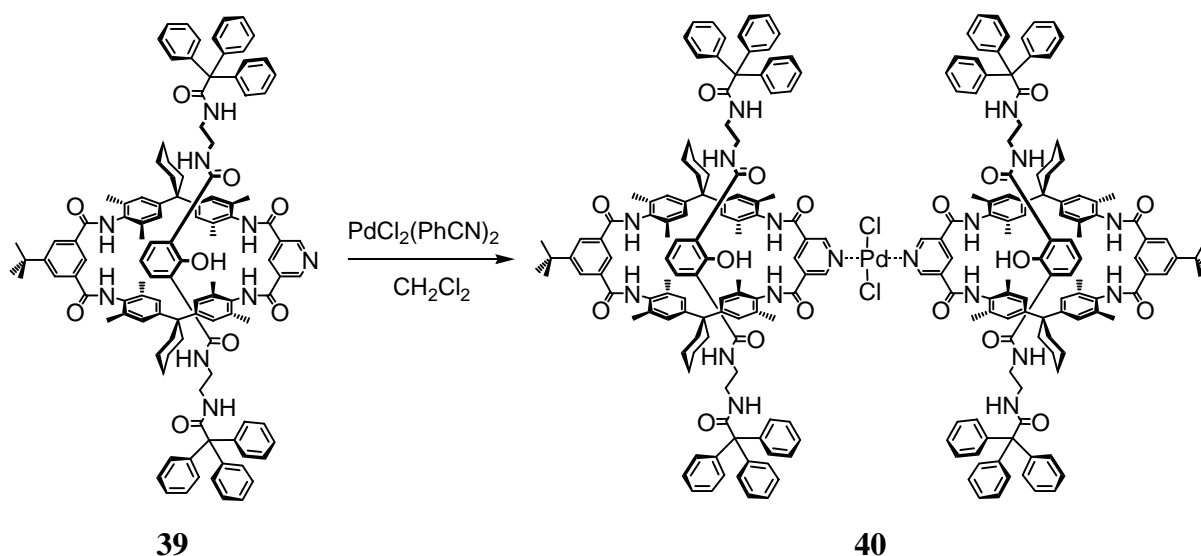


Under argon atmosphere, *tert* butylimino-tris(dimethylamino)-phosphorane (P₁ base) (0.24 mL, 1.02 mmol) was added to a suspension of **38** (176 mg, 0.66 mmol) in 300 mL CH₂Cl₂. After the reaction mixture was stirred for 1 h at room temperature, macrocycle **3** (662 mg, 0.69 mmol) was added, and stirring was continued for 15 min. Upon addition of 0.18 mL triethylamine, the reaction mixture was cooled down to 0–5°C, and a solution of triphenylacetyl chloride (405 mg, 1.32 mmol) in 10 mL CH₂Cl₂ was added dropwise. The reaction mixture was stirred for three days at room temperature, washed two times with saturated aqueous ammonium chloride solution and two times with deionized water. The

organic layer was dried over magnesium sulfate, the solvents were then evaporated off and the residue was purified by column chromatography (silica gel, EtOAc) and again by column chromatography (silica gel, CH₂Cl₂/EtOAc/MeOH 14:2:1). The product was taken up in diethyl ether, and after evaporation of solvents, **39** (165 mg, 0.09 mmol, 14%) was obtained as a white solid.

R_f	0.41 (CH ₂ Cl ₂ /EtOAc/MeOH = 14/2/1)
C₁₁₅H₁₁₇N₉O₉	1769.21 g/mol
M.p.	>200°C
¹H-NMR	(500 MHz, CD ₂ Cl ₂ , 298 K) δ [ppm] = 1.46 (s, 9H; ^t Bu-CH ₃), 1.59 (s, 4H; Cy-CH ₂), 1.69 (br, 8H; Cy-CH ₂), 1.92-1.94 (br, 24H; Ar-CH ₃), 2.21-2.24 (br, 8H; Cy-CH ₂), 2.43 (br, 4H; NCH ₂ , covered by macrocycle), 3.52-3.63 (br, 4H; NCH ₂ , free), 6.64 (br, 4H; NH), 6.81 (t, ³ J(H,H)=8.0 Hz, 1H; Ar-H), 6.97-7.22 (br, 40H; Ar-H), 8.15 (m, 2H; NH), 8.19 (br, 2H; NH), 8.52 (br, 2H; Ar-H), 8.62 (br, 1H; Ar-H), 9.08 (br, 1H; Ar-H (py)), 9.25 (d, ⁴ J(H,H)=1.0 Hz, 2H; Ar-H (py)), 15.54 (s, 1H; OH).
¹³C-NMR	(125 MHz, CD ₂ Cl ₂ , 298 K) δ [ppm] = 18.6 (PhCH ₃), 23.5 (Cy-CH ₂), 26.7 (Cy-CH ₂), 31.5 (^t Bu-CH ₃), 35.6 (^t Bu-C _q), 36.1 (Cy-CH ₂), 37.0 (Cy-C _q), 45.6 (NCH ₂), 119.4, 124.1, 126.7, 126.9, 127.1, 127.8, 128.4, 128.5, 129.9, 130.5, 131.5, 132.1, 134.1, 135.0, 135.6, 135.8, 149.2, 149.3, 152.3, 153.9, 161.7 (Ar-CH oder Ar-C _q), 164.4 (C=O), 166.4 (C=O), 177.5 (C=O). (Not observable in the spectrum: Ph ₃ -C _q , ppm = 55 to 70; This peak is probably hidden under a solvent peak)
NMR file	13m5m001.06
FT-ICR-MS	(ESI ⁻ , from MeOH) <i>m/z</i> (%): 1767 (100) [<i>M</i> -H] ⁻ .
HR-MS	(ESI ⁻ , from MeOH) <i>m/z</i> calcd for C ₁₁₅ H ₁₁₆ N ₉ O ₉ ⁻ : 1766.8901 [<i>M</i> -H] ⁻ ; found: 1766.8863 (Δ = 2.2 ppm).

Bis([2]{[2-Hydroxy-*N,N'*-bis-(2-(2,2,2-triphenyl-acetyl-amino)-ethyl)-isophthalamide]-rotaxa-[23⁵-*tert*-butyl-7³,7⁵,13²,13⁶,20³,20⁵,26³,26⁵-octamethyl-8,10⁵,12,21,25-pentaaza-7,13,20,26(1,4),10,23(1,3)-hexabenzendispiro[5.7.5¹⁴.7⁶]hexacosaphane-9,11,22,24-tetrone}})palladium(II)chloride (compound **40** from section C) [72,127,131,133]



Under argon atmosphere, a solution of rotaxane **39** (20.4 mg; 0.012 mmol) in 2.5 mL CH_2Cl_2 was slowly added to a solution of bis(benzonitrile)palladium(II)-dichloride (2.15 mg; 0.006 mmol) in 1.5 mL CH_2Cl_2 . The reaction mixture was stirred at room temperature for a day and was then stored in the refrigerator. After a week, a pale precipitation was obtained which was filtered, yielding 5 mg (0.0013 mmol; 11%) of the complex **40**.

C₂₃₀H₂₃₄Cl₂N₁₈O₁₈Pd 3715.75 g/mol

M.p. >200°C

¹H-NMR (500 MHz, CDCl_3 , 298 K)
 δ [ppm] = 1.43 (s, 9H; ^tBu-CH₃), 1.57-1.62 (br, 12H; Cy-CH₂), 1.88-1.95 (br, 24H; Ar-CH₃), 2.15-2.21 (br, 8H; Cy-CH₂), 2.34-2.36 (br, 4H; NCH₂, covered), 3.55-3.68 (br, 4H; NCH₂, free), 6.59 (br, 4H; NH), 6.85-7.24 (br, 40H; Ar-H), 8.02 (br, 2H; NH), 8.17 (br, 2H; NH), 8.51-8.59 (br, 3H; Ar-H), 9.19 (br, 1H; Ar-H (py)), 9.53 (br, 2H; Ar-H (py)).

¹³C-NMR (125 MHz, CDCl_3 , 298 K)
 δ [ppm] = 18.5-18.6 (Ar-CH₃), 23.1 (CH₂), 26.4 (CH₂), 31.5 (^tBu-CH₃), 35.6 (^tBu-C_q), 36.1 (CH₂), 36.9 (Cy-C_q), 45.3 (NCH₂), 51.1 (Ph₃-C_q), 119.5, 123.8, 127.1, 127.6, 127.9, 128.1, 128.4, 128.7, 130.2, 130.4,

130.5, 131.5, 131.6, 134.6, 135.0, 135.4, 135.8, 141.7, 142.7, 153.7, 155.6, 161.3, 161.4, 166.4 ((Ar-CH oder Ar-C_q oder C=O).

NMR file 18x5m001.08

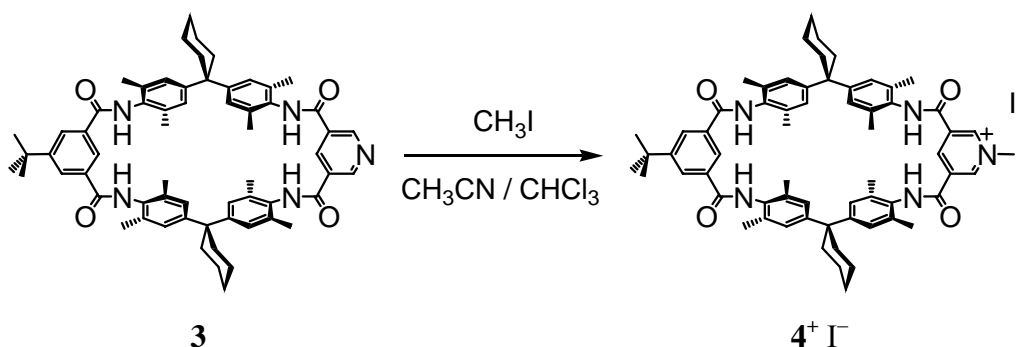
FT-ICR-MS (ESI⁺, from acetone)

m/z (%): 3738 (100) [M+Na]⁺.

HR-MS (ESI⁺, from acetone)

m/z: calcd for C₂₃₀H₂₃₄Cl₂N₁₈NaO₁₈Pd⁺: 3738.6328 [M+Na]⁺; found: 3738.6191 (Δ = 3.7 ppm).

23⁵-tert-butyl-7³,7⁵,10⁵,13²,13⁶,20³,20⁵,26³,26⁵-nonamethyl-8,12,21,25-tetraaza-10⁵-azonia-7,13,20,26(1,4),10,23(1,3)-hexabenzena-dispiro[5.7.5¹⁴.7⁶]hexacosaphane-9,11,22,24-tetrone iodide (compound **4**⁺ I⁻ from section D) [109,127,134]



Methyl iodide (0.25 mL, 4 mmol) was added to a solution of **3** (38.6 mg, 0.04 mmol) in 2 mL CH₃CN and 0.5 mL CHCl₃. The mixture was left stirring for 48h, then a yellowish precipitation was obtained which was filtered and dried in vacuo, yielding **4**⁺ I⁻ as a pale yellow solid (28.5 mg, 0.026 mmol, 65%).

C₆₄H₇₄IN₅O₄ 1104.21 g/mol

M.p. >200°C

¹H NMR (500 MHz, [D₇]DMF, 298 K)

δ [ppm] = 1.39 (s, 9H; ^tBu-CH₃), 1.50 (br, 4H; CH₂), 1.62 (br, 8H; CH₂), 2.16 (s, 12H; Ar-CH₃), 2.21 (s, 12H; Ar-CH₃), 2.45–2.50 (br, 8H; CH₂), 4.81 (s, 3H; N⁺CH₃), 7.22 (s, 4H; Ar-H), 7.25 (s, 4H; Ar-H), 8.18 (d, ⁴J(H,H)=1.5 Hz, 2H; Ar-H), 8.74 (t, ⁴J(H,H)=1.5 Hz, 1H; Ar-H), 9.38

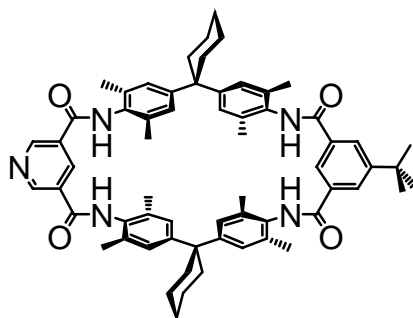
	(br, 2H; NH), 9.70 (d, $^4J(\text{H,H})=1.2$ Hz, 2H; Ar-H(py)), 10.03 (br, 1H; Ar-H(py)), 10.62 (br, 2H; NH)
^{13}C NMR	(125 MHz, $[\text{D}_7]$ DMF, 298 K) δ [ppm] = 18.9 (Ar-CH ₃), 19.1 (Ar-CH ₃), 23.5 (CH ₂), 26.8 (CH ₂), 31.4 (^t Bu-CH ₃), 32.4 (CH ₂), 34.7 (^t Bu-C _q), 45.5 (C _q), 49.3 (N ⁺ CH ₃), 119.3 (Ar-CH), 119.5 (Ar-CH), 126.3 (Ar-CH), 126.5 (Ar-CH), 128.5 (Ar-CH), 130.4 (Ar-CH), 132.6 (Ar-C _q), 133.7 (Ar-C _q), 134.1 (Ar-C _q), 135.3 (Ar-C _q), 135.5 (Ar-C _q), 135.6 (Ar-C _q), 144.0 (Ar-CH), 148.8 (Ar-CH), 153.0 (Ar-C _q), 160.8 (C=O), 165.7 (C=O).
NMR file	40x5m001.08
FT-ICR-MS	(ESI ⁺ , from MeOH) m/z (%): 977 (100) [M] ⁺ .
HR-MS	(ESI ⁺ , from MeOH) m/z calcd for C ₆₄ H ₇₄ N ₅ O ₄ ⁺ : 976.5735 [M] ⁺ ; found: 976.5701 (Δ = 3.5 ppm).

E6 Data of crystal structures

Single-crystal X-ray diffraction studies were carried out on a Bruker Nonius Kappa-CCD diffractometer or a Bruker Nonius APEX II diffractometer. Direct methods (SHELXS-97)^[115] were used for structure solution and refinement was carried out using SHELXL-97 (full-matrix least-squares on F^2). H atoms were localized by difference electron density determination and refined using a riding model (H(N) free).

X-ray diffraction studies of compounds **3** and **34** (from section C) were conducted by Prof. K. Rissanen's group at the University of Jyväskylä, Finland, while the crystal structure of compound **4**⁺ Γ^- (from section D) was determined by Dr. Jörg Daniels from Prof. J. Beck's group at Bonn University, Germany.

23⁵-tert-butyl-7³,7⁵,13²,13⁶,20³,20⁵,26³,26⁵-octamethyl-8,10⁵,12,21,25-pentaaza-7,13,20,26(1,4),10,23(1,3)-hexabenzendispiro[5.7.5¹⁴.7⁶]hexacosaphane-9,11,22,24-tetrone (compound **3** from sections C, D)^[72,127,128]



Identification code	ext070
Chemical formula (moiety)	$C_{63}H_{71}N_5O_4 \cdot 4.33CH_2Cl_2 \cdot 2.66HCl$
Chemical formula (total)	$C_{67.33}H_{82.33}Cl_{11.33}N_5O_4$
Formula weight	1427.48
Temperature	173(2) K
Radiation, wavelength	MoK $_{\alpha}$, 0.71073 Å
Crystal system, space group	triclinic, $P\bar{1}$
Unit cell parameters	a = 14.105(3) Å α = 70.38(3) deg. b = 18.436(4) Å β = 88.36(3) deg. c = 22.291(5) Å γ = 89.41(3) deg.
Cell volume	5458.0(19) Å ³
Z, Calculated density	Z = 3, $\rho(\text{calcd}) = 1.303 \text{ g/cm}^3$
Absorption coefficient μ	0.480 mm ⁻¹
F(000)	2238
Crystal colour and size	colourless, 0.40 × 0.12 × 0.06 mm ³
Reflections for cell refinement	78313 (θ range 2.5 to 27.5 deg.)
Data collection method	Nonius KappaCCD diffractometer ϕ and ω scans
θ range for data collection	5.7 to 22.5°
Index ranges	h 0 to 15, k -19 to 19, l -23 to 23
Completeness to $\theta = 22.5^\circ$	98.0 %
Reflections collected / unique	13974 / 13974 [R(int) = 0.0000]
Reflections with $I > 2\sigma$	11756
Absorption correction	gaussian
Min. and max. transmission	0.8311 and 0.9718
Structure solution	direct methods
Refinement method	Full-matrix least-squares on F^2
Data / restraints / parameters	13974 / 2121 / 1220
Final R indices [$F^2 > 2\sigma$]	R1 = 0.1609, wR2 = 0.4740
R indices (all data)	R1 = 0.1757, wR2 = 0.4863

Table E1: To be continued on next page

Goodness-of-fit on F^2	2.296
Largest diff. peak and hole	2.57 and $-1.04 \text{ e } \text{\AA}^{-3}$
CCDC number	CCDC-687761

Table E1: Crystal data and structure refinement for **3**

	x	y	z	U(eq)
N(1)	1.3989(5)	-0.5244(4)	0.1131(4)	0.0496(17)
C(2)	1.4480(6)	-0.5110(4)	0.1585(4)	0.0410(17)
C(3)	1.4140(5)	-0.4686(4)	0.1953(3)	0.0378(16)
C(4)	1.3195(5)	-0.4400(4)	0.1841(3)	0.0362(16)
C(5)	1.2703(5)	-0.4503(4)	0.1359(4)	0.0388(16)
C(6)	1.3122(6)	-0.4937(4)	0.1013(4)	0.0443(18)
C(7)	1.4676(5)	-0.4437(4)	0.2421(3)	0.0369(16)
N(7)	1.5554(4)	-0.4677(3)	0.2544(3)	0.0343(13)
O(7)	1.4273(4)	-0.3990(3)	0.2658(3)	0.0482(14)
C(8)	1.6152(5)	-0.4357(4)	0.2899(3)	0.0334(15)
C(9)	1.6413(5)	-0.3567(4)	0.2643(3)	0.0350(16)
C(10)	1.6954(5)	-0.3273(4)	0.2987(3)	0.0338(15)
C(11)	1.7307(5)	-0.3701(4)	0.3584(3)	0.0338(15)
C(12)	1.7034(5)	-0.4474(4)	0.3818(3)	0.0354(16)
C(13)	1.6470(5)	-0.4805(4)	0.3490(3)	0.0361(16)
C(14)	1.7893(5)	-0.3301(4)	0.3955(3)	0.0337(15)
C(15)	1.8228(6)	-0.3882(4)	0.4603(4)	0.0427(17)
C(16)	1.8861(7)	-0.3512(6)	0.4941(5)	0.059(2)
C(17)	1.9751(7)	-0.3132(6)	0.4520(6)	0.071(3)
C(18)	1.9453(6)	-0.2566(6)	0.3889(5)	0.062(2)
C(19)	1.8769(5)	-0.2942(5)	0.3553(4)	0.0444(18)
C(20)	1.7200(5)	-0.2690(4)	0.4075(3)	0.0294(15)
C(21)	1.7179(5)	-0.1930(4)	0.3666(3)	0.0293(15)
C(22)	1.6450(5)	-0.1410(4)	0.3685(3)	0.0303(15)
C(23)	1.5728(5)	-0.1683(4)	0.4139(3)	0.0317(15)
C(24)	1.5755(5)	-0.2439(4)	0.4597(3)	0.0362(16)
C(25)	1.6491(5)	-0.2916(4)	0.4546(4)	0.0389(17)
C(26)	1.4811(5)	-0.0531(4)	0.4184(3)	0.0327(15)
N(26)	1.4883(4)	-0.1254(3)	0.4142(3)	0.0361(14)
O(26)	1.5471(4)	-0.0201(3)	0.4320(3)	0.0430(13)
C(27)	1.3855(5)	-0.0183(4)	0.4014(3)	0.0300(15)
C(28)	1.3503(5)	0.0375(4)	0.4268(3)	0.0350(16)

Table E2: To be continued on next page

	x	y	z	U(eq)
C(29)	1.2642(6)	0.0727(4)	0.4108(4)	0.0406(17)
C(30)	1.2096(5)	0.0519(4)	0.3663(3)	0.0353(16)
C(31)	1.2441(5)	-0.0021(4)	0.3400(3)	0.0347(16)
C(32)	1.3322(5)	-0.0354(4)	0.3574(3)	0.0347(16)
C(33)	1.1909(5)	-0.0299(4)	0.2962(4)	0.0404(18)
N(33)	1.1208(4)	0.0159(3)	0.2623(3)	0.0323(13)
O(33)	1.2095(5)	-0.0921(4)	0.2899(3)	0.0646(19)
C(34)	1.0607(5)	-0.0105(4)	0.2234(3)	0.0323(15)
C(35)	1.0925(5)	-0.0073(4)	0.1625(3)	0.0332(15)
C(36)	1.0350(5)	-0.0373(4)	0.1291(3)	0.0297(15)
C(37)	0.9452(5)	-0.0707(4)	0.1520(3)	0.0304(15)
C(38)	0.9172(5)	-0.0724(4)	0.2121(3)	0.0323(15)
C(39)	0.9714(5)	-0.0419(4)	0.2493(3)	0.0333(15)
C(40)	0.8919(5)	-0.1104(4)	0.1130(3)	0.0300(14)
C(41)	0.8756(5)	-0.0543(4)	0.0453(3)	0.0317(15)
C(42)	0.8055(5)	0.0103(5)	0.0428(4)	0.0411(17)
C(43)	0.7082(6)	-0.0237(5)	0.0701(4)	0.0479(19)
C(44)	0.7192(5)	-0.0796(5)	0.1381(4)	0.0434(18)
C(45)	0.7918(5)	-0.1418(4)	0.1411(3)	0.0346(16)
C(46)	0.9570(5)	-0.1780(4)	0.1114(3)	0.0297(14)
C(47)	0.9698(6)	-0.2396(4)	0.1677(4)	0.0383(17)
C(48)	1.0359(6)	-0.2955(4)	0.1723(4)	0.0400(17)
C(49)	1.0927(5)	-0.2914(4)	0.1200(4)	0.0374(16)
C(50)	1.0821(5)	-0.2332(4)	0.0619(3)	0.0334(15)
C(51)	1.0115(5)	-0.1768(4)	0.0583(3)	0.0344(16)
C(52)	1.1773(6)	-0.4093(5)	0.1174(4)	0.0427(18)
N(52)	1.1729(5)	-0.3413(4)	0.1265(3)	0.0415(15)
O(52)	1.1128(4)	-0.4354(3)	0.0948(3)	0.0535(15)
C(53)	1.6042(7)	-0.3052(5)	0.1997(4)	0.047(2)
C(54)	1.6200(8)	-0.5644(5)	0.3764(4)	0.055(2)
C(55)	1.6458(6)	-0.0614(5)	0.3214(4)	0.0450(19)
C(56)	1.4992(7)	-0.2729(5)	0.5125(5)	0.062(3)
C(57)	1.2297(7)	0.1309(6)	0.4393(4)	0.063(2)
C(58)	1.3080(9)	0.2019(6)	0.4181(6)	0.083(3)
C(59)	1.1309(8)	0.1678(8)	0.4129(6)	0.092(4)
C(60)	1.2218(8)	0.0978(8)	0.5106(5)	0.084(3)
C(61)	1.1882(6)	0.0250(5)	0.1366(4)	0.0456(19)
C(62)	0.9398(6)	-0.0439(5)	0.3140(4)	0.046(2)
C(63)	1.0482(8)	-0.3606(6)	0.2364(4)	0.063(2)
C(64)	1.1454(6)	-0.2259(5)	0.0037(4)	0.051(2)
N(1A)	0.781(3)	0.211(2)	0.3368(12)	0.061(6)
C(2A)	0.7471(6)	0.2821(5)	0.3052(4)	0.054(2)
C(3A)	0.7844(5)	0.3288(4)	0.2494(3)	0.0327(16)
C(4A)	0.8718(5)	0.3094(4)	0.2287(3)	0.0320(15)
C(5A)	0.9195(5)	0.2444(4)	0.2670(3)	0.0333(15)

Table E2: To be continued on next page

	x	y	z	U(eq)
C(6A)	0.8757(7)	0.2002(5)	0.3230(4)	0.055(2)
C(7A)	0.7293(5)	0.3994(4)	0.2105(3)	0.0326(15)
N(7A)	0.7741(5)	0.4489(3)	0.1602(3)	0.0386(15)
O(7A)	0.6491(4)	0.4099(3)	0.2253(3)	0.0444(13)
C(8A)	0.7335(5)	0.5161(4)	0.1170(3)	0.0360(16)
C(9A)	0.7605(5)	0.5887(4)	0.1181(4)	0.0369(17)
C(10A)	0.7244(5)	0.6534(4)	0.0743(3)	0.0330(15)
C(11A)	0.6607(5)	0.6502(4)	0.0269(3)	0.0302(15)
C(12A)	0.6349(5)	0.5783(4)	0.0280(3)	0.0304(15)
C(13A)	0.6696(5)	0.5100(4)	0.0733(3)	0.0334(15)
C(14A)	0.6293(5)	0.7229(4)	-0.0273(3)	0.0285(14)
C(15A)	0.5300(5)	0.7133(4)	-0.0496(3)	0.0344(16)
C(16A)	0.4516(6)	0.7113(5)	-0.0002(4)	0.0422(17)
C(17A)	0.4513(6)	0.7836(5)	0.0150(4)	0.0475(19)
C(18A)	0.5487(5)	0.7977(4)	0.0378(4)	0.0390(17)
C(19A)	0.6276(5)	0.7973(4)	-0.0090(3)	0.0332(15)
C(20A)	0.7086(5)	0.7316(4)	-0.0803(3)	0.0306(15)
C(21A)	0.7962(5)	0.7628(4)	-0.0765(4)	0.0379(17)
C(26A)	0.6954(5)	0.7040(4)	-0.1294(3)	0.0349(16)
C(29A)	0.796(4)	0.223(3)	0.3492(16)	0.061(6)
C(48A)	1.2304(5)	0.2968(4)	0.1724(3)	0.0379(17)
C(49A)	1.1428(5)	0.2669(4)	0.1660(3)	0.0347(16)
C(50A)	1.1293(5)	0.2354(4)	0.1175(4)	0.0385(17)
C(52A)	1.0122(5)	0.2213(4)	0.2463(3)	0.0338(16)
N(52A)	1.0630(4)	0.2770(4)	0.2032(3)	0.0382(14)
O(52A)	1.0407(4)	0.1532(3)	0.2688(2)	0.0457(14)
C(53A)	0.6438(7)	0.4333(5)	0.0699(4)	0.050(2)
C(54A)	0.8293(7)	0.5950(5)	0.1670(4)	0.053(2)
C(57A)	0.7600(10)	0.1773(8)	0.4157(7)	0.055(3)
C(58A)	0.6525(12)	0.1405(11)	0.4158(10)	0.066(4)
C(59A)	0.8290(14)	0.1099(11)	0.4523(9)	0.073(4)
C(60A)	0.7518(15)	0.2318(11)	0.4532(9)	0.069(4)
C(63A)	1.2430(6)	0.3336(5)	0.2227(4)	0.051(2)
C(64A)	1.0355(6)	0.2012(6)	0.1118(4)	0.052(2)
C(71)	0.7115(10)	0.1549(8)	0.2004(6)	0.092(3)
Cl(72)	0.7083(3)	0.2353(2)	0.13521(16)	0.1076(13)
Cl(73)	0.8082(2)	0.09456(16)	0.19820(17)	0.0870(10)
C(74)	1.4567(13)	-0.3331(11)	0.3706(9)	0.121(4)
Cl(75)	1.3586(5)	-0.2767(5)	0.3723(3)	0.175(2)
Cl(76)	1.4536(5)	-0.4204(4)	0.4470(3)	0.162(2)
C(77)	0.4174(16)	-0.1047(12)	0.1441(11)	0.146(5)
Cl(78)	0.4671(5)	-0.1285(4)	0.2297(3)	0.168(2)
Cl(79)	0.4414(4)	-0.0237(3)	0.0948(3)	0.162(2)
C(80)	0.4260(14)	0.1555(11)	0.2606(9)	0.136(4)
Cl(81)	0.5030(3)	0.2427(3)	0.2482(2)	0.1216(14)
Cl(82)	0.4519(3)	0.1048(2)	0.2197(2)	0.1257(15)

Table E2: To be continued on next page

	x	y	z	U(eq)
C(83)	0.9790(14)	0.3972(12)	0.3430(10)	0.132(4)
Cl(84)	1.0284(4)	0.4289(3)	0.2691(3)	0.1499(19)
Cl(85)	0.8914(4)	0.4557(3)	0.3537(3)	0.1366(17)
C(86)	1.243(2)	-0.4695(16)	0.3610(13)	0.171(6)
Cl(87)	1.2772(6)	-0.5663(5)	0.3641(4)	0.196(3)
Cl(88)	1.1482(5)	-0.4542(4)	0.3912(3)	0.180(2)
C(89)	0.794(2)	0.1795(18)	0.5146(14)	0.106(6)
Cl(90)	0.8924(9)	0.1347(8)	0.4892(6)	0.161(4)
Cl(91)	0.7892(6)	0.2770(5)	0.4704(4)	0.115(2)
Cl(92)	0.9952(6)	-0.5676(4)	0.1162(4)	0.180(2)
Cl(93)	0.9818(7)	-0.3858(6)	-0.0069(4)	0.218(3)
Cl(94)	1.3076(5)	-0.2708(4)	0.1864(4)	0.178(2)
Cl(95)	1.1716(7)	-0.1894(5)	0.2275(4)	0.203(3)

Table E2: Atomic coordinates and equivalent isotropic displacement parameters (\AA^2) for the crystal structure of **3**. U(eq) is defined as one third of the trace of the orthogonalized U_{ij} tensor.

Bis{23⁵-*tert*-butyl-7⁵,7⁵,13²,13⁶,20³,20⁵,26³,26⁵-octamethyl-8,10⁵,12,21,25-pentaaza-7,13,20,26(1,4),10,23(1,3)-hexabenzendispiro[5.7.5¹⁴.7⁶]hexacosaphane-9,11,22,24-tetrone}palladium(II)chloride (compound **34** from section C) ^[72,127,129]

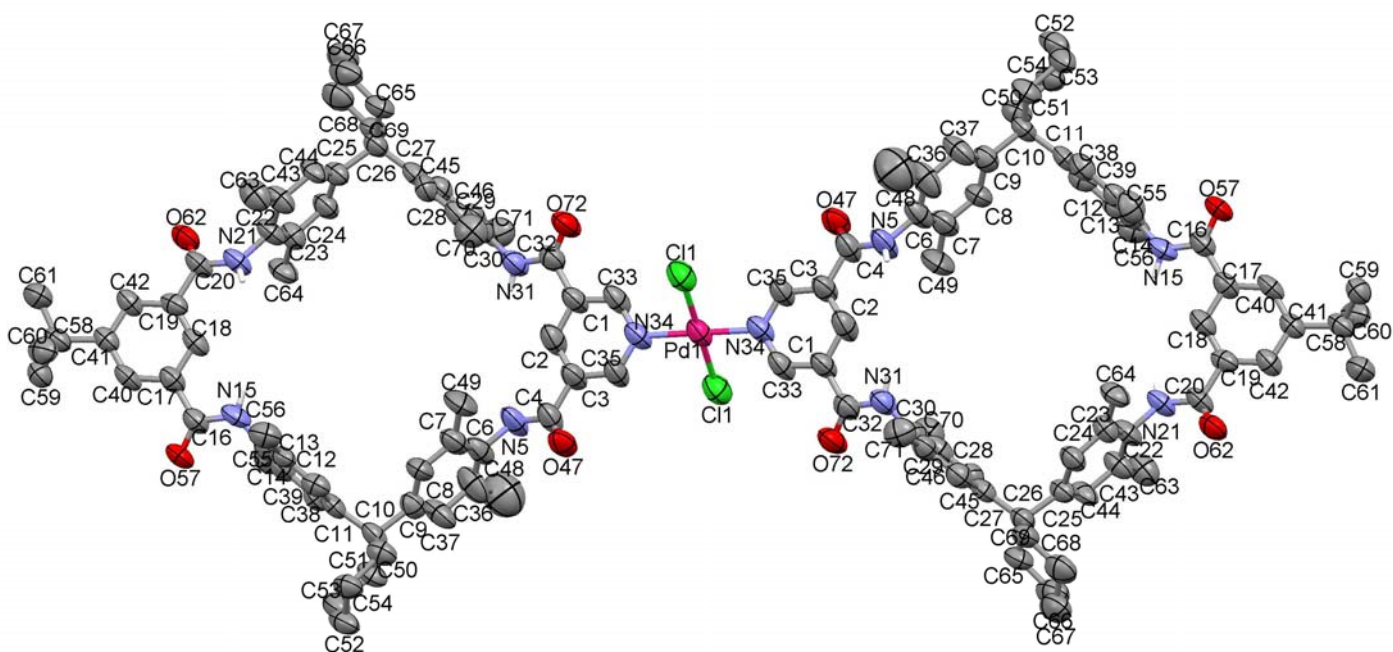
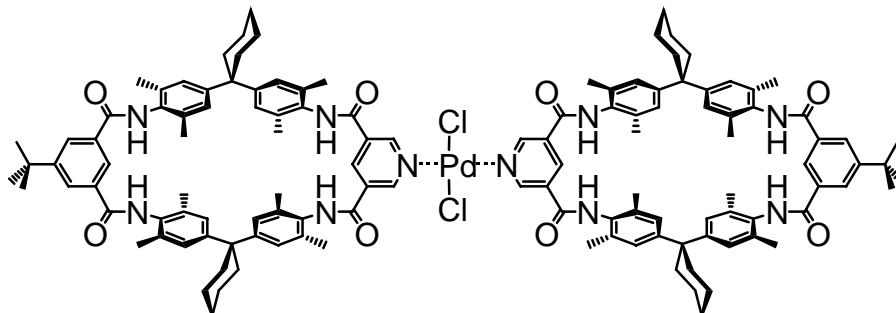


Figure E4: Crystal structure of **34** (with 50% probability ellipsoids), all protons except NH protons omitted;
Color code: C gray, Cl green, H white, N blue, O red, Pd magenta.

Identification code	cca062
Chemical formula	$C_{144.40}H_{164.40}Cl_3N_{10}O_{23.80}Pd$
Formula weight	2633.63
Temperature	173.0(1) K
Radiation, wavelength	CuK $_{\alpha}$, 1.54184 Å
Crystal system, space group	triclinic, $P\bar{1}$
Unit cell parameters	a = 12.0618(8) Å α = 72.443(4) deg. b = 16.091(2) Å β = 82.028(4) deg. c = 24.424(2) Å γ = 69.181(3) deg.
Volume	4221.8(6) Å ³
Z, Calculated density	Z = 1, $\rho(\text{calcd}) = 1.036 \text{ g/cm}^3$
Absorption coefficient μ	1.800 mm ⁻¹
F(000)	1388.2
Crystal colour and size	colourless, 0.10 × 0.15 × 0.20 mm ³
Data collection method	Bruker Nonius APEX II diffractometer
Reflections unique	9747
Reflections with $I > 2\sigma$	5581
Absorption correction	multi-scan absorption correction
Max. and min. transmission	0.7148 and 0.8405
Data / restraints / parameters	9747 / 2121 / 883
Goodness-of-fit on F ²	1.067
Final R indices [$I > 2\sigma(I)$]	R1 = 0.1457, wR2 = 0.3410
R indices (all data)	R1 = 0.2167, wR2 = 0.3825
Largest diff. peak and hole	1.078 and -0.66 e Å ⁻³
CCDC number	CCDC-687762

Table E3: Crystal data and structure refinement for 34

	x	y	z	U(eq)
Pd1	0	1	0	0.0798(7)
C11	0.0132(4)	0.9186(3)	-0.0646(2)	0.0993(18)
O47	0.1667(10)	0.6320(7)	0.1173(5)	0.091(5)
O57	0.9562(10)	0.0678(6)	0.4212(5)	0.091(5)
O62	1.2135(11)	0.4133(7)	0.3834(5)	0.089(5)
O72	0.3989(10)	0.9802(7)	0.0958(6)	0.103(5)
N5	0.3676(12)	0.5855(8)	0.1162(7)	0.101(6)
N15	0.8341(13)	0.2186(8)	0.3969(6)	0.080(5)
N21	1.0135(11)	0.4594(7)	0.3763(5)	0.076(5)
N31	0.5337(12)	0.8357(8)	0.1047(6)	0.085(6)
N34	0.1492(12)	0.9042(8)	0.0369(6)	0.080(5)
C1	0.3350(14)	0.8682(9)	0.0768(7)	0.082(7)
C2	0.3419(15)	0.7750(10)	0.0944(8)	0.094(7)
C3	0.2574(14)	0.7464(10)	0.0822(8)	0.080(6)
C4	0.2577(17)	0.6487(11)	0.1065(8)	0.091(7)
C6	0.3889(14)	0.4936(11)	0.1555(10)	0.087(7)
C7	0.3756(16)	0.4838(11)	0.2129(10)	0.090(8)
C8	0.4020(15)	0.3940(10)	0.2496(8)	0.085(7)
C9	0.4357(13)	0.3175(10)	0.2298(8)	0.074(7)
C10	0.4639(14)	0.2191(9)	0.2719(7)	0.074(6)
C11	0.5649(15)	0.2104(9)	0.3104(8)	0.071(7)
C12	0.5425(16)	0.2312(9)	0.3632(8)	0.071(7)
C13	0.6322(19)	0.2306(9)	0.3918(7)	0.073(7)
C14	0.7455(17)	0.2094(10)	0.3699(9)	0.074(7)
C16	0.9356(15)	0.1500(10)	0.4180(7)	0.076(6)
C17	1.0277(14)	0.1819(9)	0.4344(7)	0.074(6)
C18	1.0335(15)	0.2713(9)	0.4062(7)	0.075(6)
C19	1.1162(15)	0.3005(9)	0.4220(7)	0.070(6)
C20	1.1210(18)	0.3959(10)	0.3924(7)	0.079(7)
C22	0.9950(14)	0.5508(9)	0.3379(7)	0.076(6)
C23	1.0263(13)	0.5628(9)	0.2806(7)	0.072(6)
C24	1.0035(14)	0.6540(9)	0.2453(7)	0.079(6)
C25	0.9496(13)	0.7306(9)	0.2670(7)	0.065(6)
C26	0.9175(14)	0.8279(9)	0.2236(7)	0.070(6)
C27	0.8138(15)	0.8368(9)	0.1901(8)	0.069(7)
C28	0.7042(16)	0.8414(9)	0.2176(8)	0.076(7)
C29	0.6088(17)	0.8466(10)	0.1906(9)	0.084(8)
C30	0.6273(15)	0.8418(9)	0.1324(9)	0.077(7)
C32	0.4268(16)	0.9012(11)	0.0923(7)	0.081(7)
C33	0.2341(14)	0.9306(10)	0.0501(7)	0.083(7)
C35	0.1620(13)	0.8139(10)	0.0532(7)	0.084(6)
C36	0.424(2)	0.4205(14)	0.1352(8)	0.117(9)
C37	0.4453(18)	0.3305(11)	0.1718(9)	0.108(9)
C38	0.6820(16)	0.1870(9)	0.2888(7)	0.073(6)
C39	0.7730(14)	0.1870(9)	0.3183(9)	0.073(7)
C40	1.1068(14)	0.1247(9)	0.4776(7)	0.072(6)
C41	1.1908(14)	0.1542(9)	0.4928(6)	0.066(6)

Table E4: To be continued on next page

C42	1.1963(13)	0.2425(9)	0.4643(7)	0.072(6)
C43	0.9430(15)	0.6255(10)	0.3612(7)	0.081(6)
C44	0.9207(14)	0.7154(9)	0.3235(7)	0.078(7)
C45	0.8265(16)	0.8352(10)	0.1326(9)	0.078(7)
C46	0.7356(15)	0.8390(9)	0.1027(8)	0.074(7)
C48	0.440(3)	0.434(2)	0.0672(12)	0.199(9)
C49	0.338(2)	0.5644(11)	0.2369(10)	0.141(10)
C50	0.3478(14)	0.2150(10)	0.3079(7)	0.081(7)
C51	0.3606(15)	0.1185(10)	0.3477(7)	0.082(7)
C52	0.4023(18)	0.0454(10)	0.3181(7)	0.092(8)
C53	0.5179(18)	0.0479(10)	0.2834(8)	0.094(8)
C54	0.4990(15)	0.1430(9)	0.2414(7)	0.080(6)
C55	0.8950(14)	0.1699(11)	0.2905(8)	0.091(7)
C56	0.6007(16)	0.2539(11)	0.4499(8)	0.094(8)
C58	1.2777(15)	0.0869(10)	0.5394(7)	0.080(6)
C59	1.3437(14)	-0.0027(9)	0.5230(7)	0.081(6)
C60	1.2041(16)	0.0643(11)	0.5970(7)	0.092(8)
C61	1.3691(16)	0.1270(11)	0.5496(8)	0.101(8)
C63	0.9102(17)	0.6122(12)	0.4249(7)	0.102(5)
C64	1.0801(15)	0.4833(9)	0.2558(7)	0.086(7)
C65	0.8785(16)	0.9073(10)	0.2537(8)	0.085(7)
C66	0.977(2)	0.9133(12)	0.2822(8)	0.106(9)
C67	1.087(2)	0.9198(13)	0.2407(9)	0.125(10)
C68	1.1261(18)	0.8401(12)	0.2132(8)	0.102(8)
C69	1.0252(14)	0.8372(10)	0.1838(7)	0.076(6)
C70	0.4880(16)	0.8509(13)	0.2226(8)	0.105(8)
C71	0.7529(16)	0.8361(12)	0.0412(8)	0.096(8)
O73	0.6799(18)	0.5466(10)	0.1961(9)	0.090(5)
O76	0.7490(19)	0.5023(10)	0.3050(9)	0.090(5)
C74	0.707(3)	0.4535(11)	0.2286(10)	0.090(5)
C75	0.677(2)	0.4608(18)	0.2895(11)	0.090(5)
C77	0.710(3)	0.5954(11)	0.2722(10)	0.090(5)
C78	0.751(3)	0.5882(19)	0.2120(11)	0.090(5)
O79	0.167(2)	0.2856(13)	0.0883(10)	0.110(6)
O82	0.166(2)	0.1970(14)	0.2043(10)	0.110(6)
C80	0.166(3)	0.330(2)	0.1305(11)	0.110(6)
C81	0.097(3)	0.2906(15)	0.1824(14)	0.110(6)
C83	0.149(3)	0.157(2)	0.1636(11)	0.110(6)
C84	0.212(3)	0.1883(13)	0.1074(14)	0.110(6)
O85	0.832(3)	0.400(2)	0.0694(12)	0.129(8)
O88	0.750(3)	0.283(2)	0.0875(13)	0.129(8)
C86	0.852(4)	0.357(3)	0.0247(18)	0.129(8)
C87	0.740(4)	0.334(3)	0.0292(14)	0.129(8)
C89	0.738(4)	0.307(3)	0.1395(16)	0.129(8)
C90	0.820(4)	0.363(3)	0.1293(13)	0.129(8)
O98	0.544(2)	0.0873(16)	0.0450(9)	0.101(11)
C99	0.597(4)	0.097(2)	0.0906(15)	0.090(16)
Cl3	0.4753(15)	0.2016(14)	0.0440(9)	0.121(7)

Table E4: To be continued on next page

C14	0.7010(15)	0.0853(15)	0.1018(9)	0.121(7)
C111	0.573(8)	0.0873(12)	0.073(7)	0.121(7)
O95	0.3354(19)	0.5352(12)	0.3880(10)	0.112(10)
C96	0.260(3)	0.6275(14)	0.3634(15)	0.123(16)
O102	0.342(3)	0.441(4)	0.450(2)	0.09(2)
C103	0.421(6)	0.476(7)	0.409(3)	0.09(2)
O91	0.7919(12)	0.4051(9)	0.4248(5)	0.081(4)
C92	0.7932(19)	0.3769(13)	0.4862(5)	0.081(4)
O106	0.169(3)	0.717(2)	0.4615(16)	0.070(8)
O100	0.550(2)	0.5267(18)	0.4136(13)	0.104(11)
O110	0.523(5)	0.703(4)	0.402(3)	0.106(12)
C101	0.568(4)	0.600(3)	0.429(2)	0.104(11)
O93	0.8516(16)	0.0963(12)	0.5553(8)	0.102(7)
C94	0.789(2)	0.0881(18)	0.6099(9)	0.102(7)
O104	0.826(3)	0.614(3)	0.031(2)	0.14(2)
C105	0.917(5)	0.592(4)	0.070(2)	0.14(2)
O109	0.5985(11)	0.6407(10)	0.0839(7)	0.133(7)
O107	0.344(4)	0.725(3)	0.3348(19)	0.117(9)

Table E4: Atomic coordinates and equivalent isotropic displacement parameters (\AA^2) for the crystal structure of **34**. $U(\text{eq})$ is defined as one third of the trace of the orthogonalized U_{ij} tensor.

23⁵-tert-butyl-7³,7⁵,10⁵,13²,13⁶,20³,20⁵,26³,26⁵-nonamethyl-8,12,21,25-tetraaza-10⁵-azonia-7,13,20,26(1,4),10,23(1,3)-hexabenzena-dispiro[5.7.5¹⁴.7⁶]hexacosaphane-9,11,22,24-tetrone iodide (compound **4⁺ I⁻** from section D) ^[109,127,134]

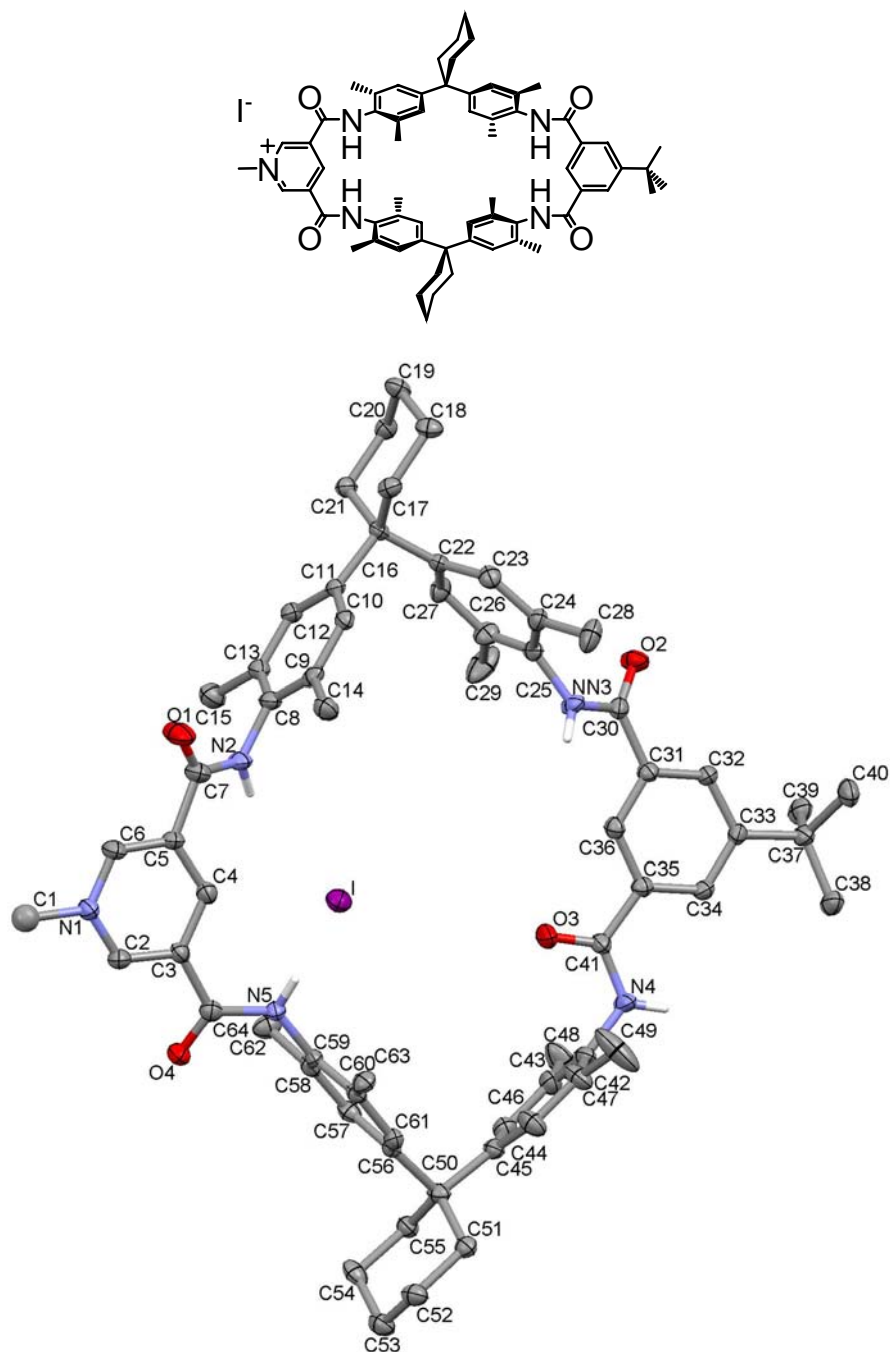


Figure E4: Crystal structure of **4⁺ I⁻** (with 50% probability ellipsoids), all protons except NH protons omitted; Color code: C gray, H white, I purple, N blue, O red.

Identification code	joerg173
Empirical formula	$C_{64}H_{74}I_{0.5}N_5O_4$
Formula weight	1040.73
Temperature	100(2) K
Radiation, Wave length	MoK α , 0.71073 Å
Crystal system, space group	Monoclinic, C2/c (No.15)
Unit cell dimensions	a = 27.9903(5) Å α = 90 deg. b = 17.1774(3) Å β = 107.1480(10) deg. c = 30.9747(6) Å γ = 90 deg.
Volume	14230.6(4) Å ³
Z, Calculated density	Z = 8, ρ (calcd) = 0.972 g/cm ³
Absorption coefficient μ	0.274 mm ⁻¹
F(000)	4412
Crystal colour and size	yellow, 0.12 x 0.15 x 0.19 mm ³
Data collection method	Nonius KappaCCD diffractometer
θ range for data collection	1.73 to 27.53 deg.
Index range	h – 36 to 36, k –21 to 22, l –40 to 39
Reflections collected / unique	54127 / 15809 [R(int) = 0.0754]
Completeness to $\theta = 27.53$	96.3 %
Absorption correction	Sphere
Max. and min. transmission	0.9679 and 0.9498
Refinement method	Full-matrix least-squares on F ²
Data / restraints / parameters	15809 / 0 / 670
Goodness-of-fit on F ²	0.854
Final R indices [I > 2 σ (I)]	R1 = 0.0505, wR2 = 0.1065
R indices (all data)	R1 = 0.0954, wR2 = 0.1153
Largest diff. peak and hole	0.797 and –0.657 e Å ⁻³
CCDC number	CCDC-709648

Table E5: Crystal data and structure refinement for 4⁺ I⁻

	x	y	z	U(eq)
I	0	0.7671(1)	0.2500	0.032(1)
N(1)	0.0780(1)	1.0355(1)	0.3300(1)	0.029(1)
N(2)	-0.0809(1)	0.9282(1)	0.3201(1)	0.026(1)
N(3)	-0.2327(1)	0.5676(1)	0.3332(1)	0.028(1)
N(4)	-0.0375(1)	0.3585(1)	0.4251(1)	0.031(1)
N(5)	0.0888(1)	0.7680(1)	0.3681(1)	0.022(1)
O(1)	-0.0753(1)	1.0201(1)	0.2688(1)	0.051(1)
O(2)	-0.2887(1)	0.5096(1)	0.3628(1)	0.034(1)
O(3)	-0.0598(1)	0.4817(1)	0.4064(1)	0.045(1)
O(4)	0.1480(1)	0.8517(1)	0.4101(1)	0.032(1)
C(1)	0.1058(1)	1.1054(2)	0.3234(1)	0.037(1)
C(2)	0.1026(1)	0.9736(2)	0.3519(1)	0.025(1)
C(3)	0.0777(1)	0.9061(2)	0.3558(1)	0.022(1)
C(4)	0.0260(1)	0.9049(2)	0.3393(1)	0.025(1)
C(5)	0.0007(1)	0.9704(2)	0.3187(1)	0.025(1)
C(6)	0.0276(1)	1.0349(2)	0.3132(1)	0.030(1)
C(7)	-0.0560(1)	0.9755(2)	0.2999(1)	0.033(1)
C(8)	-0.1344(1)	0.9222(2)	0.3081(1)	0.024(1)
C(9)	-0.1613(1)	0.8918(1)	0.2660(1)	0.024(1)
C(10)	-0.2128(1)	0.8822(1)	0.2578(1)	0.022(1)
C(11)	-0.2376(1)	0.9007(1)	0.2890(1)	0.020(1)
C(12)	-0.2097(1)	0.9317(1)	0.3299(1)	0.023(1)
C(13)	-0.1580(1)	0.9424(2)	0.3405(1)	0.024(1)
C(14)	-0.1372(1)	0.8699(2)	0.2310(1)	0.031(1)
C(15)	-0.1288(1)	0.9754(2)	0.3864(1)	0.036(1)
C(16)	-0.2935(1)	0.8771(1)	0.2804(1)	0.020(1)
C(17)	-0.3227(1)	0.8935(2)	0.2303(1)	0.024(1)
C(18)	-0.3791(1)	0.8766(2)	0.2193(1)	0.028(1)
C(19)	-0.4023(1)	0.9242(2)	0.2494(1)	0.028(1)
C(20)	-0.3743(1)	0.9104(2)	0.2992(1)	0.026(1)
C(21)	-0.3185(1)	0.9282(2)	0.3089(1)	0.023(1)
C(22)	-0.2903(1)	0.7919(1)	0.2933(1)	0.020(1)
C(23)	-0.2924(1)	0.7332(2)	0.2619(1)	0.026(1)
C(24)	-0.2774(1)	0.6567(2)	0.2741(1)	0.026(1)
C(25)	-0.2585(1)	0.6396(2)	0.3200(1)	0.025(1)
C(26)	-0.2599(1)	0.6944(2)	0.3530(1)	0.028(1)
C(27)	-0.2761(1)	0.7689(2)	0.3389(1)	0.026(1)
C(28)	-0.2782(1)	0.5959(2)	0.2391(1)	0.040(1)
C(29)	-0.2415(1)	0.6750(2)	0.4029(1)	0.052(1)
C(30)	-0.2476(1)	0.5088(2)	0.3555(1)	0.025(1)
C(31)	-0.2113(1)	0.4441(1)	0.3723(1)	0.022(1)
C(32)	-0.2288(1)	0.3722(1)	0.3809(1)	0.022(1)
C(33)	-0.1965(1)	0.3088(1)	0.3971(1)	0.022(1)
C(34)	-0.1452(1)	0.3214(2)	0.4059(1)	0.022(1)
C(35)	-0.1269(1)	0.3950(2)	0.3993(1)	0.022(1)
C(36)	-0.1596(1)	0.4557(2)	0.3819(1)	0.022(1)
C(37)	-0.2180(1)	0.2303(2)	0.4049(1)	0.026(1)
C(38)	-0.1783(1)	0.1663(2)	0.4152(1)	0.035(1)

Table E6: To be continued on next page

	x	y	z	U(eq)
C(39)	-0.2402(1)	0.2375(2)	0.4450(1)	0.032(1)
C(40)	-0.2594(1)	0.2063(2)	0.3620(1)	0.037(1)
C(41)	-0.0724(1)	0.4149(2)	0.4104(1)	0.025(1)
C(42)	0.0146(1)	0.3785(2)	0.4359(1)	0.028(1)
C(43)	0.0402(1)	0.3979(2)	0.4806(1)	0.030(1)
C(44)	0.0886(1)	0.4282(2)	0.4896(1)	0.029(1)
C(45)	0.1114(1)	0.4386(1)	0.4555(1)	0.023(1)
C(46)	0.0851(1)	0.4144(2)	0.4127(1)	0.034(1)
C(47)	0.0366(1)	0.3836(2)	0.4016(1)	0.034(1)
C(48)	0.0157(1)	0.3882(2)	0.5181(1)	0.052(1)
C(49)	0.0098(1)	0.3608(2)	0.3537(1)	0.071(1)
C(50)	0.1615(1)	0.4813(2)	0.4622(1)	0.023(1)
C(51)	0.1954(1)	0.4309(2)	0.4414(1)	0.025(1)
C(52)	0.2471(1)	0.4672(2)	0.4477(1)	0.030(1)
C(53)	0.2741(1)	0.4825(2)	0.4968(1)	0.031(1)
C(54)	0.2413(1)	0.5312(2)	0.5184(1)	0.031(1)
C(55)	0.1904(1)	0.4927(2)	0.5125(1)	0.025(1)
C(56)	0.1465(1)	0.5598(1)	0.4374(1)	0.020(1)
C(57)	0.1296(1)	0.6205(2)	0.4591(1)	0.025(1)
C(58)	0.1110(1)	0.6898(2)	0.4371(1)	0.025(1)
C(59)	0.1093(1)	0.6980(1)	0.3916(1)	0.020(1)
C(60)	0.1248(1)	0.6384(2)	0.3685(1)	0.022(1)
C(61)	0.1441(1)	0.5708(1)	0.3927(1)	0.022(1)
C(62)	0.0924(1)	0.7523(2)	0.4622(1)	0.032(1)
C(63)	0.1200(1)	0.6446(2)	0.3191(1)	0.027(1)
C(64)	0.1083(1)	0.8396(2)	0.3803(1)	0.025(1)

Table E6: Atomic coordinates and equivalent isotropic displacement parameters (\AA^2) for the crystal structure of $4^+ \Gamma$. U(eq) is defined as one third of the trace of the orthogonalized U_{ij} tensor.

F. References and Notes

- [1] Selected Examples: a) M. Wehner, T. Schrader, *Angew. Chem.* **2002**, *114*, 1827-1831; *Angew. Chem. Int. Ed.* **2002**, *41*, 1751-1754; b) A. K. H. Hirsch, F. R. Fischer, F. Diederich, *Angew. Chem.* **2007**, *119*, 342-357; *Angew. Chem. Int. Ed.* **2007**, *46*, 338-352; c) P. Blondeau, M. Segura, R. Perez-Fernandez, J. de Mendoza, *Chem. Soc. Rev.* **2007**, *36*, 198-210.
- [2] S. Mizukami, T. Nagano, Y. Urano, A. Odani, K. Kikuchi, *J. Am. Chem. Soc.* **2002**, *124*, 3920-3925.
- [3] a) A. Bianchi, K. Bowman-James, E. Garcia-Espana, *Supramolecular Chemistry of Anions*; Wiley-VCH: New York, **1997**; b) P. A. Gale, *Coord. Chem. Rev.* **2003**, *240*, 191-221; c) J.L. Sessler, P.A. Gale, W.-S. Cho, *Anion Receptor Chemistry*, RCS Publishing: Cambridge, **2006**.
- [4] P. A. Gale, S. E. Garcia-Garrido, J. Garric, *Chem. Soc. Rev.* **2008**, *37*, 151-190.
- [5] R. Custelcean, B. A. Moyer, *Eur. J. Inorg. Chem.* **2007**, 1321-1340.
- [6] J. Scheele, P. Timmerman, D. N. Reinhoudt, *Chem. Commun.* **1998**, 2613-2614.
- [7] A. F. Holleman, E. Wiberg, *Lehrbuch der Anorganischen Chemie*; deGruyter: Berlin, New York, **1995**.
- [8] K. Kavallieratos, S. R. de Gala, D. J. Austin, R. H. Crabtree, *J. Am. Chem. Soc.* **1997**, *119*, 2325-2326.
- [9] a) M. J. Hynes, M. B. Beatrice, V. McKee, R. M. Town, J. Nelson, *J. Chem. Soc.-Dalton Trans.* **2000**, 2853-2859; b) B. M. Maubert, J. Nelson, V. McKee, R. M. Town, I. Pal, *J. Chem. Soc.-Dalton Trans.* **2001**, 1395-1397.
- [10] M. P. Hughes, B. D. Smith, *J. Org. Chem.* **1997**, *62*, 4492-4499.
- [11] J. L. Sessler, R. S. Zimmerman, G. J. Kirkovits, A. Gebauer, M. Scherer, *J. Organomet. Chem.* **2001**, *637*, 343-348.
- [12] W. J. Belcher, M. Fabre, T. Farhan, J. W. Steed, *Org. Biomol. Chem.* **2006**, *4*, 781-786.
- [13] E. L. Doyle, L. Riera, D. S. Wright, *Eur. J. Inorg. Chem.* **2003**, 3279-3289.
- [14] C. Denekamp, K. Suwinska, H. Salman, Y. Abraham, Y. Eichen, J. B. Ari, *Chem.-Eur. J.* **2007**, *13*, 657-665.
- [15] H. Maeda, Y. Kusunose, *Chem. Eur. J.* **2005**, *11*, 5661-5666.
- [16] D. H. Lee, J. H. Im, S. U. Son, Y. K. Chung, J. I. Hong, *J. Am. Chem. Soc.* **2003**, *125*, 7752-7753.
- [17] A. P. Davis, J. F. Gilmer, J. J. Perry, *Angew. Chem.* **1996**, *108*, 1410-1413; *Angew. Chem. Int. Ed.* **1996**, *35*, 1312-1315.
- [18] M. Albrecht, C. Wesselt, M. de Groot, K. Rissanen, A. Luchow, *J. Am. Chem. Soc.* **2008**, *130*, 4600-4601.
- [19] a) S. J. Coles, J. G. Frey, P. A. Gale, M. B. Hursthouse, M. E. Light, K. Navakhun, G. L. Thomas, *Chem. Commun.* **2003**, 568-569; b) P. A. Gale, *Acc. Chem. Res.* **2006**, *39*, 465-475.
- [20] Examples for aromatic C-H...anion interactions: a) D.-W. Yoon, H. Hwang, C.-H. Lee, *Angew. Chem.* **2002**, *114*, 1835-1837; *Angew. Chem. Int. Ed.* **2002**, *41*, 1757-1759; b) K. Chellappan, N. J. Singh, I.-C. Hwang, J. W. Lee, K. S. Kim, *Angew. Chem.* **2005**, *117*, 2959-2963; *Angew. Chem. Int. Ed.* **2005**, *44*, 2899-2903.
- [21] C. A. Ilioudis, D.A. Tocher, J. W. Steed, *J. Am. Chem. Soc.* **2004**, *126*, 12395-12402.

- [22] For reviews on resorcinarene-based cavitands, see: a) P. Timmerman, W. Verboom, D. N. Reinhoudt, *Tetrahedron* **1996**, *52*, 2663-2704; b) A. Jasat, J. C. Sherman, *Chem. Rev.* **1999**, *99*, 931-968.
- [23] F. Hof, S. L. Craig, C. Nuckolls, J. Rebek, Jr., *Angew. Chem.* **2002**, *114*, 1556-1578; *Angew. Chem. Int. Ed.* **2002**, *41*, 1488-1508.
- [24] a) L. R. MacGillivray, J. L. Atwood, *Nature* **1997**, *389*, 469-472; b) T. Gerkenmeier, W. Iwanek, C. Agena, R. Fröhlich, S. Kotila, C. Näther, J. Mattay, *Eur. J. Org. Chem.* **1999**, 2257-2262; c) A. Shivanyuk, J. Rebek, Jr., *J. Am. Chem. Soc.* **2003**, *125*, 3432-3433; d) L. Avram, Y. Cohen, *Org. Lett.* **2003**, *5*, 3329-3332; e) N. K. Beyeh, M. Kogej, A. Åhman, K. Rissanen, C. A. Schalley, *Angew. Chem.* **2006**, *118*, 5339-5342; *Angew. Chem. Int. Ed.* **2006**, *45*, 5214-5218.
- [25] a) N. Cuminetti, M. H. K. Ebbing, P. Prados, J. de Mendoza, E. Dalcanale, *Tetrahedron Lett.* **2001**, *42*, 527-530; b) F. Fochi, P. Jacopozzi, E. Wegelius, K. Rissanen, P. Cozzini, E. Marastoni, E. Fisicaro, P. Manini, R. Fokkens, E. Dalcanale, *J. Am. Chem. Soc.* **2001**, *123*, 7539-7552.
- [26] O. D. Fox, M. G. B. Drew, P. D. Beer, *Angew. Chem.* **2000**, *112*, 139-144; *Angew. Chem. Int. Ed.* **2000**, *39*, 136-140.
- [27] L. Pirondini, E. Dalcanale, *Chem. Soc. Rev.* **2007**, *36*, 695-706.
- [28] R. J. Hooley, S. M. Biroš, J. Rebek, Jr., *Angew. Chem.* **2006**, *118*, 3597-3599; *Angew. Chem. Int. Ed.* **2006**, *45*, 3517-3519.
- [29] a) H. J. Schneider, *Angew. Chem.* **1991**, *103*, 1419-1439; *Angew. Chem. Int. Ed.* **1991**, *30*, 1417-1436; b) A. Shivanyuk, K. Rissanen, E. Kolehmainen, *Chem. Commun.* **2000**, 1107-1108; c) A. Shivanyuk, J. Rebek Jr., *Chem. Commun.* **2001**, 2374-2375; d) H. Mansikkamäki, M. Nissinen, K. Rissanen, *Chem. Commun.* **2002**, 1902-1903; e) H. Mänsikkamäki, M. Nissinen, C. A. Schalley, K. Rissanen, *New J. Chem.* **2003**, *27*, 88-97.
- [30] a) M. Yamanaka, A. Shivanyuk, J. Rebek, Jr., *J. Am. Chem. Soc.* **2004**, *126*, 2939-2943; b) L. Avram, Y. Cohen, *Org. Lett.* **2006**, *8*, 219-222.
- [31] Selected examples: a) H. Boerrigter, L. Grave, J. W. M. Nissink, L. A. J. Christoffels, J. H. van der Maas, W. Verboom, F. de Jong, D. N. Reinhoudt, *J. Org. Chem.* **1998**, *63*, 4174-4180; b) U. Lücking, D. M. Rudkevich, J. Rebek, Jr., *Tetrahedron Lett.* **2000**, *41*, 9547-9551; c) S. K. Kim, B.-G. Kang, H. S. Koh, Y. J. Yoon, S. J. Jung, B. Jeong, K.-D. Lee, J. Yoon, *Org. Lett.* **2004**, *6*, 4655-4658; d) J. S. Gardner, M. Conda-Sheridan, D. N. Smith, R. G. Harrison, J. D. Lamb, *Inorg. Chem.* **2005**, *44*, 4295-4300.
- [32] a) C. L. D. Gibb, E. D. Stevens, B.C. Gibb, *J. Am. Chem. Soc.* **2001**, *123*, 5849-5850; b) Z.R. Laughrey, T.G. Upton, B.C. Gibb, *Chem. Commun.* **2006**, 970-972.
- [33] a) P. Kebarle, L. Tang, *Anal. Chem.* **1993**, *65*, A972-A986; b) P. Kebarle, *J. Mass Spectrom.* **2000**, *35*, 804-817.
- [34] A. G. Marshall, C. L. Hendrickson, G. S. Jackson, *Mass Spectrom. Rev.* **1998**, *17*, 1-35.
- [35] R. G. Cooks, J. S. Patrick, T. Kotiaho, S. A. McLuckey, *Mass Spectrom. Rev.* **1994**, *13*, 287-339.
- [36] S. S. Zhu, H. Staats, K. Brandhorst, J. Grunenberg, F. Gruppi, E. Dalcanale, A. Lützen, K. Rissanen, C. A. Schalley, *Angew. Chem.* **2008**, *120*, 800-804; *Angew. Chem. Int. Ed.* **2008**, *47*, 788-792. For the synthesis of the cavitands, see also the Supporting Information of this reference.

- [37] Cavitand syntheses: a) D. J. Cram, L. M. Tunstad, C. B. Knobler, *J. Org. Chem.* **1992**, *57*, 528-535; b) J. A. Bryant, M. T. Blanda, M. Vincenti, D. J. Cram, *J. Am. Chem. Soc.* **1991**, *113*, 2167-2172; c) N. Cuminetti, M. H. K. Ebbing, P. Prados, J. de Mendoza, E. Dalcanale, *Tetrahedron Lett.* **2001**, *42*, 527-530; d) F. Fochi, P. Jacopozzi, E. Wegelius, K. Rissanen, P. Cozzini, E. Marastoni, E. Fisicaro, P. Manini, R. Fokkens, E. Dalcanale, *J. Am. Chem. Soc.* **2001**, *123*, 7539-7552.
- [38] H. Staats, *PhD thesis*, University of Bonn, in preparation.
- [39] A. I. Boldyrev, J. Simons, *J. Phys. Chem.* **1994**, *98*, 2298-2300.
- [40] a) A. T. Blades, P. Kebarle, *J. Am. Chem. Soc.* **1994**, *116*, 10761-10766; b) X.-B. Wang, J. B. Nicholas, L.-S. Wang, *J. Chem. Phys.* **2000**, *113*, 10837-10840.
- [41] Please note that for MS/MS experiments described here, the ions corresponding to the second peak from the isotope pattern were mass-selected, which contain one ^{13}C atom. Charge-separating fragmentations preferentially lead to fragments of approximately half the size of the parent ion (e.g. monomer loss from a dimer). Consequently, the ^{13}C atom can be incorporated either in the neutral or in the ionic fragment so that two product signals are observed with a peak spacing of 1 amu. Fragmentation into a product dianion and small neutral fragment (e.g. loss of SO_3 and $\text{CH}_2=\text{O}$) leaves almost all carbons within the ionic product, which then only appears as one, non-split signal. This approach permits to directly determine whether a fragment is singly or doubly charged and thus facilitates interpretation of the MS/MS experiments.
- [42] This experiment is a variant of Cooks' kinetic method and used here only for a qualitative ranking, not for the determination of quantitative binding energies. For a review on this method, see: R. G. Cooks, J. S. Patrick, T. Kotiaho, S. A. McLuckey, *Mass Spectrom. Rev.* **1994**, *13*, 287-339.
- [43] O. B. Berryman, V. S. Bryantsev, D. P. Stay, D. W. Johnson, B. P. Hay, *J. Am. Chem. Soc.* **2007**, *129*, 48-58 and literature cited therein.
- [44] A. D. Becke, *J. Chem. Phys.* **1993**, *98*, 5648-5652.
- [45] M. J. Frisch, G. W. Trucks, H. B. Schlegel, G. E. Scuseria, M. A. Robb, J. R. Cheeseman, J. Montgomery, J. A., T. Vreven, K. N. Kudin, J. C. Burant, J. M. Millam, S. S. Iyengar, J. Tomasi, V. Barone, B. Mennucci, M. Cossi, G. Scalmani, N. Rega, G. A. Petersson, H. Nakatsuji, M. Hada, M. Ehara, K. Toyota, R. Fukuda, J. Hasegawa, M. Ishida, T. Nakajima, Y. Honda, O. Kitao, H. Nakai, M. Klene, X. Li, J. E. Knox, H. P. Hratchian, J. B. Cross, C. Adamo, J. Jaramillo, R. Gomperts, R. E. Stratmann, O. Yazyev, A. J. Austin, R. Cammi, C. Pomelli, J. W. Ochterski, P. Y. Ayala, K. Morokuma, G. A. Voth, P. Salvador, J. J. Dannenberg, V. G. Zakrzewski, S. Dapprich, A. D. Daniels, M. C. Strain, O. Farkas, D. K. Malick, A. D. Rabuck, K. Raghavachari, J. B. Foresman, J. V. Ortiz, Q. Cui, A. G. Baboul, S. Clifford, J. Cioslowski, B. B. Stefanov, G. Liu, A. Liashenko, P. Piskorz, I. Komaromi, R. L. Martin, D. J. Fox, T. Keith, M. A. Al-Laham, C. Y. Peng, A. Nanayakkara, M. Challacombe, P. M. W. Gill, B. Johnson, W. Chen, M. W. Wong, C. Gonzalez, J. A. Pople, Revision B.02 ed., Gaussian, Inc., Pittsburgh PA, **2003**.
- [46] K. Brandhorst, J. Grunenberg, *ChemPhysChem* **2007**, *8*, 1151-1156 and references therein. The generalized compliance constants were computed using their own code COMPLIANCE, which will be available free of charge from the homepage (<http://www.oc.tu-bs.de/grunenberg>) soon.
- [47] Calculations in section A3.2 were done with: CAChe 5.0 for Windows, Fujitsu, Krakow (Poland), **2001**.

- [48] Selected example: M. Albrecht, C. Wesselt, M. de Groot, K. Rissanen, A. Lüchow, *J. Am. Chem. Soc.* **2008**, *130*, 4600-4601.
- [49] J.-M. Lehn, A. Rigault, J. Siegel, J. Harrowfield, B. Chevrier, D. Moras, *Proc. Natl. Acad. Sci. U.S.A.* **1987**, *84*, 2565-2569.
- [50] C. Piguët, G. Bernardinelli, G. Hopfgartner, *Chem. Rev.* **1997**, *97*, 2005-2062.
- [51] For reviews on self-assembly, see: a) G. M. Whitesides, J. P. Mathias, C. T. Seto, *Science* **1991**, *254*, 1312-1319; b) C. A. Schalley, A. Lützen, M. Albrecht, *Chem. Eur. J.* **2004**, *10*, 1072-1080.
- [52] For helicates, it is more unambiguous to use the terms “homo-/heterostranded” instead of “homo-/heteroleptic”. “Homo-/heteroleptic” usually refers to one metal center which is either bound to identical or non-identical ligands, so a metal center in heterotopic homostranded helicates can also be considered as “heteroleptic” in a certain sense.
- [53] M. Barley, E. C. Constable, S. Corr, R. C. S. McQueen, J. C. Nutkins, M. D. Ward, M. G. B. Drew, *J. Chem. Soc., Dalton Trans.* **1988**, 2655-2662.
- [54] E. C. Constable, J. V. Walker, *J. Chem. Soc., Chem. Commun.* **1992**, 884-886.
- [55] E. C. Constable, S. M. Elder, J. Healy, M. D. Ward, *J. Am. Chem. Soc.* **1990**, *112*, 4590-4592.
- [56] B. Hasenknopf, J.-M. Lehn, G. Baum, D. Fenske, *Proc. Natl. Acad. Sci. U.S.A.* **1996**, *93*, 1397-1400.
- [57] C. Piguët, G. Bernardinelli, B. Bocquet, A. Quattropiani, A. F. Williams, *J. Am. Chem. Soc.* **1992**, *114*, 7440-7451.
- [58] B. Hasenknopf, J.-M. Lehn, B. O. Kneisel, G. Baum, D. Fenske, *Angew. Chem.* **1996**, *108*, 1987-1900; *Angew. Chem. Int. Ed.* **1996**, *35*, 1838-1840.
- [59] a) G. C. L. Wong, J. X. Tang, A. Lin, Y. L. Li, P. A. Janmey, C. R. Safinya, *Science* **2000**, *288*, 2035-2039; b) L. M. Greig, D. Philp, *Chem. Soc. Rev.* **2001**, *30*, 287-302; c) A. Aggeli, I. A. Nyrkova, M. Bell, R. Harding, L. Carrick, T. C. B. McLeish, A. N. Semenov, N. Boden, *Proc. Natl. Acad. Sci. U. S. A.* **2001**, *98*, 11857-11862.
- [60] a) J. Elemans, A. E. Rowan, R. J. M. Nolte, *J. Am. Chem. Soc.* **2002**, *124*, 1532-1540; b) F. Würthner, S. Yao, U. Beginn, *Angew. Chem.* **2003**, *115*, 3368-3371; *Angew. Chem. Int. Ed.* **2003**, *42*, 3247-3250; c) O. Ikkala, G. ten Brinke, *Chem. Commun.* **2004**, 2131-2137.
- [61] J. Hamblin, L. J. Childs, N. W. Alcock, M. J. Hannon, *J. Chem. Soc.-Dalton Trans.* **2002**, 164-169.
- [62] J. R. Nitschke, D. Schultz, G. Bernardinelli, D. Gerard, *J. Am. Chem. Soc.* **2004**, *126*, 16538-16543.
- [63] M. Albrecht, S. Mirtschin, M. de Groot, I. Janser, J. Runsink, G. Raabe, M. Kogej, C. A. Schalley, R. Fröhlich, *J. Am. Chem. Soc.* **2005**, *127*, 10371-10387.
- [64] M. Albrecht, M. Fiege, M. Baumert, M. de Groot, R. Fröhlich, L. Russo, K. Rissanen, *Eur. J. Inorg. Chem.* **2007**, 609-616.
- [65] For recent MS studies on metallosupramolecular aggregates, see: a) A. Marquis-Rigault, A. Dupont-Gervais, P. N. W. Baxter, A. Van Dorsselaer, J.-M. Lehn, *Inorg. Chem.* **1996**, *35*, 2307-2310; b) S. König, C. Brückner, K. N. Raymond, J. A. Leary, *J. Am. Soc. Mass Spectrom.* **1998**, *9*, 1099-1103; c) S. Sakamoto, M. Fujita, K. Kim, K. Yamaguchi, *Tetrahedron* **2000**, *56*, 955-964; d) C. A. Schalley, T. Müller, P. Linnartz, M. Witt, M. Schäfer, A. Lützen, *Chem. Eur. J.* **2002**, *8*, 3538-3551; e) I. M. Müller, D. Möller, C. A. Schalley, *Angew. Chem.* **2005**, *117*, 485-488; *Angew. Chem. Int. Ed.* **2005**, *44*, 480-484; f) M. Hutin, C. A. Schalley, G. Bernardinelli, J. R. Nitschke, *Chem. Eur. J.* **2006**, *12*, 4069-4076.

- [66] a) F. M. Romero, R. Ziessel, A. Dupont-Gervais, A. Van Dorsselaer, *Chem. Commun.* **1996**, 551-552; b) A. Marquis-Rigault, A. Dupont-Gervais, A. Van Dorsselaer, J.-M. Lehn, *Chem. Eur. J.* **1996**, *2*, 1395-1398.
- [67] An analogous experiment was also conducted with the 1:1 mixture of $[\text{Li}_3(\mathbf{1})_6\text{Ni}_2]^+$ and $[\text{Li}_3(\mathbf{2})_6\text{Ni}_2]^+$. In the mass spectra of pure $[\text{Li}_3(\mathbf{2})_6\text{Ni}_2]^+$, the mono-sodiated adduct $[\text{Li}_2\text{Na}(\mathbf{2})_6\text{Ni}_2]^+$ is already observable to some extent. Therefore, the mass spectra of the 1:1 mixture of $[\text{Li}_3(\mathbf{1})_6\text{Ni}_2]^+$ and $[\text{Li}_3(\mathbf{2})_6\text{Ni}_2]^+$ showed mono-sodiated adducts for all helicates containing at least three ligands **2**. If only the lithium peaks (those peaks which definitely do not contain sodium) were considered, the mass spectra of the 1:1 mixture of $[\text{Li}_3(\mathbf{1})_6\text{Ni}_2]^+$ and $[\text{Li}_3(\mathbf{2})_6\text{Ni}_2]^+$ show almost the same picture like the mass spectra of the 1:1 mixture of $[\text{Li}_3(\mathbf{1})_6\text{Zn}_2]^+$ and $[\text{Li}_3(\mathbf{2})_6\text{Zn}_2]^+$.
- [68] M. Albrecht, Y. Liu, S. S. Zhu, C. A. Schalley, R. Fröhlich, *Chem. Commun.* **2009**, 1195-1197.
- [69] a) C. Piguet, G. Hopfgartner, B. Bocquet, O. Schaad, A. F. Williams, *J. Am. Chem. Soc.* **1994**, *116*, 9092-9102; b) C. Piguet, G. Hopfgartner, A. F. Williams, J.-C. G. Bünzli, *J. Chem. Soc., Chem. Commun.* **1995**, 491-492; c) C. Piguet, G. Bernardinelli, J.-C. G. Bünzli, S. Petoud, G. Hopfgartner, *J. Chem. Soc., Chem. Commun.* **1995**, 2575-2577; d) C. Piguet, C. Edder, S. Rigault, G. Bernardinelli, J.-C. G. Bünzli, G. Hopfgartner, *J. Chem. Soc., Dalton Trans.* **2000**, 3999-4006; e) C. Edder, C. Piguet, J.-C. G. Bünzli, G. Hopfgartner, *Chem. Eur. J.* **2001**, *7*, 3014-3024; f) see also: T. B. Jensen, R. Scopelliti, J.-C. G. Bünzli, *Dalton Trans.* **2008**, 1027-1036.
- [70] F. E. Hahn, M. Offermann, C. Schulze Isfort, T. Pape, R. Fröhlich, *Angew. Chem.* **2008**, *120*, 6899-6902; *Angew. Chem. Int. Ed.* **2008**, *47*, 6794-6797.
- [71] a) H. M. Ali, S. Puvaneswary, W. J. Basirun, S. W. Ng, *Acta Crystallogr., Sect. E* **2005**, *61*, o1013-o1014; b) P. Melnyk, V. Leroux, C. Sergheraert, P. Grellier, *Bioorg. Med. Chem. Lett.* **2006**, *16*, 31-35; c) O. Pouralimardan, A.-C. Chamayou, C. Janiak, H. Hosseini-Monfared, *Inorg. Chim. Acta* **2007**, *360*, 1599-1608; For related semicarbazone derived ligands and their mononuclear complexes, see: d) M. Albrecht, O. Osetska, R. Fröhlich, *Dalton Trans.* **2005**, 3757-3762; e) M. Albrecht, S. Mirtschin, O. Osetska, S. Dehn, D. Enders, R. Fröhlich, T. Pape, E. F. Hahn, *Eur. J. Inorg. Chem.* **2007**, 3276-3287.
- [72] B. Baytekin, S. S. Zhu, B. Brusilowskij, J. Illigen, J. Ranta, J. Huuskonen, L. Russo, K. Rissanen, L. Kaufmann, C. A. Schalley, *Chem. Eur. J.* **2008**, *14*, 10012-10028.
- [73] For reviews on self-assembly, see: a) D. Philp, J. F. Stoddart, *Angew. Chem.* **1996**, *108*, 1242-1286; *Angew. Chem. Int. Ed.* **1996**, *35*, 1155-1196; b) P. J. Stang, B. Olenyuk, *Acc. Chem. Res.* **1997**, *30*, 502-518; c) C. A. Schalley, A. Lützen, M. Albrecht, *Chem. Eur. J.* **2004**, *10*, 1072-1080.
- [74] Selected examples: a) I. Higler, H. Boerrigter, W. Verboom, H. Kooijman, A. L. Spek, D. N. Reinhoudt, *Eur. J. Org. Chem.* **1998**, 1597-1607; b) E. S. Barrett, J. L. Irwin, P. Turner, M. S. Sherburn, *J. Org. Chem.* **2001**, *66*, 8227-8229; c) B. M. O'Leary, T. Szabo, N. Svenstrup, C. A. Schalley, A. Lützen, M. Schäfer, J. Rebek, *J. Am. Chem. Soc.* **2001**, *123*, 11519-11533; d) S. Y. Yu, H. Huang, H. B. Liu, Z. N. Chen, R. B. Zhang, M. Fujita, *Angew. Chem.* **2003**, *115*, 710-714; *Angew. Chem. Int. Ed.* **2003**, *42*, 686-690; e) J. W. Steed, *Chem. Commun.* **2006**, 2637-2649.

- [75] Selected examples: a) T. Iijima, S. A. Vignon, H. R. Tseng, T. Jarrosson, J. K. M. Sanders, F. Marchioni, M. Venturi, E. Apostoli, V. Balzani, J. F. Stoddart, *Chem. Eur. J.* **2004**, *10*, 6375-6392; b) A. B. Braunschweig, W. R. Dichtel, O. S. Miljanic, M. A. Olson, J. M. Spruell, S. I. Khan, J. R. Heath, J. F. Stoddart, *Chem. Asian J.* **2007**, *2*, 634-647.
- [76] Selected examples: a) D. M. Tiede, R. T. Zhang, L. X. Chen, L. H. Yu, J. S. Lindsey, *J. Am. Chem. Soc.* **2004**, *126*, 14054-14062; b) J. Otsuki, T. Narita, K. Tsutsumida, M. Takatsuki, M. Kaneko, *J. Phys. Chem. A* **2005**, *109*, 6128-6134; c) E. Iengo, E. Zangrando, E. Alessio, *Acc. Chem. Res.* **2006**, *39*, 841-851.
- [77] Y. Tanaka, H. Katagiri, Y. Furusho, E. Yashima, *Angew. Chem.* **2005**, *117*, 3935-3938; *Angew. Chem. Int. Ed.* **2005**, *44*, 3867-3870.
- [78] Selected examples: a) C. J. Pedersen, *J. Am. Chem. Soc.* **1967**, *89*, 2495-2496; b) R. M. Izatt, K. Pawlak, J. S. Bradshaw, R. L. Bruening, *Chem. Rev.* **1995**, *95*, 2529-2586.
- [79] Selected examples: a) R. A. Bissell, E. Cordova, A. E. Kaifer, J. F. Stoddart, *Nature* **1994**, *369*, 133-137; b) J. P. Sauvage, *Acc. Chem. Res.* **1998**, *31*, 611-619; c) C. A. Schalley, K. Beizai, F. Vögtle, *Acc. Chem. Res.* **2001**, *34*, 465-476; d) A. M. Brouwer, C. Frochot, F. G. Gatti, D. A. Leigh, L. Mottier, F. Paolucci, S. Roffia, G. W. H. Wurpel, *Science* **2001**, *291*, 2124-2128.
- [80] Selected examples: a) M. Kocak, A. I. Okur, O. Bekaroglu, *J. Chem. Soc. Dalton Trans.* **1994**, 323-326; b) J. D. Badjic, V. Balzani, A. Credi, S. Silvi, J. F. Stoddart, *Science* **2004**, *303*, 1845-1849; c) S. J. Loeb, D. A. Tramontozzi, *Org. Biomol. Chem.* **2005**, *3*, 1393-1401; d) X. Z. Zhu, C. F. Chen, *J. Am. Chem. Soc.* **2005**, *127*, 13158-13159; e) O. Hayashida, M. Uchiyama, *J. Org. Chem.* **2007**, *72*, 610-616.
- [81] a) C. A. Hunter, *J. Chem. Soc. Chem. Commun.* **1991**, 749-751; b) C. A. Hunter, *J. Am. Chem. Soc.* **1992**, *114*, 5303-5311.
- [82] a) F. Vögtle, S. Meier, R. Hoss, *Angew. Chem.* **1992**, *104*, 1628-1631; *Angew. Chem. Int. Ed.* **1992**, *31*, 1619-1622; b) S. Ottens-Hildebrandt, S. Meier, W. Schmidt, F. Vögtle, *Angew. Chem.* **1994**, *106*, 1818-1821; *Angew. Chem. Int. Ed.* **1994**, *33*, 1767-1670.
- [83] a) C. A. Schalley, W. Reckien, S. Peyerimhoff, B. Baytekin, F. Vögtle, *Chem. Eur. J.* **2004**, *10*, 4777-4789; b) C. Spickermann, T. Felder, C. A. Schalley, B. Kirchner, *Chem. Eur. J.* **2008**, *14*, 1216-1227.
- [84] Selected examples: a) F. Vögtle, M. Händel, S. Meier, S. Ottens-Hildebrandt, F. Ott, T. Schmidt, *Liebigs Annalen* **1995**, 739-743; b) B. A. Blight, K. A. Van Noortwyk, J. A. Wisner, M. C. Jennings, *Angew. Chem.* **2005**, *117*, 1523-1528; *Angew. Chem. Int. Ed.* **2005**, *44*, 1499-1504; c) P. Ghosh, G. Federwisch, M. Kogej, C. A. Schalley, D. Haase, W. Saak, A. Lützen, R. M. Gschwind, *Org. Biomol. Chem.* **2005**, *3*, 2691-2700; d) B. A. Blight, X. Wei, J. A. Wisner, M. C. Jennings, *Inorg. Chem.* **2007**, *46*, 8445-8447.
- [85] a) R. Jäger, F. Vögtle, *Angew. Chem.* **1997**, *109*, 966-980; *Angew. Chem. Int. Ed.* **1997**, *36*, 930-944; b) C. A. Schalley, T. Weilandt, J. Brüggemann, F. Vögtle, *Top. Curr. Chem.* **2005**, *248*, 141-200.
- [86] X. Y. Li, J. Illigen, M. Nieger, S. Michel, C. A. Schalley, *Chem. Eur. J.* **2003**, *9*, 1332-1347.
- [87] The term "post-macrocyclization pathway" has previously been used in: W. Van Rossom, W. Maes, L. Kishore, M. Ovaere, L. Van Meervelt, W. Dehaen, *Org. Lett.* **2008**, *10*, 585-588.
- [88] For x-ray crystallographic data of **3**, see section E6.

- [89] C. Bilton, J. A. K. Howard, N. N. L. Madhavi, A. Nangia, G. R. Desiraju, F. H. Allen, C. C. Wilson, *Chem. Commun.* **1999**, 1675-1676.
- [90] a) K. Sonogashira, Y. Tohda, N. Hagihara, *Tetrahedron Lett.* **1975**, 4467-4470; b) R. Chinchilla, C. Najera, *Chem. Rev.* **2007**, *107*, 874-922.
- [91] A. S. Hay, *J. Org. Chem.* **1962**, *27*, 3320-3321.
- [92] Recent review: J. E. Moses, A. D. Moorhouse, *Chem. Soc. Rev.* **2007**, *36*, 1249-1262.
- [93] T. Ishiyama, M. Murata, N. Miyaura, *J. Org. Chem.* **1995**, *60*, 7508-7510.
- [94] N. Miyaura, A. Suzuki, *Chem. Rev.* **1995**, *95*, 2457-2483.
- [95] a) D. M. T. Chan, K. L. Monaco, R. P. Wang, M. P. Winters, *Tetrahedron Lett.* **1998**, *39*, 2933-2936; b) P. Y. S. Lam, C. G. Clark, S. Saubern, J. Adams, M. P. Winters, D. M. T. Chan, A. Combs, *Tetrahedron Lett.* **1998**, *39*, 2941-2944.
- [96] The bromo derivatives of pyridines, pyrimidines and terpyridines are relatively unreactive in Suzuki coupling reactions, therefore their boronates need to be used. See also: a) W. Goodall, K. Wild, K. J. Arm, J. A. G. Williams, *J. Chem. Soc., Perkin Trans.* **2002**, 1669-1681; b) C. J. Aspley, J. A. G. Williams, *New J. Chem.* **2001**, *25*, 1136-1147.
- [97] a) G. M. Hübner, J. Gläser, C. Seel, F. Vögtle, *Angew. Chem.* **1999**, *111*, 395-398; *Angew. Chem. Int. Ed.* **1999**, *38*, 383-386; b) C. A. Schalley, G. Silva, C.-F. Nising, P. Linnartz, *Helv. Chim. Acta* **2002**, *85*, 1578-1596. See also: P. Ghosh, O. Mermagen, C.A. Schalley, *Chem. Commun.* **2002**, 2628-2629.
- [98] C. A. Schalley, P. Ghosh, M. Engeser, *Int. J. Mass Spectrom.* **2004**, *232-233*, 249-258. See also: C. A. Schalley, J. Hörschemeyer, X.-Y. Li, G. Silva, P. Weis, *Int. J. Mass Spectrom.* **2003**, *228*, 373-388.
- [99] T. Felder, C. A. Schalley, *Angew. Chem.* **2003**, *115*, 2360-2363; *Angew. Chem. Int. Ed.* **2003**, *42*, 2258-2260.
- [100] a) A. Affeld, G. M. Hübner, C. Seel, C. A. Schalley, *Eur. J. Org. Chem.* **2001**, 2877-2890; b) P. Linnartz, S. Bitter, C. A. Schalley, *Eur. J. Org. Chem.* **2003**, 4819-4829; c) P. Linnartz, C.A. Schalley, *Supramol. Chem.* **2004**, *16*, 263-267.
- [101] J. Kagan, S. K. Arora, *J. Org. Chem.* **1983**, *48*, 4317-4320.
- [102] a) C. Goze, G. Ulrich, L. J. Mallon, B. D. Allen, A. Harriman, R. Ziessel, *J. Am. Chem. Soc.* **2006**, *128*, 10231-10239; b) Y.-H. Yu, A. B. Descalzo, Z. Shen, H. Röhr, Q. Liu, Y.-W. Wang, M. Spieles, Y.-Z. Li, K. Rurack, X.-Z. You, *Chem. Asian. J.* **2006**, *1-2*, 176-187; c) A. Harriman, L. J. Mallon, B. Stewart, G. Ulrich, R. Ziessel, *Eur. J. Org. Chem.* **2007**, 3191-3198; d) A. Loudet, K. Burgess, *Chem. Rev.* **2007**, *107*, 4891-4932.
- [103] a) B. Turfan, E. U. Akkaya, *Org. Lett.* **2002**, *4*, 2857-2859; b) A. Coskun, B. T. Baytekin, E. U. Akkaya, *Tetrahedron Lett.* **2003**, *44*, 5649-5651.
- [104] a) Y. Li, H. Zheng, Y. Li, S. Wang, Z. Wu, P. Liu, Z. Gao, H. Liu, D. Zhu, *J. Org. Chem.* **2007**, *72*, 2878-2885; b) H. T. Baytekin, *Fluorescent Sensing of Cations, Anions and Neutral Molecules Towards Information Processing at Molecular Level*, The Graduate School of Natural and Applied Sciences of Middle East Technical University, Ankara, **2002**.
- [105] B. J. Holliday, C. A. Mirkin, *Angew. Chem.* **2001**, *113*, 2076-2097; *Angew. Chem. Int. Ed.* **2001**, *40*, 2022-2043.
- [106] P. J. Stang, D. H. Cao, *J. Am. Chem. Soc.* **1994**, *116*, 4981-4982.

- [107] For x-ray crystallographic data of **34**, see section E6.
- [108] Calculations in section C2.10 were done with: CAChe 5.0 for Windows, Fujitsu, Krakow (Poland), **2001**.
- [109] S. S. Zhu, M. Nieger, J. Daniels, T. Felder, I. Kossev, T. Schmidt, M. Sokolowski, F. Vögtle, C. A. Schalley, *Chem. Eur. J.* **2009**, *15*, 5040-5046.
- [110] This type of macrocycle was first reported in: C. A. Hunter, *J. Chem. Soc., Chem. Commun.* **1991**, 749-751.
- [111] Selected examples: a) S. Y. Chang, H. S. Kim, K. J. Chang, K. S. Jeong, *Org. Lett.* **2004**, *6*, 181-184; b) G. Kleefisch, C. Kreutz, J. Bargon, G. Silva, C. A. Schalley, *Sensors* **2004**, *4*, 136-146.
- [112] Selected example: Q. Y. Li, E. Vogel, A. H. Parham, M. Nieger, M. Bolte, R. Fröhlich, P. Saarenketo, K. Rissanen, F. Vögtle, *Eur. J. Org. Chem.* **2001**, 4041-4049.
- [113] W. Reckien, S. Peyerimhoff, *J. Phys. Chem. A* **2003**, *107*, 9634-9640.
- [114] If the macrocycle is divided into two halves by a plane bisecting the two isophthalamides, we can distinguish one 2-in-2-out conformation, where the A_{out} groups lie in the same half, from another 2-in-2-out conformation, where the A_{out} groups lie in different halves. The latter is observed in the crystal structures.
- [115] G. M. Sheldrick, *Acta Crystallogr.* **2008**, *A64*, 112-122.
- [116] I. Kossev, W. Reckien, B. Kirchner, T. Felder, M. Nieger, C. A. Schalley, F. Vögtle, M. Sokolowski, *Adv. Funct. Mater.* **2007**, *17*, 513-519.
- [117] C. Fischer, M. Nieger, O. Mogck, V. Böhmer, R. Ungaro, F. Vögtle, *Eur. J. Org. Chem.* **1998**, 155-161.
- [118] M. Nieger, T. Schmidt, F. Vögtle, private communication, **2004**, CCDC-245578 (CCDC-Refcode: YAFDOZ). TLM **2** was crystallized by slow evaporation of the solvents $\text{CHCl}_3/\text{EtOAc}$.
- [119] For the synthesis of TLM **2**, see the experimental part of ref. 109 or see: T. Schmidt, *diploma thesis*, University of Bonn, **1994**.
- [120] B. A. Blight, J. A. Wisner, M. C. Jennings, *Chem. Commun.* **2006**, 4593-4595.
- [121] H. Adams, F. J. Carver, C. A. Hunter, *J. Chem. Soc., Chem. Commun.* **1995**, 809-810.
- [122] The macrocycle plane is defined by the least-squares fit plane through the two quaternary cyclohexane and the four amide α -carbon atoms.
- [123] 44.4° is the angle between the plane of A_{out} groups (formed by the four atoms H13, N13, C14 O14) and the macrocycle plane of **2**. Regarding all the crystal structures of TLMs, this is the largest angle between a plane of an A_{out} amide group and the macrocycle plane.
- [124] Compound **3** crystallizes in a centrosymmetric space group, and in the crystal structure, the *all-in* conformer **3A** is disordered in terms of the position of the pyridine group and the *tert*-butylbenzene group.
- [125] To the best of our knowledge, no other example for a similarly short aryl-C-H \cdots O=C-NH hydrogen bond is known. A comparably short hydrogen bond with a carboxylate oxygen as the acceptor has been reported in: A. Abu-Rayyana, Q. Abu-Salem, N. Kuhn, C. Maichle-Mossmer, E. Mallah, M. Steimann, *Z. Naturforsch. B* **2008**, *63*, 1015-1019. Calculations on comparable hydrogen bonds with methyl C-H as the donor has been reported in: C. E. Cannizzaro, K. N. Houk, *J. Am. Chem. Soc.* **2002**, *124*, 7163-7169.

- [126] For related amide catemers, see: S. S. Kuduva, D. Bläser, R. Boese, G. R. Desiraju, *J. Org. Chem.* **2001**, *66*, 1621-1626.
- [127] For the IUPAC nomenclature for macrocycles, see: H. A. Favre, D. Hellwinkel, W. H. Powell, H. A. Smith, S. S. C. Tsay, *Pure Appl. Chem.* **2002**, *74*, 809-834.
- [128] This compound is referred to as SSZ37 in the lab book.
- [129] This compound is referred to as SSZ74 in the lab book.
- [130] This compound is referred to as SSZ75 in the lab book.
- [131] For the IUPAC nomenclature for rotaxanes and pseudorotaxanes, see: A. Yerin, E. S. Wilks, G. P. Moss, A. Harada, *Pure Appl. Chem.* **2008**, *80*, 2041-2068.
- [132] This compound is referred to as SSZ36 in the lab book.
- [133] This compound is referred to as SSZ79 in the lab book.
- [134] This compound is referred to as SSZ56 in the lab book.

Appendix I: Acknowledgement

(Removed in this online edition / Gelöscht in dieser Online-Ausgabe)

Appendix II: Curriculum Vitae / Lebenslauf

(Removed in this online edition / Gelöscht in dieser Online-Ausgabe)

Appendix III: Publication List / Publikationsliste

Publications in Scientific Journals / Veröffentlichungen in Fachzeitschriften

- 1.** *Anionen bindende Resorcinaren-Cavitanden: die Bedeutung von C–H...Anion-Wechselwirkungen* /
Anion Binding to Resorcinarene-Based Cavitands: The Importance of C–H...Anion Interactions
S. S. Zhu, H. Staats, K. Brandhorst, J. Grunenberg, F. Gruppi, E. Dalcanale, A. Lützen, K. Rissanen, C. A. Schalley, *Angew. Chem.* **2008**, *120*, 800-804; *Angew. Chem. Int. Ed.* **2008**, *47*, 788-792.
(highlighted in: *Synfacts* **2008**, *4*, 367)
- 2.** *A Modular “Toolbox” Approach to Flexible Branched Multimacrocylic Hosts as Precursors for Multiply Interlocked Architectures*
B. Baytekin, S. S. Zhu, B. Brusilowskij, J. Illigen, J. Ranta, J. Huuskonen, L. Russo, K. Rissanen, L. Kaufmann, C. A. Schalley, *Chem. Eur. J.* **2008**, *14*, 10012-10028.
- 3.** *Self-assembly of Heterodinuclear Triple-stranded Helicates: Control by Coordination Number and Charge*
M. Albrecht, Y. Liu, S. S. Zhu, C. A. Schalley, R. Fröhlich, *Chem. Commun.* **2009**, 1195-1197.
- 4.** *Conformational Flexibility of Tetralactam Macrocycles and Their Intermolecular Hydrogen-Bonding Patterns in the Solid State*
S. S. Zhu, M. Nieger, J. Daniels, T. Felder, I. Kossev, T. Schmidt, M. Sokolowski, F. Vögtle, C. A. Schalley, *Chem. Eur. J.* **2009**, *15*, 5040-5046.

Poster Contributions / Posterbeiträge

1. *“Functionalized Macrocycles and Rotaxanes: A Toolbox for Supramolecular Assemblies”*
B. Baytekin, B. Brusilowskij, S. S. Zhu, J. Illigen, C. A. Schalley
 - International symposium “Complex Chemical Systems in Theory and Experiment” in the context of SFB 424 (special research program no. 424), Münster, 15/06/2007

2. *“Towards Complex Threaded Molecular Architectures – Functionalized Macrocycles and Rotaxanes Serving As A Toolbox”*
S. S. Zhu, B. Baytekin, B. Brusilowskij, C. A. Schalley
 - 113th BASF International Summer Course 2007, BASF, Ludwigshafen, 23/07/2007–03/08/2007

3. *“Anion Binding to Simple Resorcinarene-Based Cavitands – The Importance of C–H... Anion Interactions”*
S. S. Zhu, C. A. Schalley
 - International symposium “Templates in Chemistry and Beyond” in the context of SFB 624 (special research program no. 624), Bonn, 13/09/2007–14/09/2007

Oral Presentations / Vorträge

1. *“Molecular Shuttles, Threaded Molecular Architectures and Metallosupramolecular Aggregates”*
 - Workshop “Supramolecular Chemistry” organized by the research groups Albrecht / Lützen / Schalley / Engeser, Bonn, 21/07/2006
2. *“Anion Binding to Resorcinarene-Based Cavitands: The Importance of C–H...Anion Interactions”*
 - Workshop “Supramolecular Chemistry” organized by the research groups Albrecht / Lützen / Schalley / Engeser, Berlin, 13/08/2007
3. *“Anion Binding to Resorcinarene-Based Cavitands: A Gas-Phase Study”*
 - COST workshop Twente 2008, in the context of COST Action D31 – Working Group WG31 0004 04 “Thermodynamically Controlled Macrocyclizations: Size and Shape Selection from Dynamic Libraries through Template Effects”, Enschede, 26/05/2008–27/05/2008
4. *“More Insights into C–H...Anion Interactions in Resorcinarenes and Cavitands”*
 - Workshop “Supramolecular Chemistry” organized by the research groups Albrecht / Lützen / Schalley / Engeser, Simmerath, 09/07/2008

Appendix IV: Summary / Zusammenfassung

Summary

In the course of the development of supramolecular chemistry, weak non-covalent interactions have gained tremendous importance. In this work, comprehensive mass-spectrometric investigations combined with theoretical calculations reveal a new type of these interactions, namely C–H•••anion interactions, to be operative when anions were bound in the bowl of resorcinarene-based cavitands. A further mass-spectrometric study focuses on the formation and ligand exchange processes in helicate-type complexes, in which the hierarchical self-assembly is assisted by $\text{Li}^+\cdots\text{O}=\text{C}$ interactions, and shows that homodinuclear helicates are preferably formed rather than heterodinuclear Ni/Zn helicates in corresponding mixtures. Not an undefined mixture, but a toolbox of specific building blocks was developed on the basis of tetralactam macrocycles in a modular approach. Using this versatile toolbox, a series of multi-macrocylic hosts and some multiply interlocked architectures, in which the threading process is governed by hydrogen bonds, were obtained. In addition, interesting intermolecular hydrogen-bonding patterns and unusual conformational properties were found in crystal structures of tetralactam macrocycles. In summary, this thesis provides new insight into the nature of weak non-covalent interactions and of supramolecular phenomena.

Zusammenfassung

Im Zuge der Entwicklung der supramolekularen Chemie wird den schwachen nicht-kovalenten Wechselwirkungen eine zunehmend größere Bedeutung beigemessen. In der vorliegenden Arbeit zeigen umfangreiche massenspektrometrische Untersuchungen gemeinsam mit theoretischen Berechnungen, dass C–H•••Anion-Wechselwirkungen als eine neue Form schwacher nicht-kovalenter Wechselwirkungen vorliegen, wenn Anionen in der Kavität von resorcinaren-artigen Cavitanden gebunden werden. Eine weitere massenspektrometrische Studie ist auf Bildungs- und Ligandenaustausch-Prozesse bei helicat-artigen Komplexen, deren hierarchische Selbstorganisation von $\text{Li}^+\text{•••O}=\text{C}$ -Wechselwirkungen unterstützt wird, ausgerichtet und zeigt, dass homodinucleare Helicate gegenüber heterodinuclearen Ni/Zn-Helicates bevorzugt in den entsprechenden Mischungen gebildet wird. Keine undefinierbare Mischung, sondern ein Werkzeugkasten, der spezifische Bausteine enthält, wurde in einem modularen Ansatz auf der Grundlage von Tetralactam-Macrocyclen entwickelt. Unter Verwendung dieses vielseitigen Werkzeugkastens wurden eine Reihe von multi-macrocyclischen Gästen und einige mehrfach durchgefädelt Strukturen, bei denen der Einfädungsprozess durch Wasserstoffbrücken gesteuert wird, erhalten. Ferner wurden interessante intermolekulare Wasserstoffbrückenbindungsmuster und ungewöhnliche Konformationseigenschaften in den Kristallstrukturen von Tetralactam-Macrocyclen gefunden. Insgesamt liefert die vorliegende Arbeit neue Einblicke in das Wesen der schwachen nicht-kovalenten Wechselwirkungen und in supramolekulare Phänomene.

Declaration / Erklärung

Hiermit versichere ich an Eides statt, dass die vorliegende Dissertation von mir persönlich und selbständig angefertigt wurde und keine anderen als die angegebenen Quellen und Hilfsmittel verwendet wurden.

Wurden Ergebnisse im Rahmen einer Kooperation erhalten, so wurden entsprechende Angaben in der Fußzeile zu Beginn des jeweiligen Kapitels gemacht.

Die vorliegende Arbeit wurde an keiner anderen Hochschule als Dissertation eingereicht.

Ich habe früher noch keinen Promotionsversuch unternommen.

Teile der Arbeit sind auszugsweise veröffentlicht worden; entsprechende Angaben wurden in der Fußzeile zu Beginn des jeweiligen Kapitels gemacht.

Sascha Shuxia Zhu